AD

AMMRC CR 71-9

MATERIAL PROPERTIES MEASUREMENTS USING PULSED ELECTRON BEAMS

July 1971

T. Stefansky, A. Mazzella, K. Triebes, and J. Shea

Physics International Company
2700 Merced Street, San Leandro, California 94577

FINAL REPORT PIFR-174

Prepared for

ARMY MATERIALS AND MECHANICS RESEARCH CENTER
Watertown, Massachusetts 02172

The findings in this report are not to be construed as an official Department of the Army position, unless so designated by other authorized documents.

Mention of any trade names or manufacturers in this report shall not be construed as advertising nor as an official indorsement or approval of such products or companies by the United States Government.

DISPOSITION INSTRUCTIONS

Destroy this report when it is no longer needed.
Do not return it to the originator.

UNCLASSIFIED
Security Classification

DOCUMENT CONTROL DATA - R & D

(Security classification of title, body of abstract and indexing annotation must be entered when the overall report is classified)

1. ORIGINATING ACTIVITY (Corporate author)

Physics International Company
2700 Merced Street, San Leandro, CA. 94577

2a. REPORT SECURITY CLASSIFICATION: Unclassified

2b. GROUP: Not Applicable

3. REPORT TITLE

Material Properties Measurements Using Pulsed Electron Beams

4. DESCRIPTIVE NOTES (Type of report and inclusive dates)

Final Report

5. AUTHOR(S) (First name, middle initial, last name)

Stefansky, Tibor; Mazzella, Aldo; Triebes, Kenneth; and Shea, James

6. REPORT DATE	7a. TOTAL NO. OF PAGES	7b. NO. OF REFS
July 1971	126	21

8a. CONTRACT OR XXXXXX
DAAG 46-69-C-0126

b. PROJECT NO. DA, ITO62105A331

c. AMCMS Code 5025.11.297

d.

9a. ORIGINATOR'S REPORT NUMBER(S)
PIFR-174

9b. OTHER REPORT NO(S) (Any other numbers that may be assigned this report)
AMMRC CR 71-9

10. DISTRIBUTION STATEMENT

Approved for public release; distribution unlimited

11. SUPPLEMENTARY NOTES

12. SPONSORING MILITARY ACTIVITY
Army Materials and Mechanics
Research Center
Watertown, Massachusetts 02172

13. ABSTRACT A technique has been developed for measuring the elevated-temperature tensile properties of materials following "instantaneous" in-depth heating. High-energy pulsed electron beams are used to heat specimens to the required temperature in approximately 0.08 μsec, and a Hopkinson bar-type device, in a tensile configuration, is used to perform the mechanical tests at any desired time after irradiation. Data on the temperature-induced degradation of the Young's Modulus and the yield stress of 2014-T6 aluminum and commercially pure alpha titanium have been obtained. The data extend up to approximately 700 F for three different times at temperature: 0.2 msec, 1.0 msec and 10 msec. The results indicate that the Young's Modulus at ambient pressure appears to be a function of temperature only. The degradation of the yield strength, on the other hand, is time- and temperature-dependent but not as severe as that shown by the long-heating-time handbook data.

Results are also presented on measurements of the Gruneisen coefficient of 2014-T6 aluminum and alpha titanium at energy densities up to melt. The measurements were made using a pressure transducer located just beyond the region of energy deposition to measure the pressures generated by the deposition of electron energy at constant volume. The results agree with those calculated from equilibrium thermodynamic data and suggest a temperature independent Gruneisen coefficient at internal energies at least up to melt.

DD FORM 1473 REPLACES DD FORM 1473, 1 JAN 64, WHICH IS OBSOLETE FOR ARMY USE.

UNCLASSIFIED

Preceding Page Blank

KEY WORDS	LINK A		LINK B		LINK C	
	ROLE	WT	ROLE	WT	ROLE	WT
Pulse heating						
Yield point						
Heating rate						
Materials						
Impact						
Energy pressure coupling						
Thermal degradation						
Dynamic modulus of elasticity						
Electron beams						

AMMRC CR 71-9

MATERIAL PROPERTIES MEASUREMENTS USING PULSED ELECTRON BEAMS

T. Stefansky, A. Mazzella, K. Triebes, and J. Shea

Physics International Company
2700 Merced Street, San Leandro, California 94577

July 1971

FINAL REPORT Contract Number DAAG-46-69-C-0126

D/A Project 1TO 62105A331
AMCMS Code 5025.11.297
Reduction of Vulnerability: ABM Systems

Approved for public release; distribution unlimited

Prepared for

ARMY MATERIALS AND MECHANICS RESEARCH CENTER
Watertown, Massachusetts 02172

FOREWORD

This report describes the work performed by Physics International Company for the Army Materials and Mechanics Research Center (AMMRC) under Contract No. DAAG46-69-C-0126.

The program was entitled "Material Properties Measurements Using Pulsed Electron Beams" and its objectives were threefold:

- To develop a technique for measuring elevated-temperature high strain-rate mechanical properties under conditions where the material is heated uniformly in a few tens of nanoseconds and to determine mechanical properties of the material, for varying but generally short times at temperature thereafter.

- To demonstrate this technique by obtaining data on two structural metals.

- To further characterize the response of the same two materials to rapid heating by measuring their Gruneisen, or pressure-energy coupling, coefficient.

These objectives were successfully accomplished.

The administration of the program at AMMRC was performed by Dr. S. C. Chou; Mr. J. Dignam was the Program Manager. The program manager at Physics International was Dr. T. Stefansky.

ABSTRACT

A technique has been developed for measuring in a direct and straightforward manner the elevated-temperature tensile properties of materials following "instantaneous" in-depth heating. High-energy pulsed electron beams are used to heat specimens to the required temperature in approximately 0.08 μsec, and a Hopkinson bar-type device, in a tensile configuration, is used to perform the mechanical tests at any desired time after irradiation.

Data on the temperature-induced degradation of the Young's Modulus and the yield strength of 2014-T6 aluminum and commercially pure alpha titanium have been obtained. The data extend up to approximately 700 F for three different times at temperature: 0.2 msec, 1.0 msec and 10 msec. The strain rates were approximately 500 in./in./sec. The results indicate that the dynamic tensile properties of the materials studied are degraded at these temperatures and times at temperature, following instantaneous in-depth heating. More specifically, the Young's Modulus at ambient pressure appears to be a function of temperature only. The degradation of the yield strength, on the other hand, is time- and temperature-dependent but not as severe as that shown by the long-heating-time handbook data.

Results are also presented on direct measurements of the Gruneisen coefficient of 2014-T6 aluminum and alpha titanium at energy densities up to melt. The measurements were made using

the transmitted stress technique: a pressure transducer located just beyond the region of energy deposition measures the pressures generated by the deposition of electron energy at constant volume. The results agree well with those calculated from equilibrium thermodynamic data and they suggest, therefore, a temperature independent Gruneisen coefficient at internal energies at least up to melt.

CONTENTS

ILLUSTRATIONS

Preceding Page Blank

ILLUSTRATIONS (cont.)

ILLUSTRATIONS (cont.)

ILLUSTRATIONS (cont.)

ILLUSTRATIONS (cont.)

ILLUSTRATIONS (cont.)

TABLES

SECTION 1

PROPERTY DEGRADATION DUE TO "INSTANTANEOUS" IN-DEPTH HEATING

1.1 BACKGROUND OF THE PROBLEM AND THE CHOSEN METHOD OF APPROACH

The temperature dependence of the mechanical properties of metals and alloys is well documented (Reference 1) for times at a temperature where properties have reached steady state values. Typical long soak times yield stress data versus temperature are shown on Figure 1.1. As a general rule, for long soak times the material no longer has any significant strength at temperatures equal to half the melting point.

In the region where strength properties vary with time and temperature, the data that are available (Reference 2) are rather fragmentary and become increasingly so for high heating rates and short soak times. Although some evidence exists that strength properties can undergo significant temperature-induced degradation for times-to-heat plus times-to-test as short as one second (Reference 3),* the data are not in the range of direct interest to a nuclear radiation effects analyst concerned with structural response. From this standpoint, a more reasonable and desirable set of data would be generated under the following conditions:

- The specimen is heated in a small fraction of a microsecond.

*These data were obtained using a resistive heating technique coupled with a conventional Hopkinson bar apparatus (Reference 3).

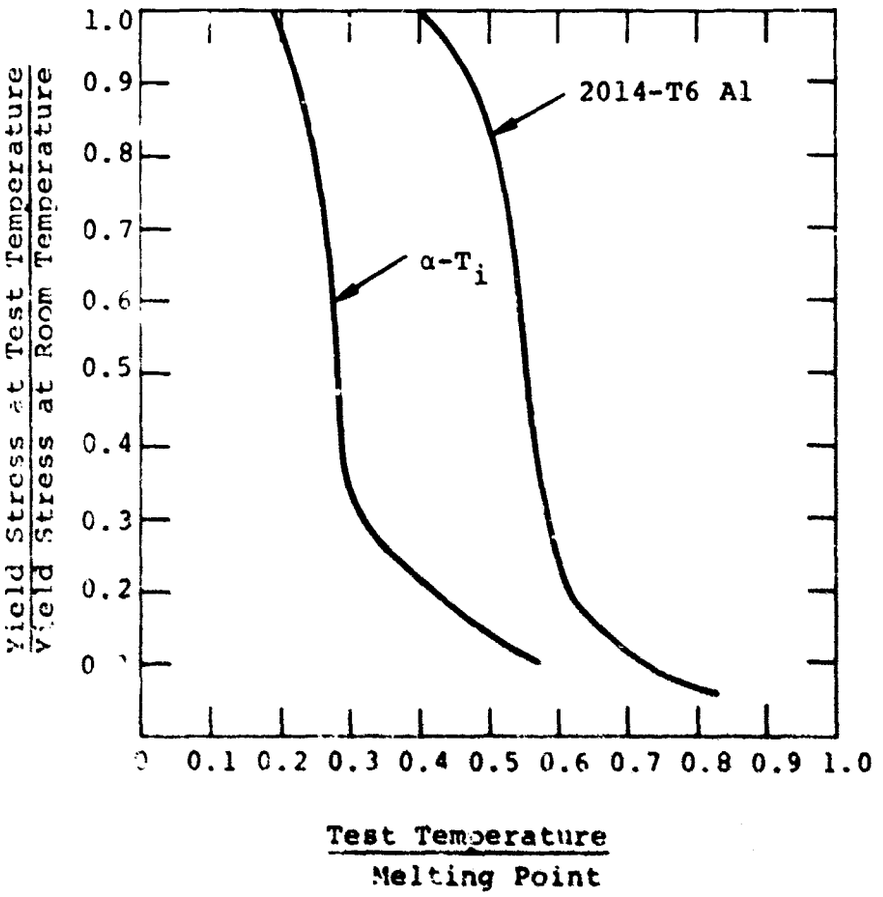

Figure 1.1 Long-heating-time temperature-induced tensile property degradation.

- The specimen is held at temperature, and its high strain rate mechanical properties (yield stress, Young's modulus, etc.) are measured for times ranging from a fraction of a millisecond to many milliseconds after heating.
- The testing time is very short compared with the time at temperature.
- The specimen must be sufficiently large so that macroscopic properties can be measured.

In this report a technique is described for measuring the dynamic yield stress and Young's modulus in tension under the above noted conditions. This technique now is state of the art. High-energy pulsed electron beams are used to achieve heating approximately 80 nanoseconds (or 60 nanoseconds at full width at the half maximum (FWHM)). A modified Hopkinson bar type device in a tensile configuration mated to the electron accelerator is used to measure the dynamic tensile properties at any desired time after irradiation. Data on the temperature degraded mechanical properties of 2014-T6 aluminum alloy and a commercially pure alpha-titanium are presented. The significance of these data for structural design is discussed.

1.2 A TECHNIQUE FOR SUBMICROSECOND HEATING BY PULSED ENERGY DEPOSITION

Rapid heating of a specimen can be readily accomplished by irradiation with a high intensity short duration electron beam pulse.

Electrons lose energy as they pass through matter primarily by ionizing the atoms in the material through electron-electron interactions. Excitation and recombination by the secondary electrons with ions increase the kinetic energy of the atoms, and thereby the temperature of the material.

The amount of energy an electron loses in passing through a given thickness of matter is proportional to the density, ρ, and the ratio of atomic number to the atomic mass number, Z/A. Since Z/A varies only from 0.5 for low-Z elements to 0.4 for high-Z elements, if distances that the electrons travel in the material are expressed in terms of the product of the density times the length, the path-length increases quite slowly with Z.

The electrons also undergo extensive elastic scattering with the nuclei. As a result, the average depth of penetration is considerably less than the average total path length. Since the scattering cross section increases with Z, the effects of decreasing stopping power and increased scattering compensate, and consequently, the depth of penetration expressed in grams/cm^2 tends to be independent of material for a given energy electron beam. The maximum depth of penetration is shown as a function of electron energy in Figure 1.2.

The extensive scattering causes some electrons which bombard a material to be scattered back out. However, upon reaching a depth representing an appreciable portion of their total range, the electrons are unlikely to reach the surface again. As a result, electron-energy deposition profiles, i.e., specific energy deposited versus distance into target, have a peak value at a point interior to the surface. An energy deposition profile for a beam with a mean electron energy of 4.5 MeV is shown in Figure 1.3.

Uniform heating of a specimen by a pulsed electron beam can be achieved by using target samples that are thin in comparison to the electron range, and sample dimensions such that the beam intensity is constant over the irradiated area.

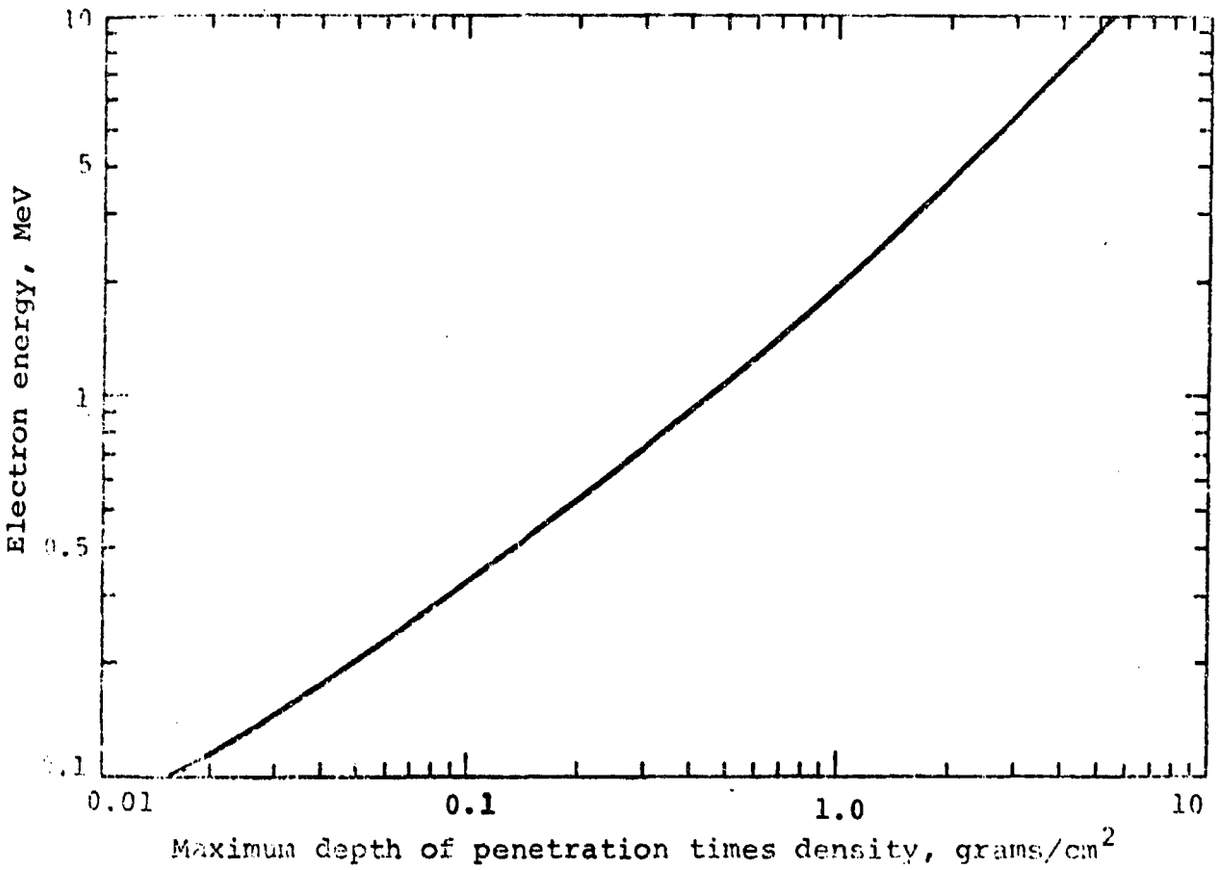

Figure 1.2 Maximum depth of penetration of monoenergetic electrons for normal incidence.

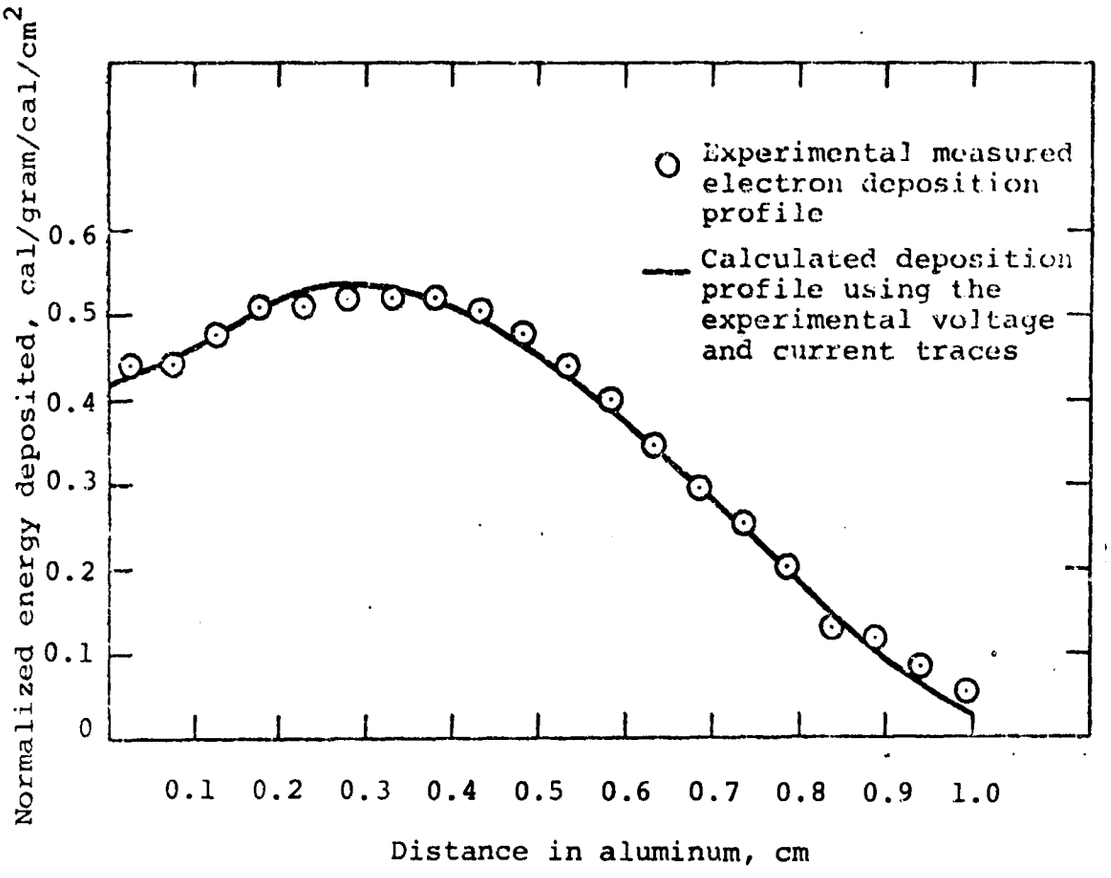

Figure 1.3 Normalized deposition profile in aluminum, <4.5 MeV>.

The heating rate obtained is dependent only upon the peak dose and the duration of the beam. The latter is a characteristic of the accelerator and for Physics International's Model 1140 Pulserad used in these experiments, is on the order of 60 nsec (FWHM). Thus the electrical conductivity, thermal conductivity, or dielectric properties of the material do not limit the heating rates in contrast with joule or microwave heating techniques.

A detailed description of the operation of pulsed electron accelerators is not pertinent to this report and can be found in References 5, 6, and 7. Very briefly, however, a resonance charged Blumlein transmission line delivers a pulse to the cathode such that the electric field causes direct field emission of electrons toward the anode. The stream of electrons passes through the thin anode into a drift chamber where experiments are performed. In these experiments, the intensity of the beam falls off as the inverse square of the distance from the anode.

Using the Model 1140 Pulserad operating with a mean electron energy of 4.5 MeV, a uniformity of heating through the thickness of ± 5 percent can be obtained for aluminum specimens 0.080-inch thick, centering the sample about the peak of the deposition profile by using a filter. Moreover, a substantial fluence is transmitted through the sample, and can be measured using total absorbing calorimeters. This, in conjunction with the energy deposition profile and the specific heat of the target, can be used to determine the radiation induced temperature increase in the specimen. Alternatively, the temperature increase in a specimen can be directly measured with thermocouples, and correlated with the transmitted fluence to obtain a calibration curve. The two methods generally agree within ± 15 percent.

The deposition profile for a given experimental configuration is computed using the PIE-1D Monte Carlo electron transport code (Reference 8) and the time dependent electron energy spectrum derived from the accelerator current and voltage recordings.

The validity of the energy deposition profile obtained in this way is confirmed by comparing the profile computed for aluminum with that obtained with an aluminum depth dosimeter (Figure 1.3). The dosimeter consists of a stack of closely spaced, thin aluminum foils that are thermally isolated (Figure 1.4). The collimated electron beam impinges normally over the center portion of the foils, such that virtually all the electrons incident are captured in the foils, despite the electron scattering. Iron-constantan thermocouples are spot-welded to the edge of each foil, outside the irradiated region; the temperature rise of each foil establishes the total energy deposited in each foil.

The total energy stored in the Model 1140 Pulserad is sufficiently large that fluences up to 300 cal/cm^2 uniform over several square centimeters can be obtained. Consequently, the uniformity in fluence (or temperature) over a 1-inch long by 0.5-inch wide target area is generally within ± 10 percent for fluence levels on the order of 100 cal/cm^2.

Although uniform heating can be obtained for sample thicknesses equivalent to as great as 0.080 inches of aluminum for the heating rates employed here, the sample thickness must be limited to prevent damage to the specimen by thermomechanical stress waves. The generation of these stresses is discussed in the second section of this report. If thermal expansion through the thickness of the specimen is incomplete after energy deposition,

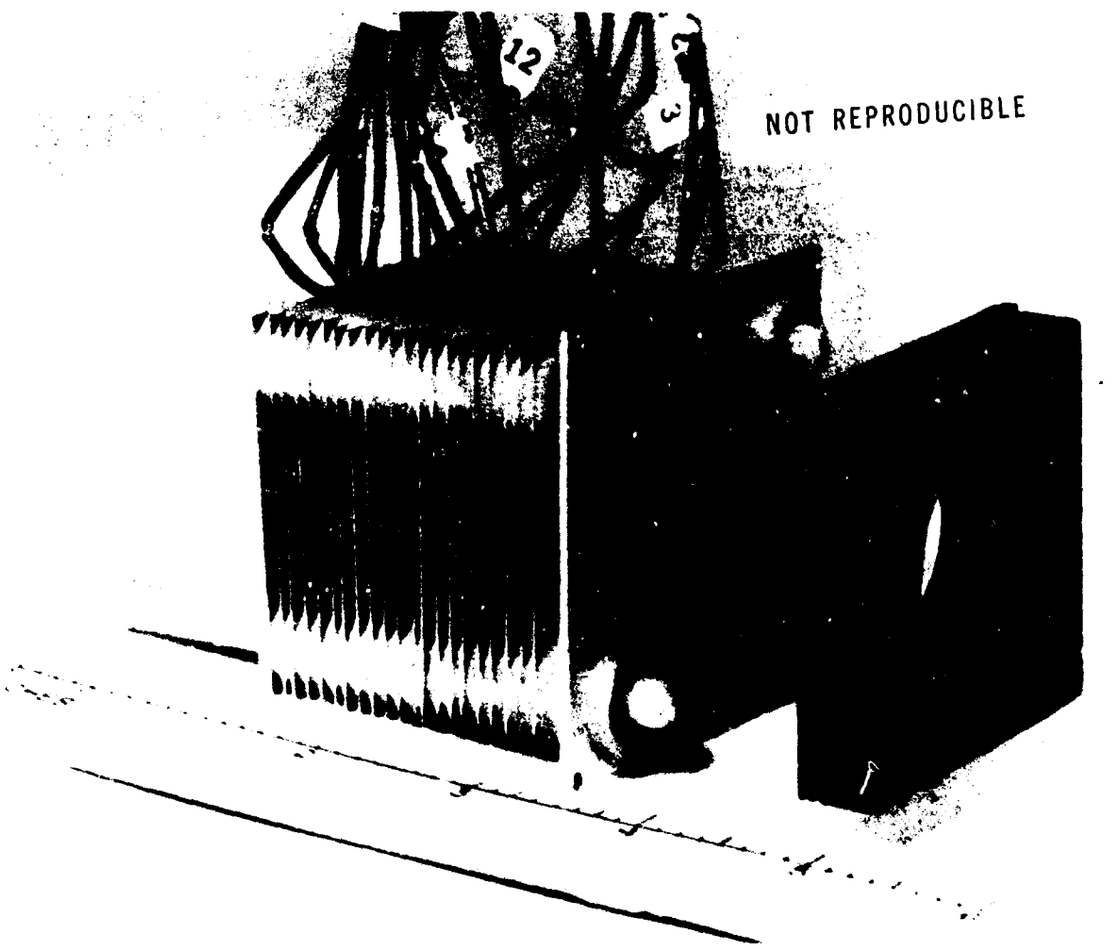

Figure 1.4 **Depth dose calorimeter array.**

the superposition of stress relief waves from the free surfaces can produce tensile failure at the midplane of the sample. Thermal expansion, i.e., stress relief, proceeds at the speed of sound in the material, so the peak tension associated with a given dose can be greatly reduced by making the specimen thickness comparable to or less than the distance a sound wave can propagate during the source duration. Data on the peak dose required to induce incipient tensile damage in this way as a function of sample thickness are given in Reference 6 for alpha titanium and 6061-T6 aluminum.

1.3 A DYNAMIC TECHNIQUE FOR MEASURING THE STRENGTH PROPERTIES OF MATERIALS FOLLOWING HIGH RATE HEATING

The technique employed to measure the yield stress and Young's modulus of materials following high rate heating is based upon observation of a tensile stress pulse that passes through a heated region in a strip of the material. Young's modulus, E, can be obtained from a measurement of the elastic wave transit time through the heated region, which determines the elastic wave velocity, C_o, in the heated region, and from the relationship

$$E = \rho C_o^2 .$$

If the amplitude of the stress pulse before passing into the heated region is at the yield stress for the unheated material, an elastic-plastic wave will result in the heated portion if the yield stress has been degraded by the temperature. The amplitude of the elastic wave will be equal to the yield stress in the heated material. The elastic wave velocity, $C_o = \sqrt{E/\rho}$ is much greater (typically a factor of seven) than the nominal plastic wave velocity, C_p, which is given by (Reference 9)

$$C_p(\sigma) = \sqrt{\frac{d\sigma}{d\varepsilon}/\rho}$$

where $d\sigma(\varepsilon)/d\varepsilon$ is the slope of the stress-strain relationship in uniaxial tension. Consequently, unless the loading pulse is much longer than length of the heated region, the elastic unloading wave will attenuate the plastic loading wave.

As the elastic wave re-enters cold material, it remains elastic. Measurement of its amplitude (in the cold material) thus provides the yield stress in the heated region, after a small correction for slight differences in the acoustic impedance between the heated and cold materials.

Strain gauges placed on either side of the heated region allow measurement of the elastic transit time; the amplitude of the elastic stress wave transmitted through the heated region can also be measured with strain gauges.

In this study, the pulsed electron beam from the Model 1140 Pulserad was used to heat a one-inch long portion of a half-inch wide strip of the materials investigated. A graphite shield was used to mask all but the desired area from the beam. Strain gauges were placed on either side of the heated region.

A tensile pulse was produced in the specimen at the desired times using an apparatus specially designed and constructed under this contract. The experimental configuration is shown in Figure 1.5.

The tensile loading device is, in essence, a Hopkinson bar apparatus in a tensile configuration. The essential features of the device are illustrated in Figures 1.5 through 1.8. A tensile wave is induced in a long and slender elastic bar upon impact of a gas driven projectile on a tup attached to the bar. The projectile is concentric with the bar and travels toward the tup.

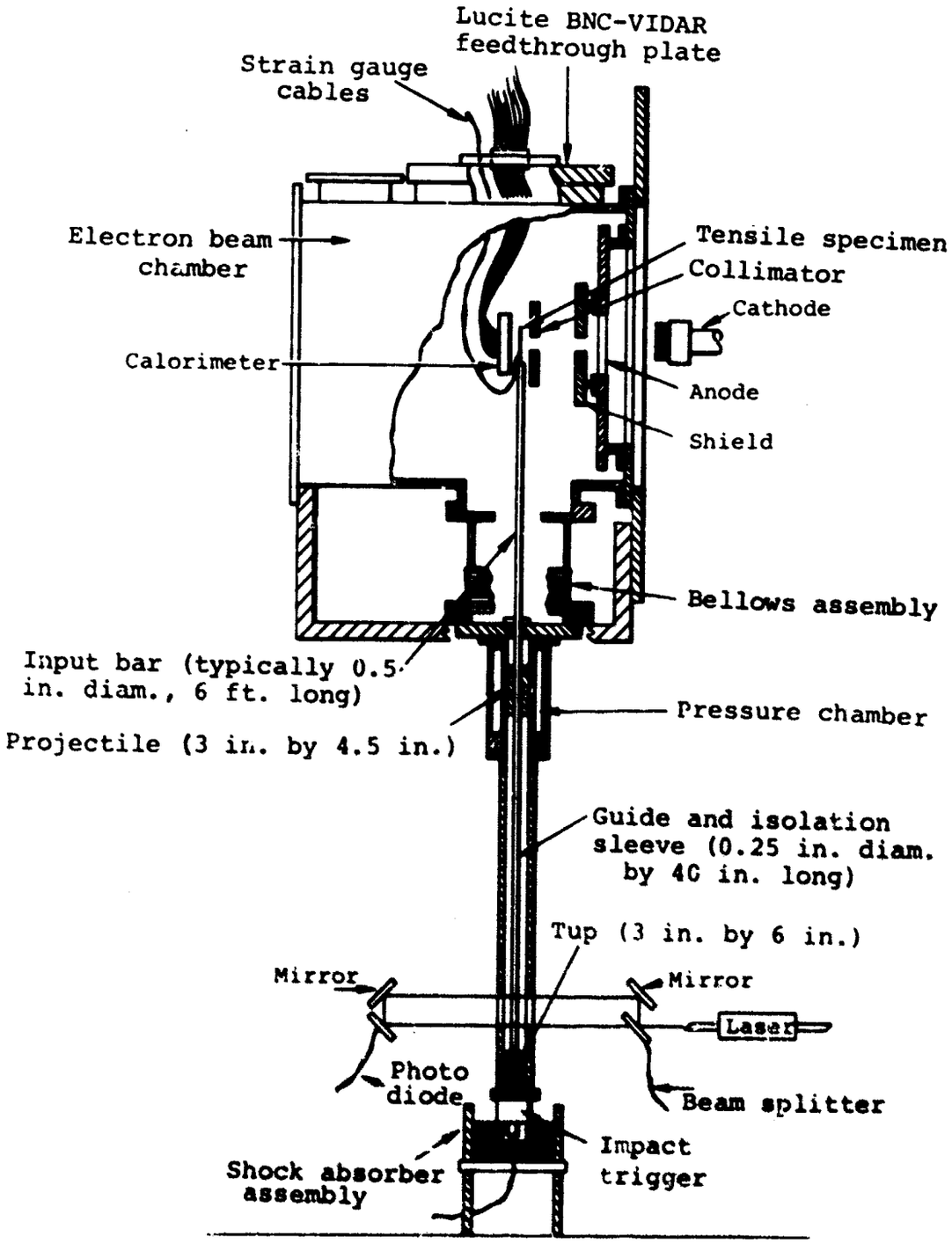

Figure 1.5 Experimental configuration.

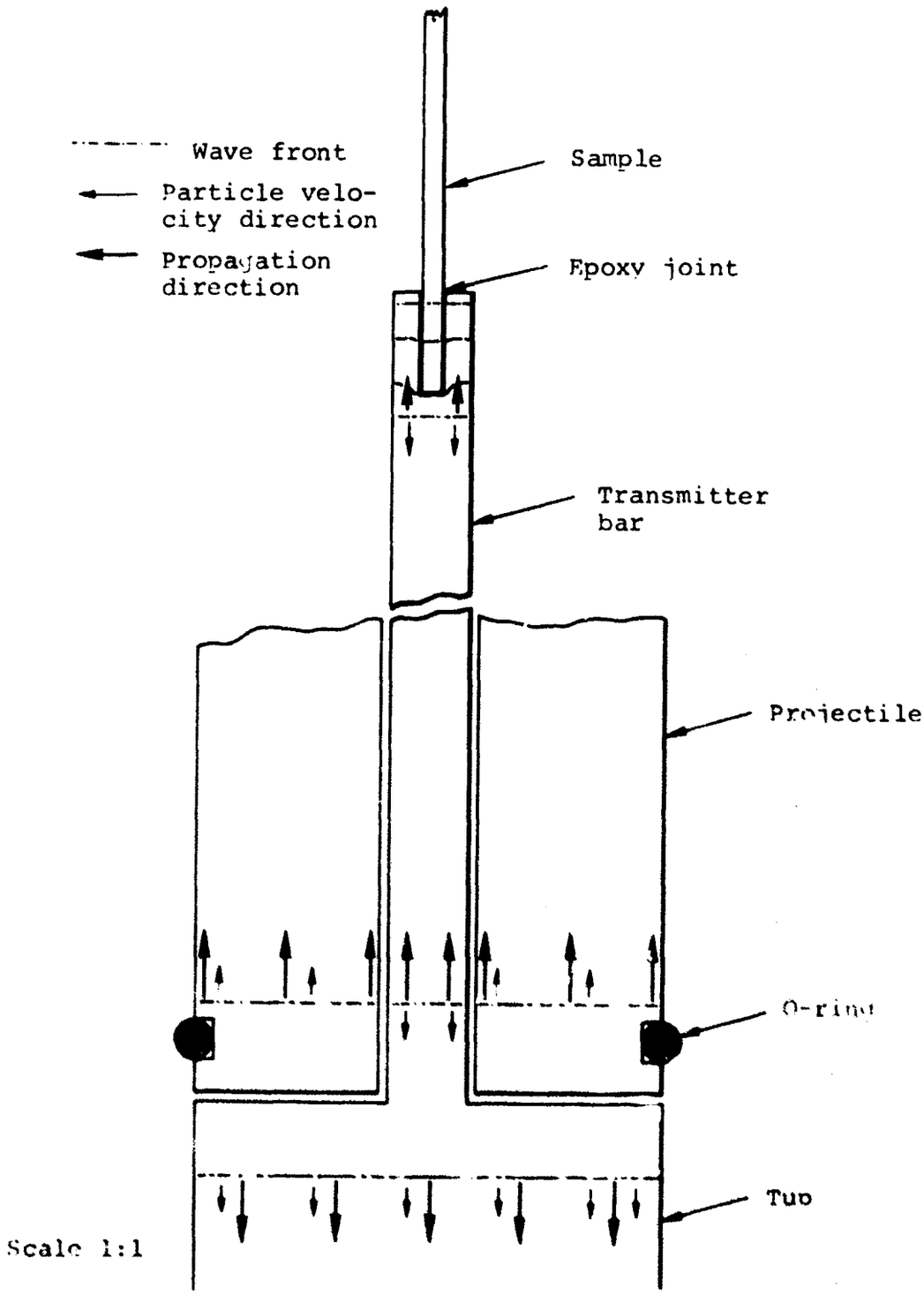

Figure 1.6 Schematic of tensile wave formation.

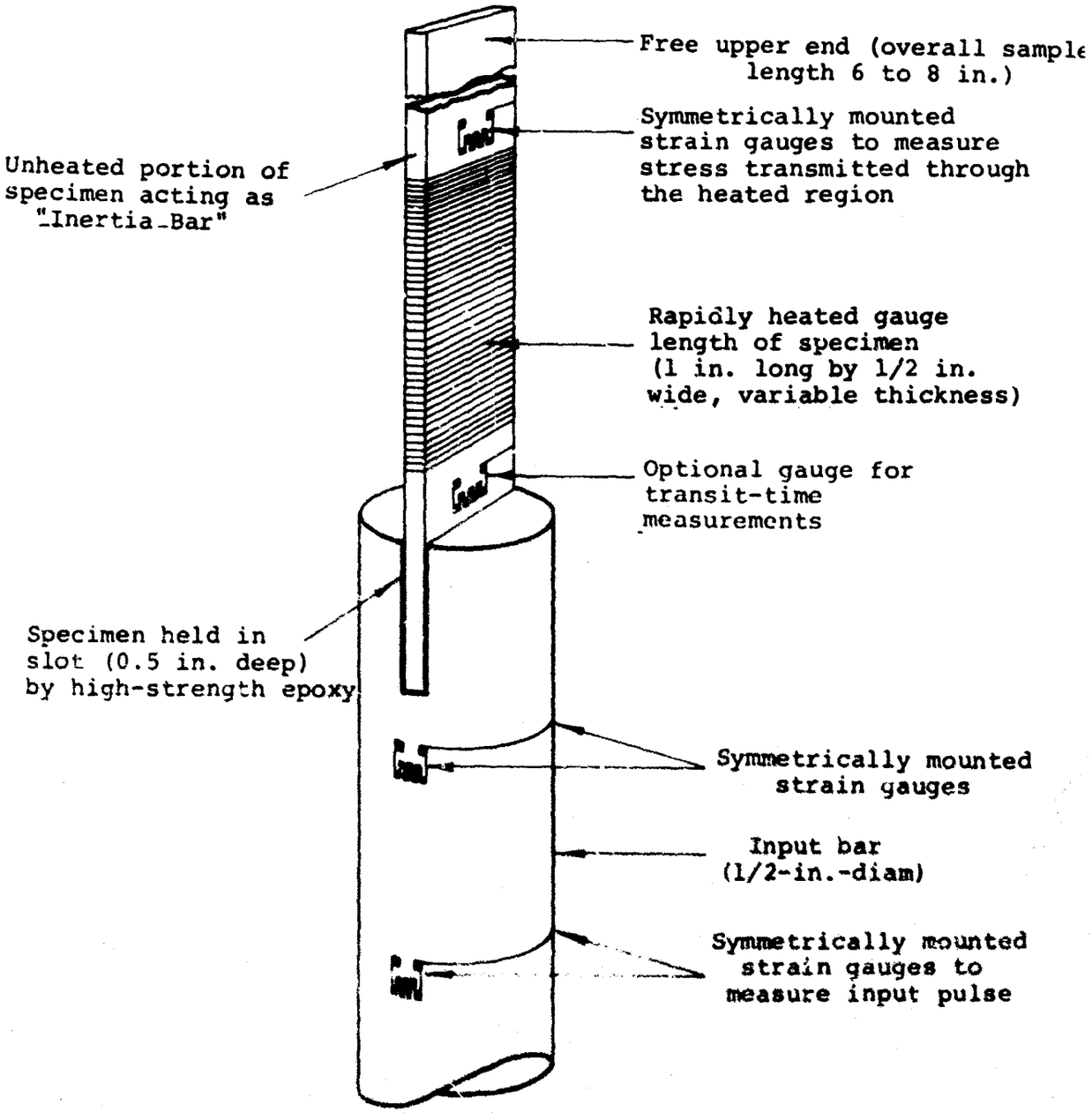

Figure 1.7 Specimen-gripping assembly and instrumentation (not to scale).

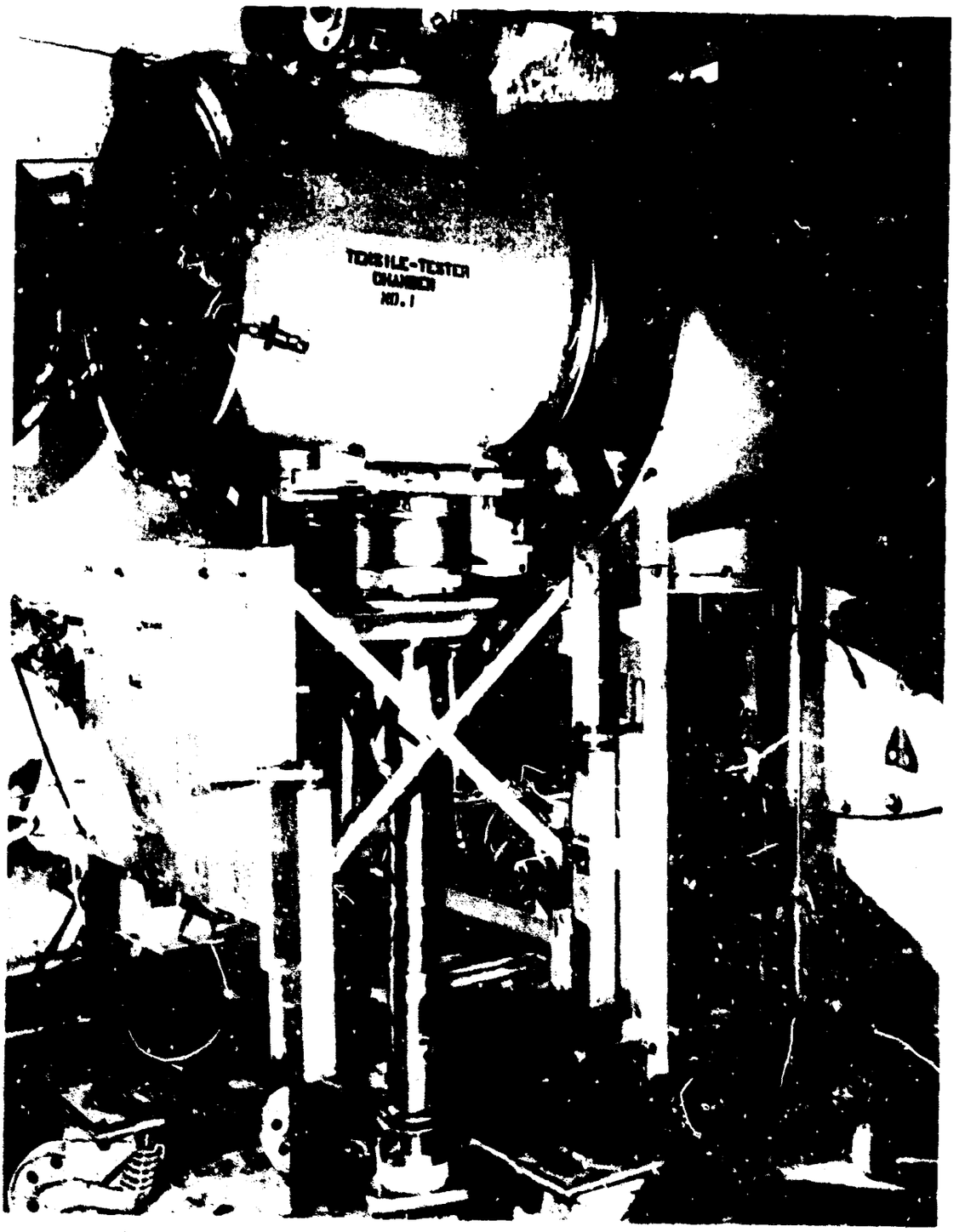

Figure 1.8 High-heating-rate test facility, 2140 Pulserad and modified Hopkinson bar device.

The tensile wave thus generated is transmitted into a specimen joined to the other end of the bar.

The formation of the tensile wave in the input bar and its transmission into the specimen is illustrated in Figure 1.6. The tensile pulse in the bar has a risetime of less than 10 μsec. Most of this appears to be due to geometric dispersion. The duration of the tensile pulse is governed by the lengths of the projectile and the tup and has generally been 100 μsec. Impact conditions are chosen so that the yield stress of the specimen is exceeded while the input wave is still rising. As a result, the measurements do not depend on the detailed shape of the input tensile wave, as long as the strain rate is held constant from shot to shot.

The impact velocity is varied by changing the pressure of the driving gas. The pressure container has, in addition, a built-in volume adjustment, which together with the various barrel extensions available, gives the system a stress capability covering the range of practical interest.

The input bar and the projectile-tup assemblies are fabricated from 7075-T6 aluminum, which has been found to be suitable for low to medium strength materials.

The specimen-gripping assembly that is used is shown in Figure 1.7. The lower portion of the specimen is inserted into a narrow slot at the top end of the input bar and is joined to the latter by a layer of Aerobond 2211 (Adhesive Engineering Company) high-strength epoxy. This is a critical area since improper gripping can lead to substantial distortions of the incoming stress-wave. The gripping technique illustrated in Figure 1.7

has held at the highest stress levels used without distorting the loading wave. The grips are not heated directly or by thermal diffusion during the test.

The upper end of the sample is not gripped, i.e., the unheated portion of the sample acts effectively as an "inertia bar." This arrangement prevents buckling of the specimen because of the thermal expansion of the rapidly heated gauge length. The input bar is supported by having the tup rest directly on the impact trigger and absorber assembly, which appears in Figure 1.5.

The stress pulse that is transmitted to the specimen can be determined by considering the requirement that the total force and the particle velocity must be continuous across the interface. This leads to the conditions that a stress increment, $\Delta\sigma_1$, and its corresponding particle velocity increment $\Delta v_1 = \Delta\sigma_1/\rho_1 C_1$, in the input bar transmit stress and particle velocity increments, $\Delta\sigma_2$ and Δv_2, into the specimen as given by

$$\Delta\sigma_2 = \frac{2\ \Delta\sigma_1}{\frac{A_2}{A_1} + \frac{\rho_1 C_1}{\rho_2 C_2}}$$

and

$$\Delta v_2 = \frac{2\ \Delta v_1}{1 + \frac{\rho_2 C_2 A_2}{\rho_1 C_1 A_1}}$$

where ρ and A denote the respective densities and cross sectional areas; C denotes the bar velocity for elastic increments, given by $\sqrt{E/\rho}$, where E is Young's modulus. For plastic increments, C is the plastic wave velocity, given by $C = \sqrt{d\sigma/d\varepsilon\ }/\rho$.

For $A_2 << A_1$, which was the case in the experiments here ($A_2/A_1 \sim 0.05$), and comparable acoustic impedances, we obtain

$$\Delta v_2 \approx 2\Delta v_1$$

This approximation improves when yielding occurs in the specimen, since C_2 decreases. Thus, the loading of the specimen is equivalent to specifying a velocity boundary condition $v_2(t) = 2v_1(t)$.

It may also be noted that as C_2 decreases, the transmitted stress increments decrease relative to the stress increments in the input bar. Making use of the fact that $v_2(t)$ is known, the transmitted stress may be computed from the relationship

$$\sigma_2(t) = \int_{v_2(o)}^{v_2(t)} \left(\rho_2 \frac{d\sigma_2}{d\varepsilon_2}\right)^{1/2} dv_2$$

if the stress strain relationship is known. Since $d\sigma/d\varepsilon$ in the plastic range is much less than E, once yielding occurs in the specimen further increases in the velocity lead to comparatively small increases in the stress transmitted to the specimen. Consequently, very high stress levels would be required in the input bar to obtain the velocities necessary to achieve fracture in ductile materials.

The strain gauges were spaced 5.7 centimeters apart, with the lower gauge located approximately 0.5 centimeters from the input bar interface. The heated region, 2.5 centimeters in length, was centered between the gauges. Sample thicknesses were 0.010 inches (0.025 cm), so despite the complex details of the boundary conditions at the interface between the input bar and

the specimen, the first gauge is located ~ 20 specimen thicknesses away. Consequently, the stress should be uniform throughout the thickness by that distance.

Specimen widths were one-half inch (1.3 cm) so the existence of transverse stress components in the plane of the strip is a potential concern. However, even if the strain in this transverse direction were completely suppressed, the effective longitudinal modulus would be increased only about 10 percent for a material with a Poisson ratio of 0.3. The yield stress for a von Mises yield condition would also be increased by about 10 percent in such a case. This, of course, is a more severe case than would actually be encountered since stress waves can cross the width of the specimen four times during the ten μsec risetime of the pulse. In addition, the farthest end of the heated region is about four strip widths away from the interface with the input bar. Finally, the strain gauge nearest the input bar need only record the arrival time of the stress pulse, and only the velocity of propagation beyond that point influences the measurement of Young's modulus.

The strain gauges used are 350 Ω, SR-4 foil gauges (BLH FAE-06S-35-59), bonded with a thin layer of non-brittle cement. The gauges were powered with continuous-operation, constant-current power supplies. The gauge output was recorded with Tektronix 556 oscilloscopes equipped with Type W preamplifiers. The gauge current used was 20 mA, which with the strain gauge factor of about 2, yields a sensitivity of 14 volts per unit strain. This provided a satisfactory signal level.

Considerable care was required to prevent direct electron irradiation, RF and bremsstrahlung induced transients in the strain gauge circuit during the electron beam pulse from saturating the amplifiers on the oscilloscope. An aluminum foil RF shield was placed around each strain gauge, and all cables were triple shielded. The type W preamplifiers have a fast recovery and were operated in differential mode.

In determining the transit time between gauges, the difference in arrival time at the two locations was used. Since the foot of the recorded pulse does not show a sharp break from the baseline, the arrival time was defined as the intercept between the baseline and an extension of the linearly rising portion of the gauge record (Figure 1.9). The elastic velocity, C_H, in the heated gauge length, ℓ, is determined from the transit time, τ, between the gauges, separated by distance, S, as

$$C_H = \frac{\ell}{\tau - \frac{(S-\ell)}{C_o}}$$

where C_o is the elastic velocity in cold material.

The yield stress is obtained from the gauge positioned beyond the heated region. The beginning of yield (elastic limit) is indicated by a knee in the traces. We have chosen to define the yield stress as the first deviation from linearity as shown in Figure 1.9. The alternative definition shown also gives consistent results, as will be discussed below.

The appearance of yield on the strain gauge traces is shown in Figures 1.10 and 1.11 for typical room temperature shots on 2014-T6 aluminum and alpha titanium. The strain rate in these

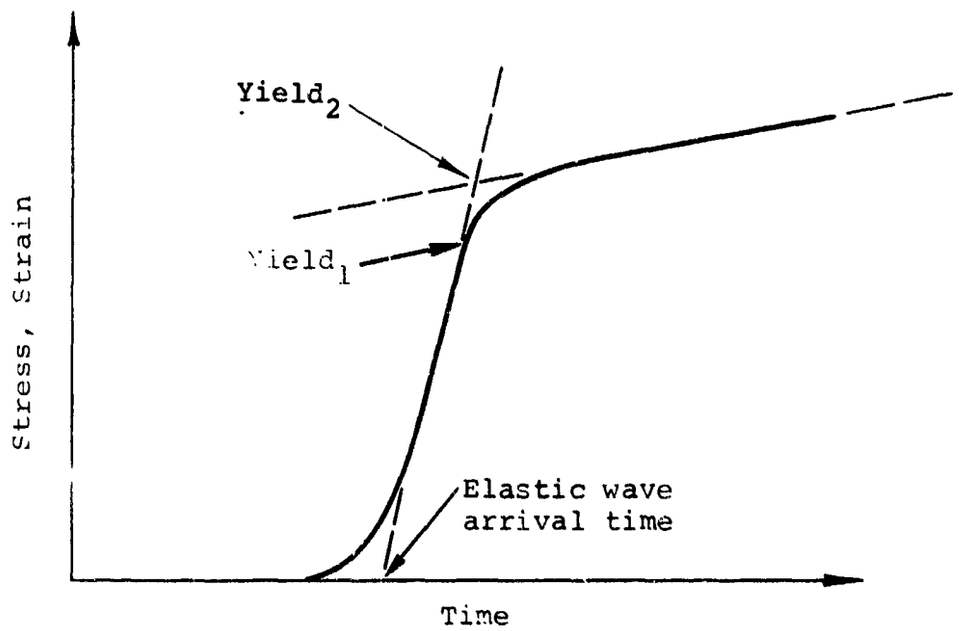

Yield$_1$ - First departure from linearity of stress-time trace

Yield$_2$ - Backward extrapolation method

Figure 1.9 Definition of yield.

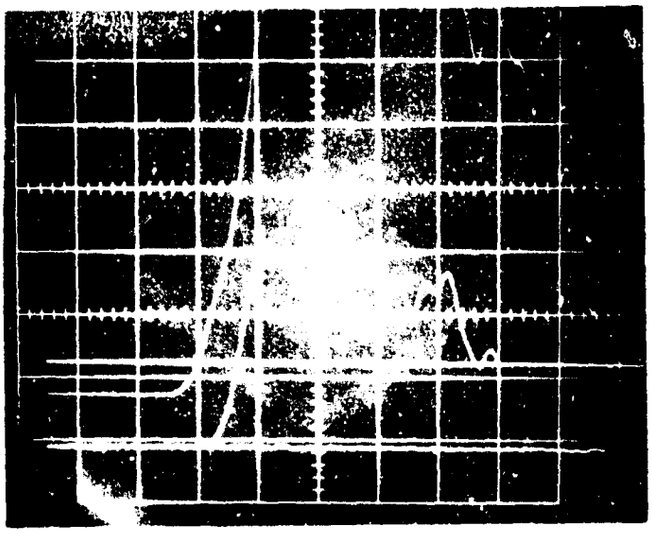

a. Yield strain trace, 20 μsec/cm

Top trace - Lower sample gauge
- 50 mV/cm

Bottom trace - Upper sample gauge
- 20 mV/cm

Shot 10404
Gauge type - BLH,FAE-06S-35-59
Gauge factor - 2.1
Gauge currents - Lower sample gauge-15.462 mA
Upper sample gauge-15.077 mA

NOT REPRODUCIBLE

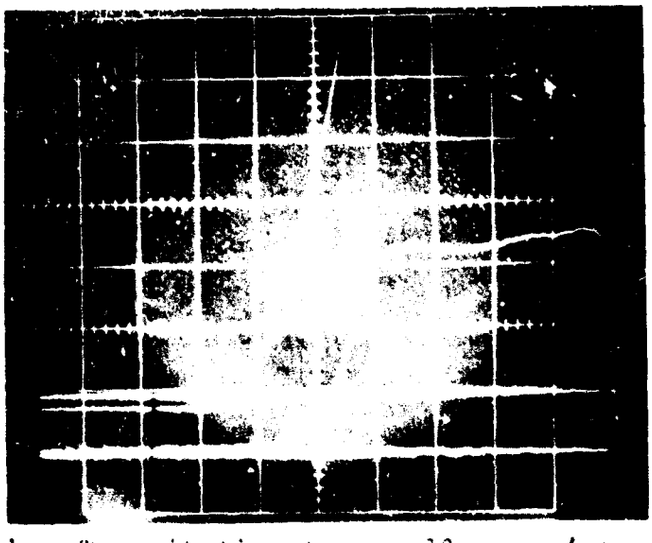

b. Transit time trace, 10 μsec/cm

Top trace - Lower sample gauge

Bottom trace - Upper sample gauge

20 mV/cm

Strain gauge traces for a room temperature shot on 2014-T6 aluminum.

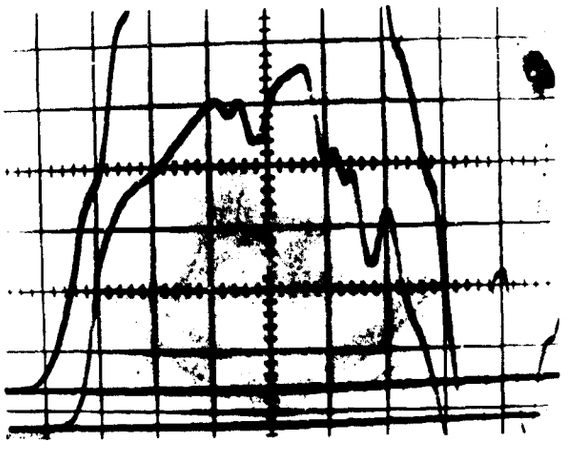

a. Yield strain trace, 20 μsec/cm

Top trace: Lower sample gauge
50 mV/cm
Bottom trace: Upper sample gauge
20 mV/cm

Shot #7-21-4D
Gauge type: BLH, FAE-06S-35-S9
Gauge factor: 1.97
Gauge currents:
Lower sample gauge:
15.077 mA
Upper sample gauge:
15.474 mA

NOT REPRODUCIBLE

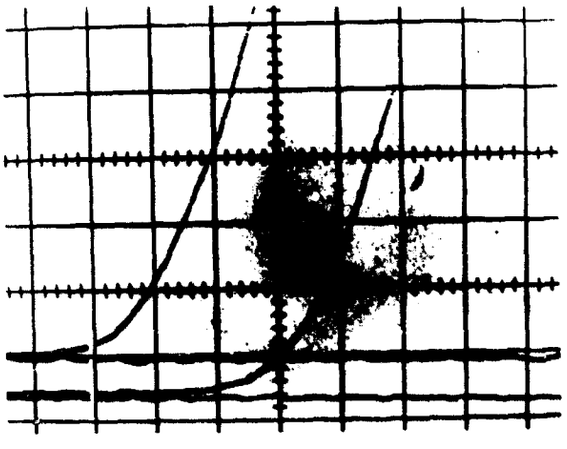

b. Transit time trace, 5 μsec/cm

Top trace: Lower sample gauge
Bottom trace: Upper sample gauge
10 mV/cm

Figure 1.11 Strain gauge traces for a room temperature shot on alpha titanium.

A693

tests was approximately 500 in./in./sec (as given by the slope of the strain-time curve).

For measurements at elevated temperature, the heated gauge length is 1-inch-long, and one must take into account the impedance mismatch at the upper boundary between the gauge length and cold portion of the sample. Since the wave that propagates through the heated region is elastic, one-dimensional elastic wave analysis supplies applies. It can be shown that the upper strain gauge measures a stress, σ_T, such that

$$\sigma_T = \frac{2}{1 + \frac{\rho_h C_h}{\rho_o C_o}} \sigma_I$$

where
ρ = density
C = velocity of sound
h = hot
c = cold

Therefore, σ_I, the stress amplitude in the heated material, is easily calculated.

Losses caused by heat conduction during the short times at temperature of interest here can be shown to be negligible by a simple steady heat-flow calculation. For a short time following the heating of the gauge length it is valid to postulate that the temperature gradient between two points a small distance on either side of the hot-cold boundary is constant.

The rate of heat conduction can then be expressed as

$$Q = - \frac{\int_{T_0}^{T} k dT}{\int_{P_1}^{P_2} \frac{dl}{A}}$$

where Q is the rate of heat flow in heat units per unit time, k is the thermal conductivity, T is the temperature of the hot material, T_0 is the initial temperature P_1 and P_2 are points in the heated and cold regions, respectively, and A is the cross-sectional area. The worst case (maximum conduction) is for aluminum heated to the maximum temperature specified with the longest specified time at temperature. Consider, herefore, that a 1-inch-long by 1/2-inch-wide by 0.025-inch-thick gauge section of 2014-T6 aluminum is rapidly heated (in less than 0.01 μsec) to 700 F.

Let P_1 be 0.5 mm within the heated region and P_2 at 0.5 mm outside the boundary. If the heat conductivity of the alloy is taken as 0.37 cal/cm^2/cm/^{o}C/sec (Reference 1) the rate of heat loss is Q = 16 cal/sec. The heat content of the gauge length at 700 F is H = 2.75 calories of which a maximum of 0.16 calories or 6 percent will be lost in 0.01 seconds. The maximum anticipated heat loss is therefore quite moderate in aluminum and also in titanium.

To obtain the various times at temperature triggering devices were located in the gas gun to fire the electron beam accelerator. For times on the order of 10 msec, a small piston placed in a radial orifice in the barrel is moved to contact a trigger electrode by the gas pressure behind the projectile after it passes the orifice. For times on the order of 1 to 0.25 msec, a spring-loaded triggering pin was placed near the bottom of the impact chamber port. Contact between the projectile and the pin triggers the machine. In both cases, the time at temperature is measured by triggering an oscilloscope simultaneously with the electron beam deposition and displaying the output of an impact trigger on the trace. The stress wave arrives at the heated gauge length 0.25 msec after impact.

The velocity of the projectile is measured on each shot by interrupting two spatially separated laser beams that illuminate a photodiode (Figure 1.5).

1.4 DEGRADED TENSILE PROPERTIES OF 2014-T6 ALUMINUM AND ALPHA TITANIUM

The data obtained on 2014-T6 aluminum are summarized in Table 1.1. Room temperature properties agree well with published values (References 1 and 4). At room temperature 2014-T6 aluminum is insensitive to strain rate, so the results should be independent of the test technique. At elevated temperatures 2014-T6 aluminum may be strain-rate dependent; however, because, as is discussed below, the amplitude of the stress pulse traveling with the elastic velocity is observed after propagating several centimeters in the heated material, the observed yield stress should be nearly equivalent to its quasistatic value.

A representative set of oscillograph records is shown in Figure 1.12.

The temperature along the gauge length is uniform approximately within 10 percent (the peak temperature is used in strength versus temperature plots). A representative temperature profile is given in Figure 1.13.

The measured Young's modulus is shown in Figure 1.14. The modulus appears to be only a function of temperature and, in fact, agrees quite well with reported values (Reference 4) for long heating times. Once the radiation induced internal pressures have decayed, one would indeed expect the modulus to be a function of temperature only. The estimated uncertainties in the modulus shown in Figure 1.14 represent the uncertainty in the measured transit time.

TABLE 1.1

DATA SUMMARY FOR TENSILE PROPERTIES OF 2014-T6 ALUMINUM FOLLOWING INSTANTANEOUS HEATING

Shot Number	Temp. (F)	Time at Temperature (msec)	Yield Stress (ksi)	Young's Modulus (x 10^6 psi)
6-11-3D	Room	-	63.6	-
10404	Room	-	60.6	10.48
10408	350	.250	55.5	9.83
10867	496	.250	48.5	-
10409	632	.250	45.8	-
10400	146	1.0	56.7	10.27
10406	242	1.1	54.8	10.27
10395	326	1.0	52.5	9.87
10864	553	0.75	45.5	7.79
10792	500	1.0	47.2	-
10863	302	10.0	50.3	-
10865	425	10.0	46.4	9.28
10862	537	10.0	44.1	7.79

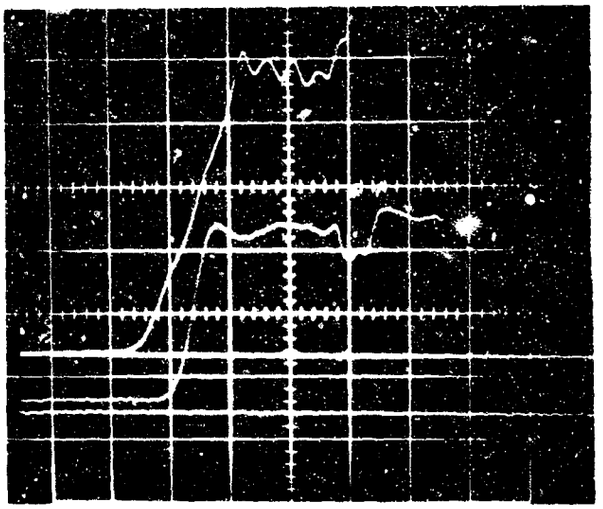

Top trace: Lower sample gauge
50 mV/cm
Bottom trace: Upper sample gauge
20 mV/cm

Shot 10395
Temperature: 326 F
Time at temperature: 1 msec
Gauge type: BLH, FAE-06S -35-S9
Gauge factor: 2.1
Gauge currents: Lower sample
Lower sample gauge:
15.462 mA
Upper sample gauge:
15.077 mA

a. Yield strain trace, 20 μsec/cm

NOT REPRODUCIBLE

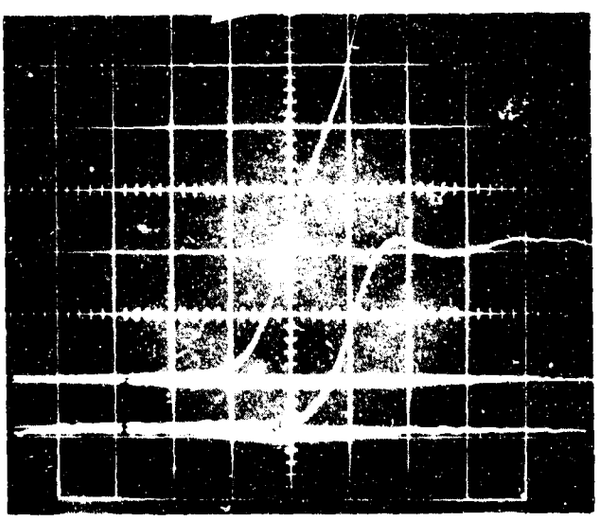

Top trace: Lower sample gauge

Bottom trace: Upper sample gauge

20 mV/cm

b. Transit time trace, 10 μsec/cm

Figure 1.12 Strain gauge traces for an elevated temperature shot on 2014-T6 aluminum with a 1 msec time at temperature, (shot 10295).

A694

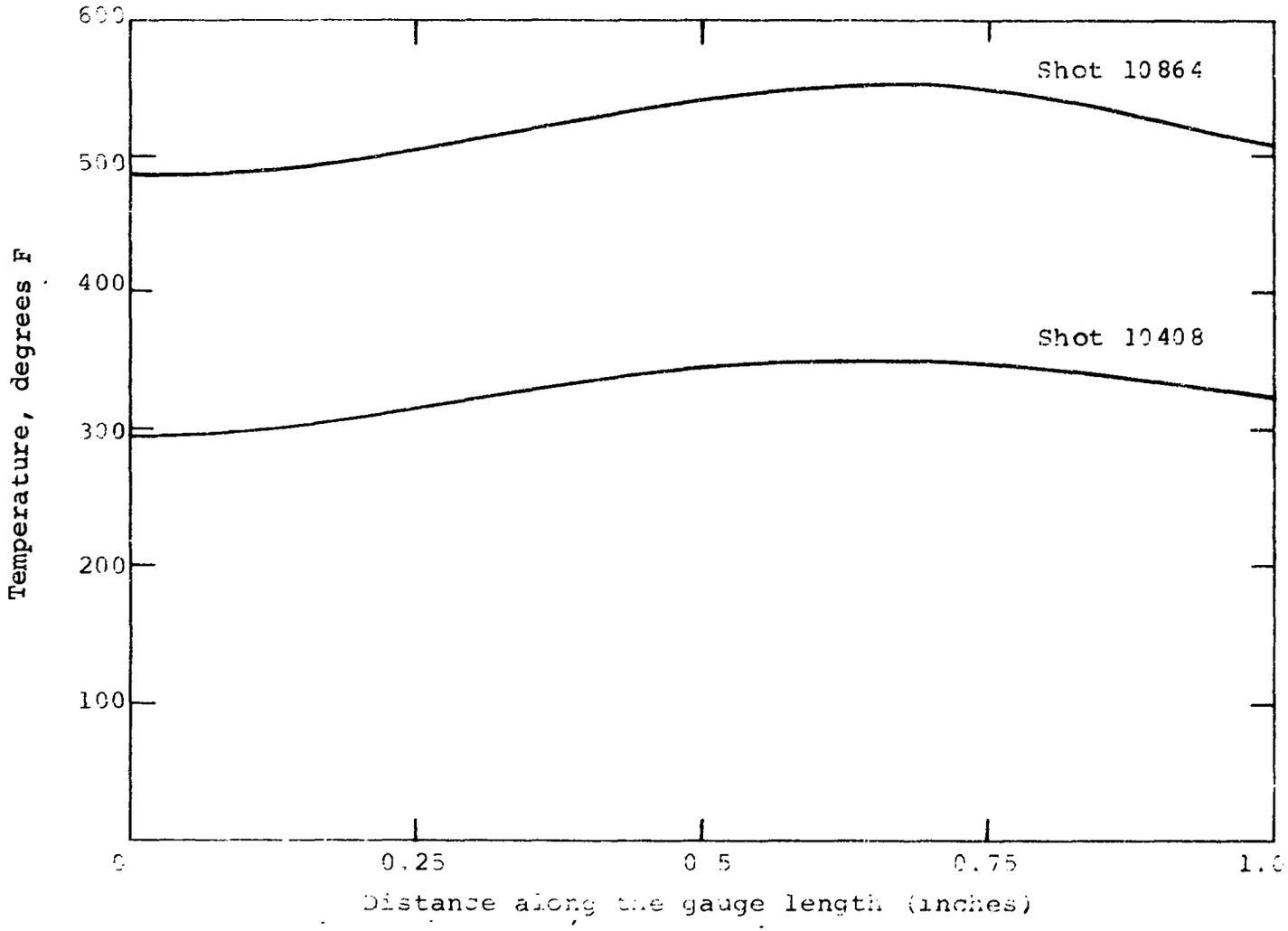

Figure 1.13 Typical temperature profiles along the gauge length for shots on 2014-T6 aluminum.

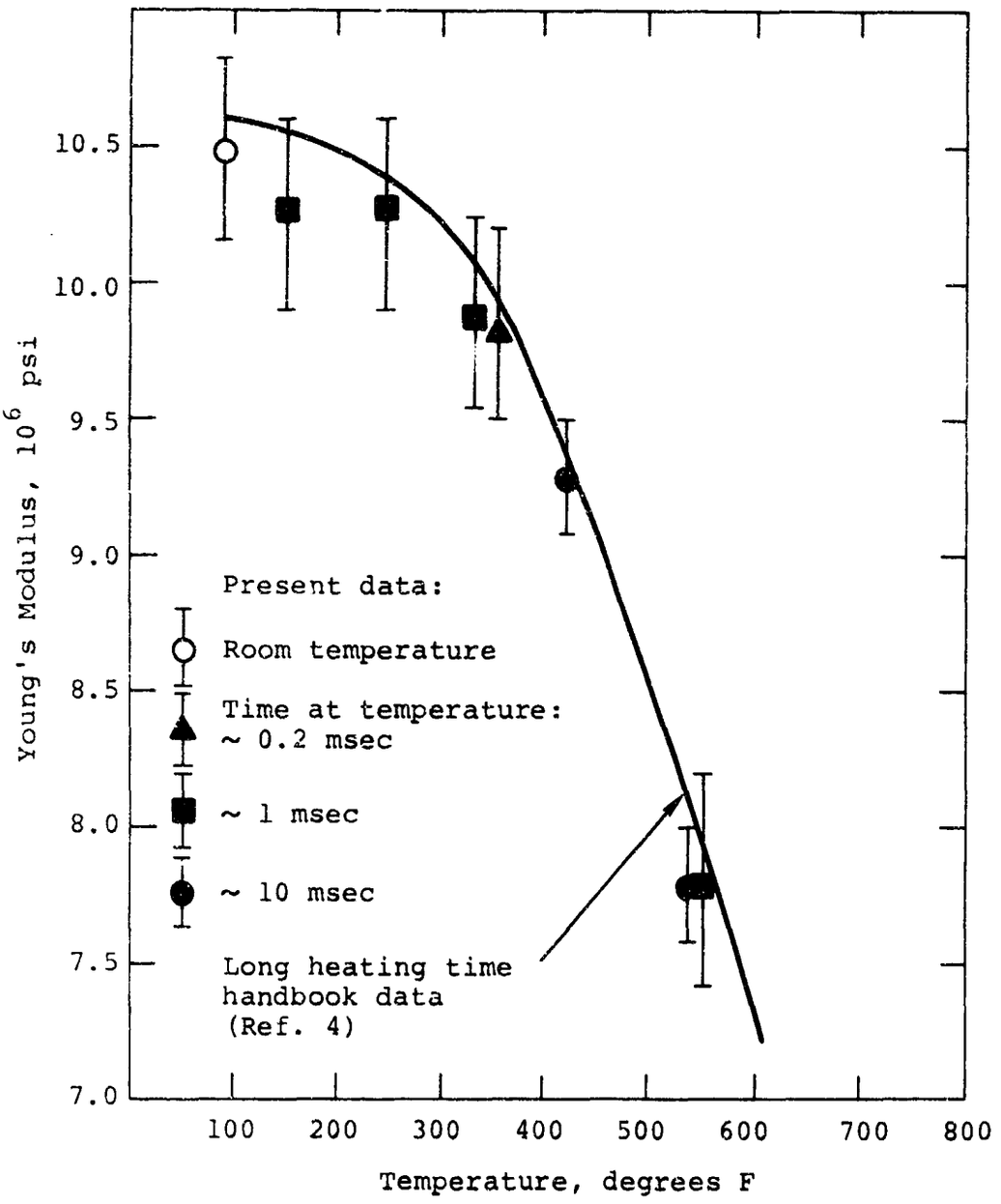

Figure 1.14 Thermal degradation of Young's Modulus for 2014-T6 aluminum.

The yield stress, on the other hand, appears to be a function of temperature as well as time at temperature. This is illustrated in Figure 1.15. The strain at yield also changes with temperature and time at temperature (Figure 1.16). The time dependence of the yield stress for these short times at temperature is probably associated with metallurgical changes in the structure of the material. It has been stated (Reference 10) that such changes, for example changes in precipitate size, can occur on a time scale of milliseconds. However, the change in yield stress might also be related to changes in both the modulus (Figure 1.14) and the strain at yield (Figure 1.16), although not enough is currently known about the structure on these time scales to provide an explanation.

An alternative way of presenting the yield stress data is shown in Figure 1.17. Degradation of the yield stress for times at temperature of significance to structural response is seen to be considerably less than for long soak times.

Data from References 1, 4 and 11 are also shown in Figures 1.15 and 1.17. The data show a nearly linear decrease in the yield stress with temperature for very short times at temperature. The curves for the 0.2 to 10 msec data were faired through the data points. However, the vertical bars about each datum point denote only the uncertainty in interpreting the strain gauge traces; an additional uncertainty results from the uncertainty in the voltage calibration of the oscilloscopes which is estimated to be on the order of 5 percent. Consequently, although the data do indicate a trend between 0.2 and 10 msec data, it is possible that all the short time heating data actually lie in a single band. This would account for the apparent differences between the 10^4 hour data and the 1 and 10 msec data below 250 F.

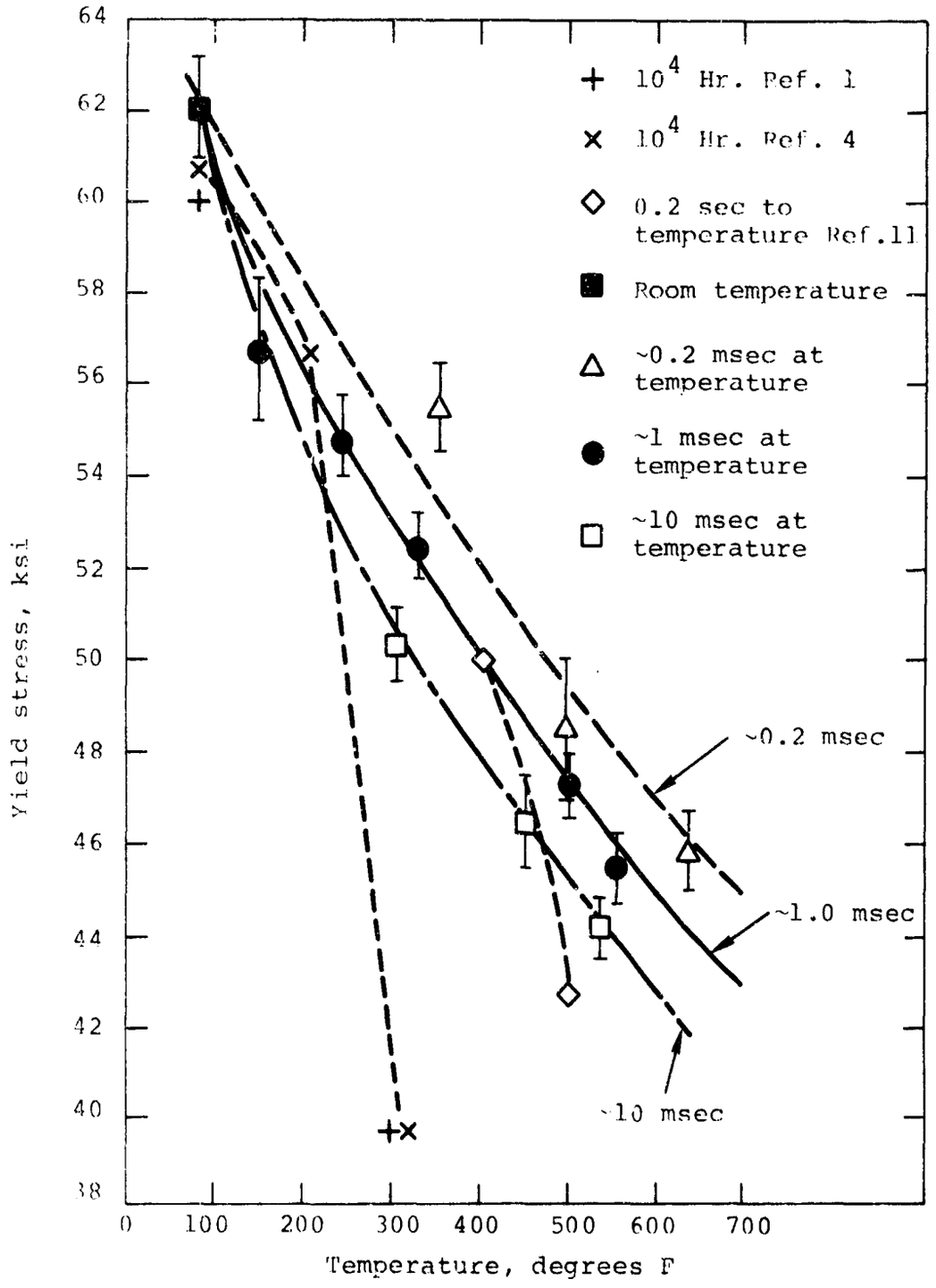

Figure 1.15 Thermal degradation of the yield stress for 2014-T6 aluminum following instantaneous heating.

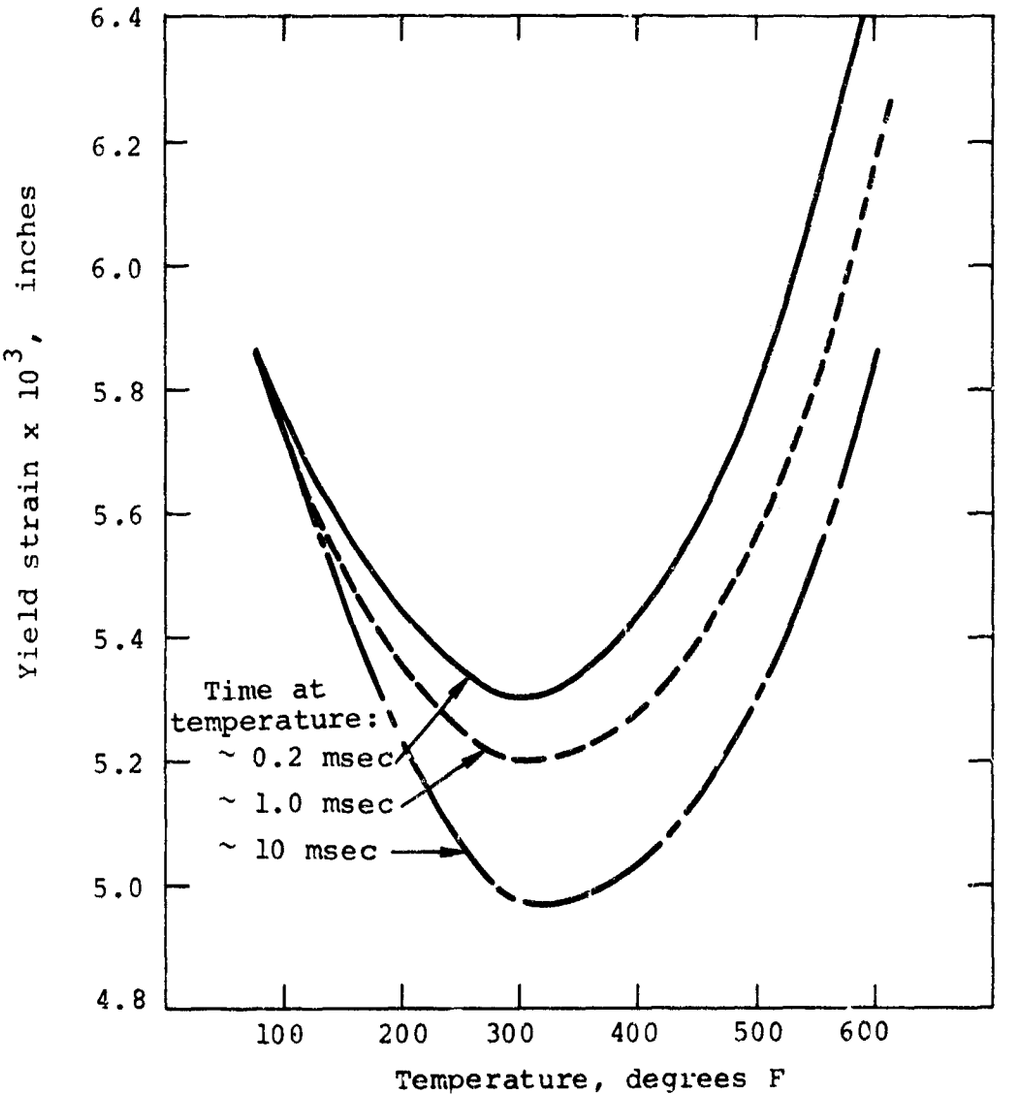

Figure 1.16 Thermal effect on yield strain in 2014-T6 aluminum following instantaneous heating.

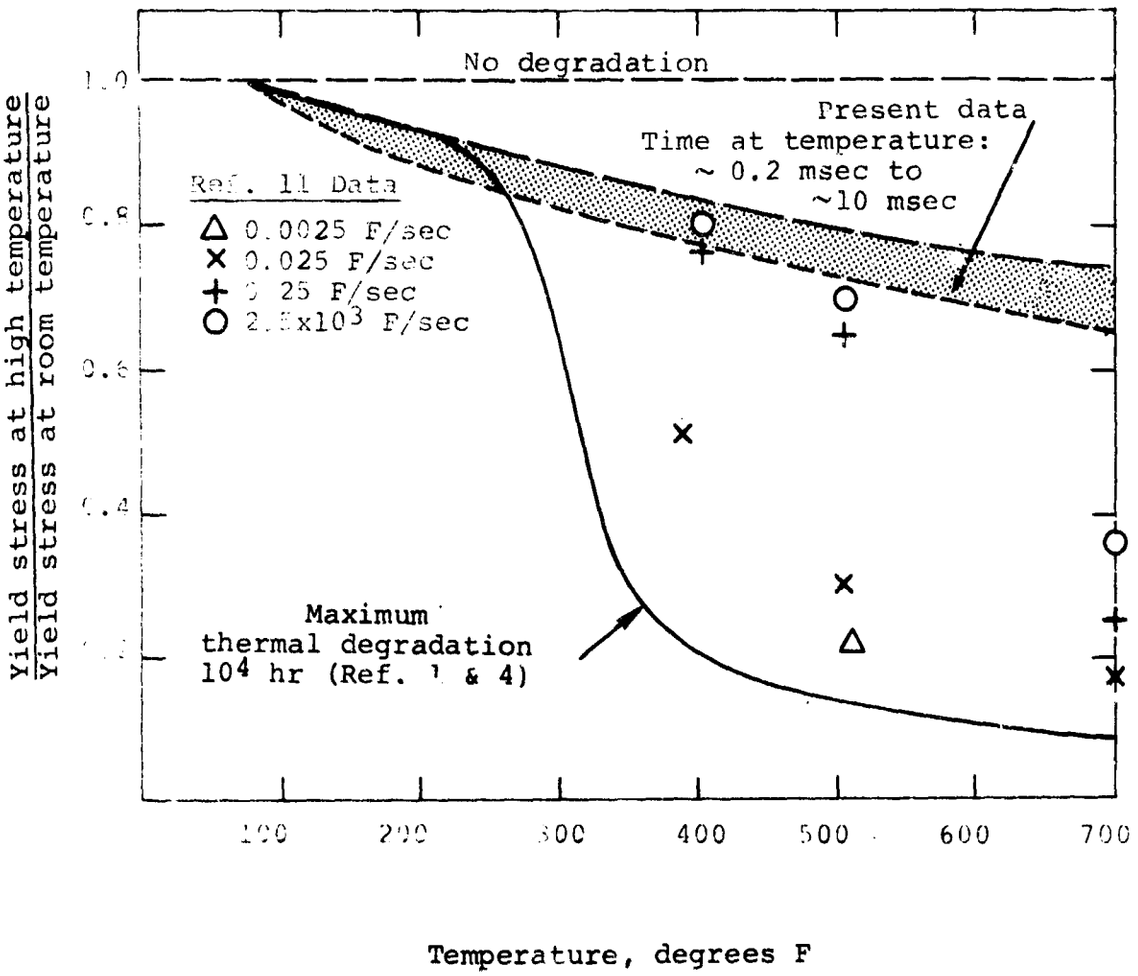

Figure 1.17 Thermal degradation of the yield stress for 2014-T6 aluminum following instantaneous heating.

The conventional rapid (less than 10^4 F/sec) heating rate data of Babcock, et al., (Reference 11) appear to follow the millisecond data band up to a temperature that increases with the heating rate. At higher temperatures, Babcock's data approach the long soak time data.

The measured yield stress values are sensitive to the definition of yield, as is shown in Figure 1.18. (Possible definitions were given in Figure 1.9.) However, the percent degradation is insensitive to the definition used as shown in Figure 1.19.

Since α-titanium is strain-rate sensitive, the effect of strain rate upon the measurement must be considered. In this experiment we observed the amplitude of the stress wave that travels with the elastic velocity. For a constitutive relationship (in uniaxial stress) of the form

$$E_o \frac{\partial \varepsilon}{\partial t} - \frac{\partial \sigma}{\partial t} = g(\sigma, \varepsilon)$$

where E_o is the elastic modulus and g is some function of the stress and strain, Malvern (Reference 12) has shown that for a step-function velocity boundary condition

$$\int_{\sigma^y}^{\sigma} \frac{d\bar{\sigma}}{g(\bar{\sigma}, \frac{\bar{\sigma}}{\rho C_o^2})} = -1/2\ t$$

along $x = C_o t$, where $C_o = \sqrt{E_o/\rho}$ and σ^y is the static yield stress. Assuming the particular form for the function g equivalent to that used by Rubin (Reference 13)

$$g(\sigma, \varepsilon) = \frac{1}{\tau} (\sigma - E_1 \varepsilon)$$

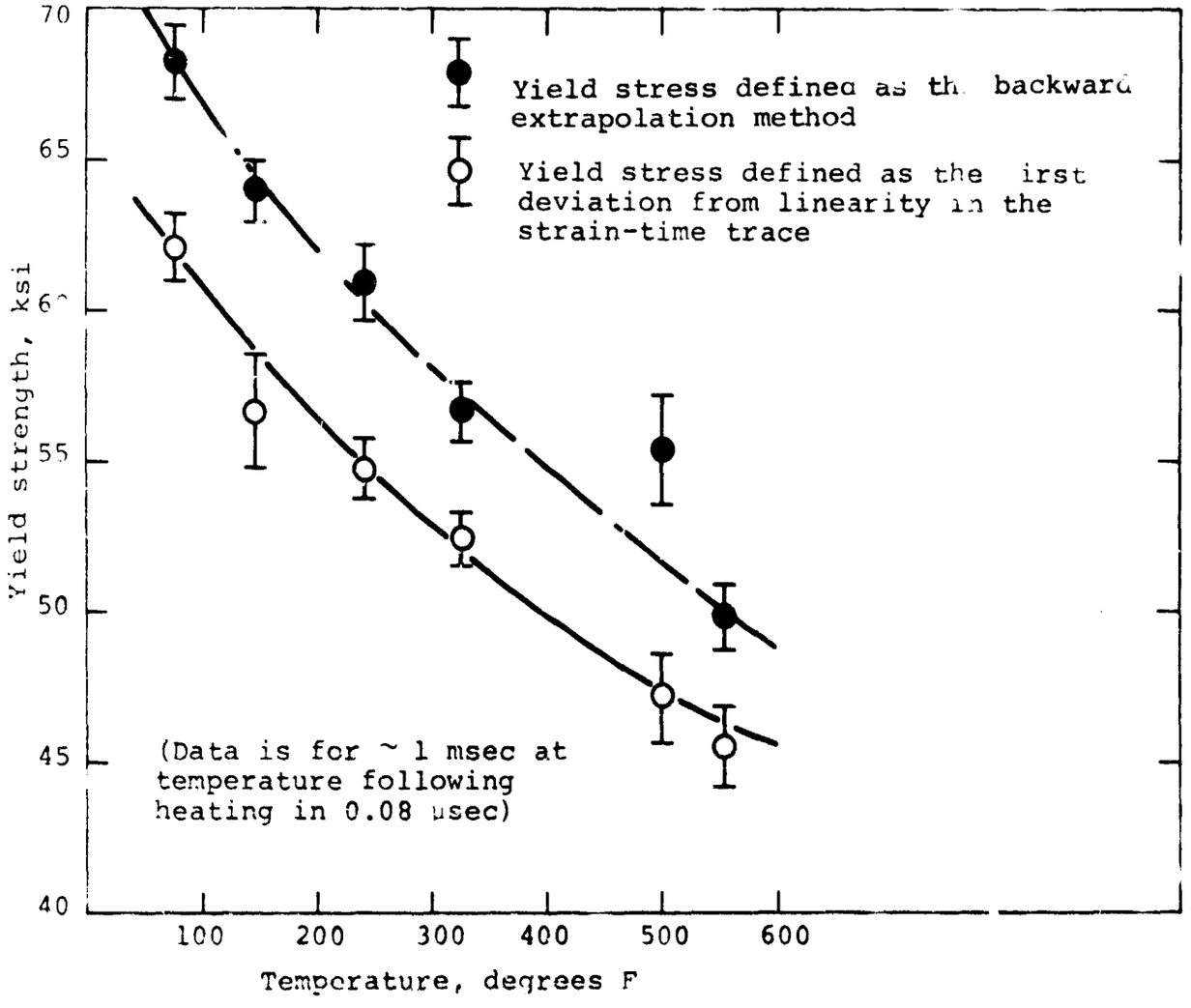

Figure 1.18 Sensitivity of the results to the definition of the yield strength for 2014-T6 aluminum.

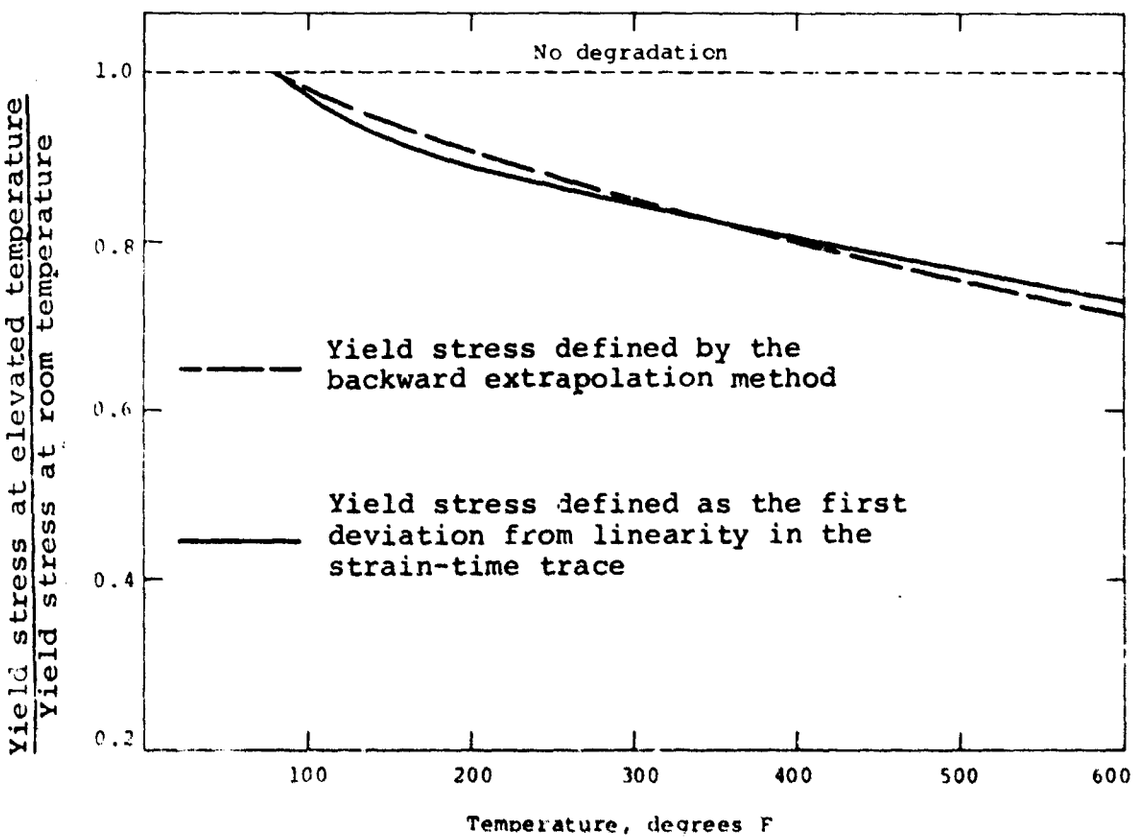

Figure 1.19 Sensitivity of the results to the definition of yield stress for 2014-T6 aluminum.

where E_1 is the slope of the static stress-strain curve in the plastic region, and τ is a characteristic relaxation time, the amplitude of the dynamic overstress, i.e., the difference between the dynamic stress and the static stress for corresponding strains, in the leading portion of the pulse is given by

$$\sigma - \sigma^Y = \sigma^Y_e - (1-\frac{E_1}{E_o})x/2\ C_o\tau$$

Thus the dynamic overstress decays to 1/e of its initial value in a distance

$$X = \frac{2\ C_o\tau}{1-E_1/E_o}$$

An upper bound for the relaxation time can be obtained from split Hopkinson bar data. For the special case of a constant strain rate, the constitutive relation we have assumed can be integrated with the result

$$t = \frac{\sigma - \hat{\sigma}}{\dot{\varepsilon}\ E_c(1-\frac{E_1}{E_o})}$$

where $\hat{\sigma}$ is the static stress.

The split Hopkinson bar data on alpha titanium from Reference 14 shows a 3 kbar dynamic overstress for a strain rate of 600 sec^{-1} at 75 F and a 3 kbar dynamic overstress for a strain rate of 1100 sec^{-1} at 700 F. Consequently, relaxation times of 4.0 and 2.2 μsec are indicated for 75 F and 700 F, respectively.

The distances for the dynamic overstress to decay to 1/e of its initial value in alpha titanium is thus on the order of 4 centimeters at 75 F and 2 centimeters at 700 F. These compare to the 5.7 centimeter distance from the input bar to the strain gauge used to define yield and the 2.5 centimeter long heated gauge length. Moreover, the loading to the specimen is not a step-function as assumed in deriving the relaxation distances; the loading time is several relaxation times. Consequently, the value obtained for the yield stress in these experiments should be the quasistatic value or very nearly so.

The results for α-titanium are listed in Table 1.2. A representative oscillograph of the elevated temperature data is shown in Figure 1.20. Examining the upper gauge record (i.e., the gauge beyond the region that is heated) in Figure 1.11 which was obtained at room temperature, a pronounced ramp after initial yield is observed. Such behavior is indicative that considerable work hardening occurs in the vicinity of the yield, since the arrival time of a given strain level depends upon the slope of the stress-strain curve at that strain. In contrast, there is no ramp after yield for the corresponding gauge record in Figure 1.20 indicating a more abrupt yielding at elevated temperatures. In addition, a slight drop is observed. Such a drop would not be expected from the rate independent model of elastic-plastic wave propagation (Reference 9), and is probably due to residual stress relaxation (strain rate effects).

Degraded property data for this material are shown in Figures 1.21 through 1.24. As is the case of 2014-T6 aluminum, Young's modulus is temperature dependent only and in good agreement with reported long soak time values (Reference 14). Comparisons for the yield stress are shown with longer heating time, low strain rate and high strain rate data from Reference 15.

TABLE 1.2

DATA SUMMARY FOR TENSILE PROPERTIES OF ALPHA TITANIUM FOLLOWING INSTANTANEOUS HEATING

Shot Number	Temp. (F)	Time at Temperature (msec)	Yield Stress (ksi)	Young's Modulus (x 10^6 psi)
7-31-3D	Room	-	92.7	18.01
7-21-4D	Room	-	89.1	17.04
7-22-2D	Room	-	97.5	17.51
7-24-3D	Room	-	94.5	17.21
7-31-5D	Room	-	90.7	17.04
10959	488	1.0	83.2	16.15
10960	545	1.0	77.2	14.93
10958	360	10.0	81.8	16.45
10875	650	10.0	73.8	14.94
10876	652	10.0	74.3	14.88

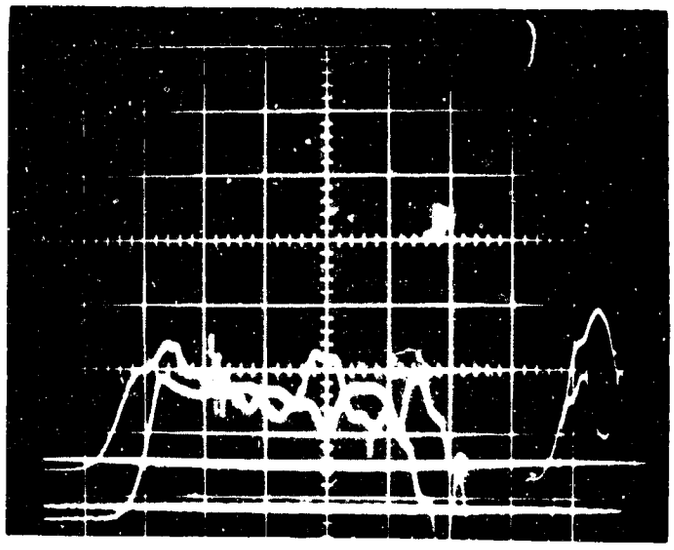

a. Yield strength trace, 20 μsec/cm

Top trace: Lower sample gauge
50 mV/cm
Bottom trace: Upper sample gauge
20 mV/cm

Shot #10876

Temperature: 652 F
Time at temperature:
10 msec
Gauge type: BLH,
FAE-06S-35-S9
Gauge factor: 1.97
Gauge currents:
Upper sample gauge:
15.077 mA
Lower sample gauge:
15.462 mA

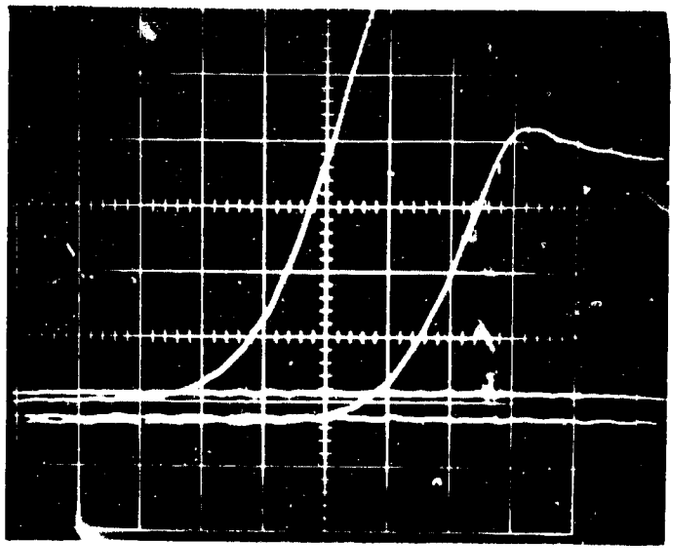

b. Transit time trace, 5 μsec/cm

Top trace: Lower sample gauge
Bottom trace: Upper sample gauge
10 mV/cm

Figure 1.20 Strain gauge traces for an elevated temperature shot on alpha titanium with a 10 msec time at temperature.

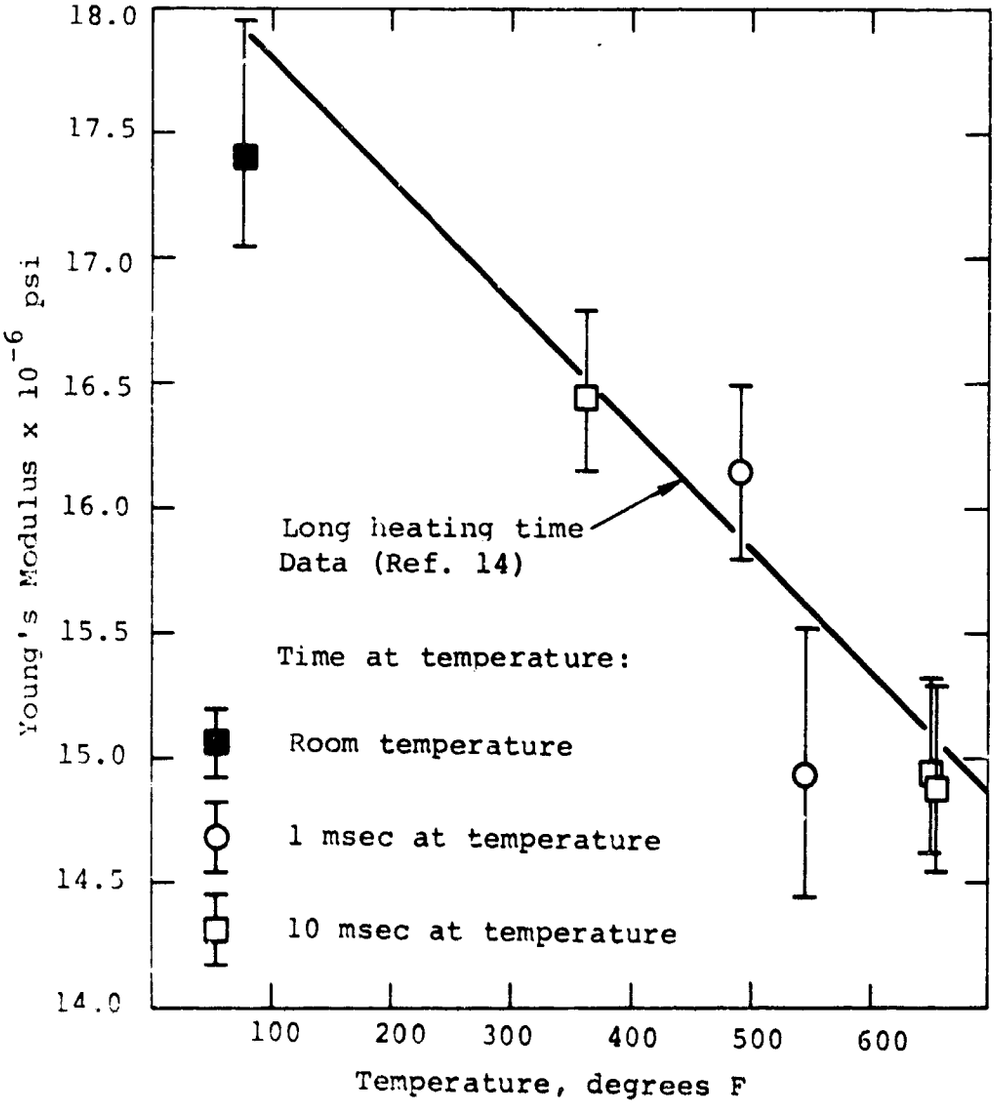

Figure 1.21 Thermal degradation of Young's Modulus for alpha-titanium following instantaneous heating.

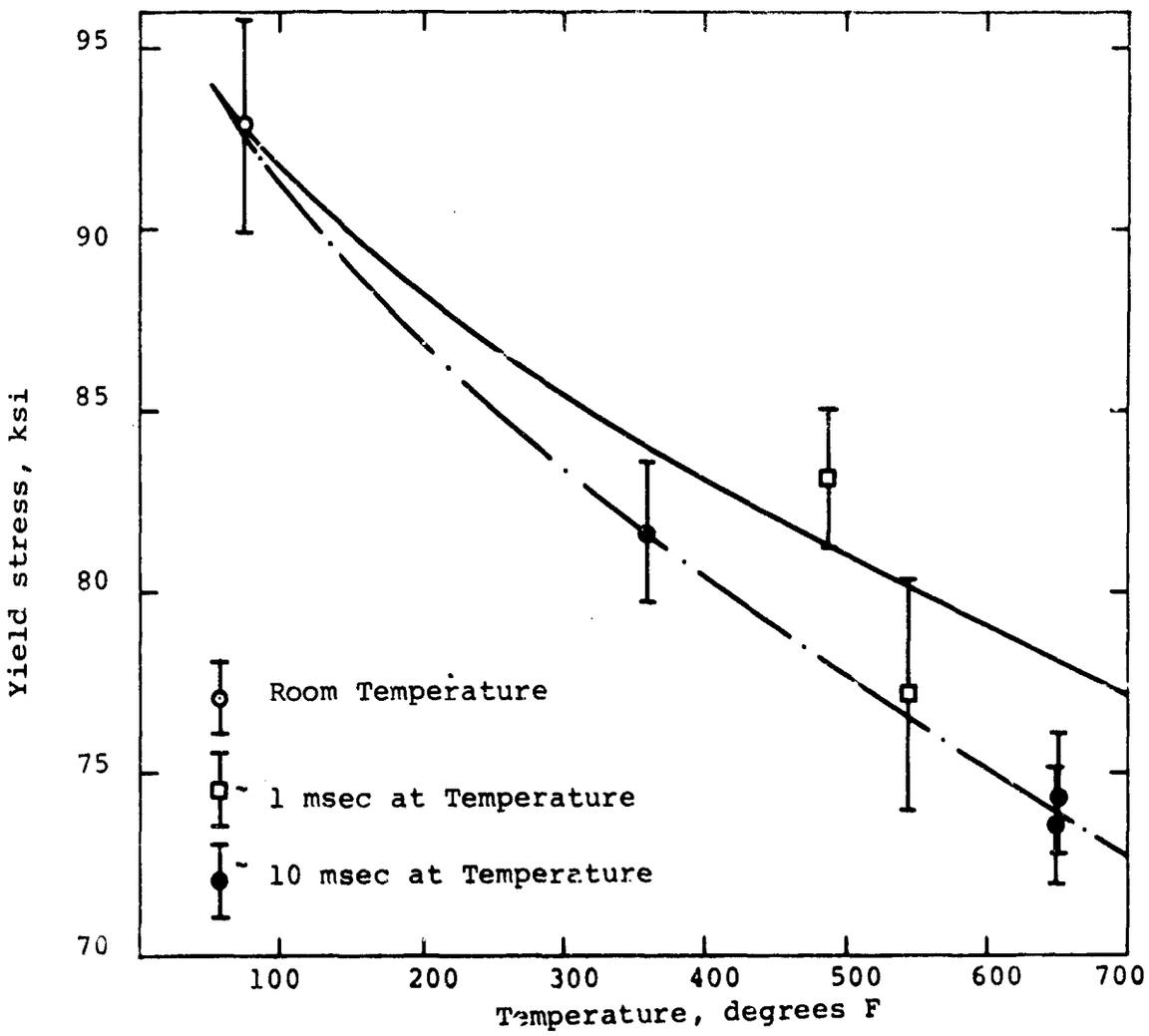

Figure 1.22 Thermal degradation of the yield stress for alpha titanium following instantaneous heating.

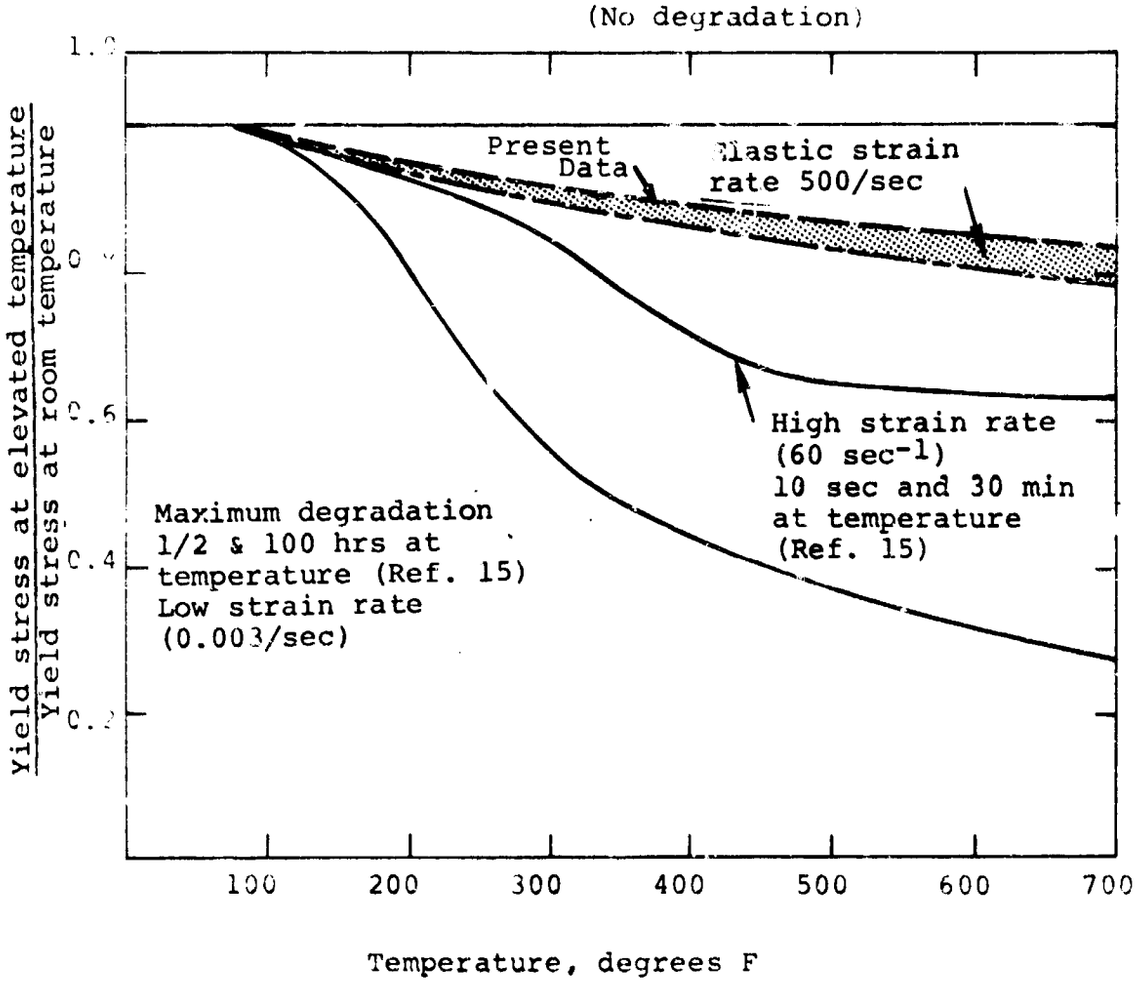

Figure 1.23 Thermal degradation of the yield stress for alpha titanium following instantaneous heating.

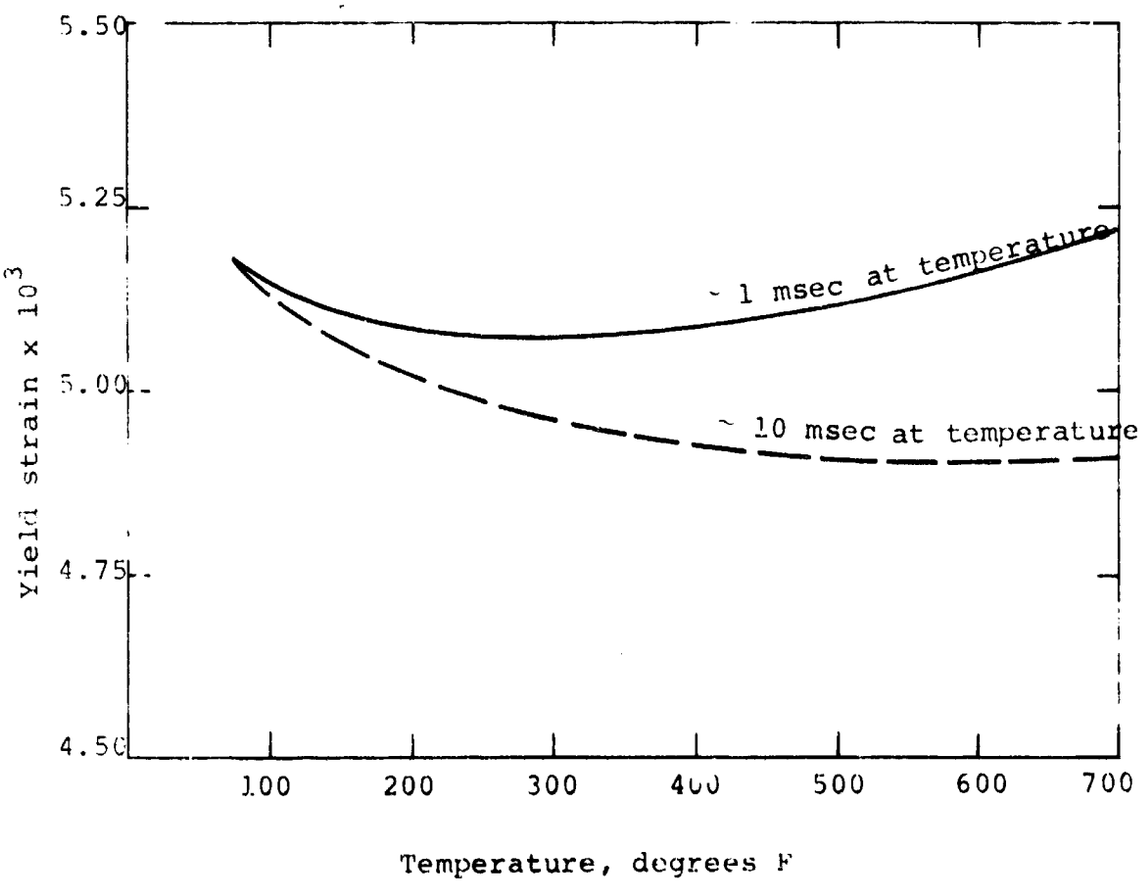

Figure 1.24 Temperature induced changes in the yield strain for alpha titanium following instantaneous heating.

1.5 CONCLUSIONS

A new technique has been developed and demonstrated that can be used to measure the tensile yield stress and elastic modulus of materials at elevated temperatures where the heating times are less than a microsecond, and the time at temperature is as short as 0.1 msec. The technique, which combines a high energy pulsed electron beam, and a Hopkinson bar in a tensile configuration, is independent of the electrical or thermal properties of the material tested.

Data have been obtained on 2014-T6 aluminum and alpha titanium, for temperatures up to 650 F and times at temperature between 0.20 and 10 msec. The data for both materials show a gradual, nearly linear decrease in the yield stress with temperature up to the maximum temperature tested, in contrast with other data obtained on longer time scales.

The results of these measurements show that the time variation of the temperature dependent mechanical properties can be measured on the time scales of interest to structural response. Moreover, the use of long-heating-time data can greatly overestimate the extent of strength degradation, and thus lead to inefficiencies and severe penalties in design.

There is not enough presently known to identify the physical processes associated with the time-dependence of the yield stress at elevated temperatures and short times. However, aluminum alloys in particular, where the strengthening mechanisms are associated with the size and spacing of precipitates, could be investigated by calculating the diffusion controlled size of the precipitates as a function of time, and the stress field interactions between an array of precipitates and a dislocation.

The precipitate particles are compounds of copper, iron, magnesium, silicon, etc., which in general will have different thermal properties from the aluminum matrix. Since a nearly uniform dose is delivered to the sample by the electron beam, differences in specific heat will produce differences in the initial temperatures. For example, the specific heat of $CuAl_2$, which is a compound that may be present, is approximately half that of aluminum (Reference 16). Consequently, when an alloy containing $CuAl_2$ is heated with a pulsed electron beam, a $CuAl_2$ particle will be heated to a temperature twice that of the aluminum matrix. Although the precipitate particles are small and will quickly lose heat by thermal conduction, the large initial temperature gradient may lead to rapid diffusion (or even melting or vaporization) over short distances and possibly to changes in strength.

The mechanisms that influence the time dependence of the yield stress can also be studied experimentally by obtaining data on laboratory controlled alloys, varying the composition, size, and spacing of the precipitates.

SECTION 2

ENERGY-PRESSURE COUPLING IN HOMOGENEOUS MATERIALS

2.1 BACKGROUND AND METHOD OF APPROACH

The thermomechanical response of materials to a pulsed radiation environment is directly dependent upon the energy-pressure-coupling relationship of the material. This relationship is determined by the Gruneisen coefficient, Γ, and may be defined thermodynamically as

$$\Gamma = V\left(\frac{\partial P}{\partial E}\right)_V \qquad (1)$$

where P is the pressure, V is the specific volume, and E is the specific internal energy. The Gruneisen coefficient thus defined appears in the Gruneisen equation of state (Reference 17), which forms the basis for most finite-difference material response codes currently in use throughout the community (Reference 18). This equation, which can be written in the form:

$$P = f(V) + \frac{\Gamma E}{V} \qquad (2)$$

is strictly applicable only to homogeneous media, and its extension to heterogeneous materials must be undertaken with caution. Generalizations of the equation have been developed for porous materials by Herrmann (References 19 and 20) and Seaman and Linde (Reference 21). Additional compications arise for composites and mixtures subjected to a pulsed radiation environment since thermodynamic equilibrium may not be achieved during the times of interest for the material response.

In the case of heterogeneous materials, depending upon the model adopted, the Gruneisen coefficient may be considered either on a microscopic scale, where the constituent materials are homogeneous (References 20 and 21), or on a microscopic scale (Reference 21), in which case all quantities in Equation 1 are averaged over dimensions that are large compared to the inhomogeneities.

The value of the Gruneisen coefficient for homogeneous materials can be computed from thermodynamic quantities (Reference 17) as

$$\Gamma = \frac{\beta k}{\rho c_p} \qquad (3)$$

where β is the volume-expansion coefficient, k is the adiabatic bulk modulus, ρ is the density and c_p is the specific heat at constant pressure. The Gruneisen coefficient is a function of volume (Reference 17) and is probably also a function of temperature (Reference 22); the significance of this variation is somewhat uncertain, particularly since it is difficult to measure the parameters in Equation 3) as a function of temperature without also varying the volume.

For heterogeneous materials, the Gruneisen coefficient defined in the macroscopic sense is often referred to as the "effective" Gruneisen coefficient. It is likely to be strongly energy dependent (Reference 23), energy-rate dependent (Reference 24), or both.

This report describes measurements that provide a determination of the macroscopic Gruneisen coefficient, which for homogeneous materials is equivalent to the microscopic value. The technique is also applicable directly to heterogeneous materials.

for computational models using macroscopic descriptions, and indirectly for models using the microscopic description, provided the measurements are made on macroscopic samples of the individual constituents.

If the pressure in a substance is determined as a function of energy at constant volume, the value of the Gruneisen coefficient can be obtained from Equation 1. Sudden volume heating can readily be achieved using high-intensity pulsed electron beams and the problem is then reduced t measuring the resulting pressure. One technique that can be used to obtain the pressure is to use a sample (slab geometry) thick enough to absorb all the incident electrons. A compressive stress wave propagates from the heated, high-pressure region toward the rear surface of the sample. A pressure transducer, such as a quartz or manganin gauge, located just beyond the deposition depth, can be used to record the stress pulse.

Material response calculations can be used to deduce the initial pressure distribution, by assuming a value for the Gruneisen coefficient and iterating until the computed stress history agrees with the experimental data (References 25 to 30). This requires a knowledge of the equation of state (the relationship between pressure, volume, and energy) and the constitutive relationship (the relationship between the stress and strain deviators). In practice, however, this is not generally a serious limitation, even if hugoniot or other data are not available. The transducer is located just beyond the deposition region, so the stress pulse travels only a short distance; consequently, the stress-time profile at the gauge is not seriously perturbed by slight variations in the sound speed with pressure (due to curvature of the hugoniot), elastic-plastic, or other dispersive effects. In addition, the arrival time of the stress pulse can be used to determine the sound velocity for a given experiment

since the sample geometry, energy deposition profile and the energy deposition time are known. The Bremsstrahlung radiation during energy deposition produces a signal in the transducer cables that provides a convenient fiducial mark for the energy deposition time.

In the event that substantial changes do occur in the stress pulse during its transit to the transducer, comparison of the measured stress history with that computed from the assumed equation of state and constitutive relationship will reveal any serious inconsistencies.

The materials investigated in this study were 2014-T6 aluminum and alpha titanium. The equation of state for alpha titanium has been investigated under the PREDIX program (Reference 14), and so is well known. Considerable data are available on the properties of 2014-T6 aluminum and aluminum alloys similar in composition, such as 2024 aluminum (References 11, 14, and 31). Consequently, 2014-T6 aluminum and alpha titanium are appropriate materials to evaluate the suitability of the technique employed here for measurement of the Gruneisen coefficient.

2.2 EXPERIMENTAL CONFIGURATION AND PROCEDURE

In the present experiments, pressures were generated by the sudden deposition of electron energy in the target material. Quartz transducers, (Reference 32), located just beyond the region of energy deposition, were used to record the resulting stress pulse.

Electron beam energies were chosen such that the heated region was acoustically thick, i.e., pressure relief during deposition was confined to a small region near the front surface. The duration of the stress pulse increases with the maximum range of the electrons. Consequently, the energy of the electrons must be limited such that the duration of the stress pulse does not exceed the reading time of the transducer used; Valpey Corporation type QH JA-3 gauges were used, which have a nominal 0.5 μsec record time. Based upon these considerations, nominal beam energies of 0.6 MeV and 1.1 MeV were selected for use in the experiments. Two electron spectra were chosen to investigate the sensitivity of the results to the shape of the deposition profile.

The time dependent energy deposition must be known to input to the material response calculation. This can be computed from a knowledge of the beam energy spectrum and the incident fluence (i.e., time-integrated energy flux) using Monte Carlo electron transport techniques (Reference 8). In addition, when high current beams are used the plasma properties of the beam must be considered.

Intense electron beams are characterized by the parameter ν/γ here

$$\nu = \frac{I(\text{amps})}{17{,}000\ \beta}$$

$$\gamma = (1-\beta^2)^{-1/2}$$

and

β = electron velocity/velocity of light.

In cases where v/γ is not small compared to unity, transverse energy components exist in the beam. This implies that on the average, the electrons are incident upon the target at an angle. This produces differences in the deposition profile from that obtained for electrons incident normal to the target. The mean angle of incidence can be computed from the relationship (Reference 33)

$$\langle\theta\rangle = \tan^{-1}\left[\frac{2}{\sqrt{\frac{\alpha(\alpha+2)(1.16\times10^{9})I_{pr}^{2}}{I_{net}^{4}}+1}-1}\right]^{1/2}$$

where α is the ratio of the mean kinetic energy of the beam electrons, $\langle E\rangle$, to the rest mass of the electron, 511 keV, I_{pr} is the primary beam current in amps and I_{net} is the sum of the primary current and the plasma current in amps. Thus, measurements of the primary current, net current and mean electron energy determine the mean angle of incidence.

The parameters necessary to determine the mean angle are measureable, and favorable correlations have been made between the current transmitted through various thickness foils,* and the computed values based upon the electron energy spectra and angles of incidence obtained from the accelerator diagnostics (Reference 33).

The experimental configuration employed in this study was not directly compatible with the measurements necessary to obtain

*The relative current transmitted through the foils determines the number of electrons deposited in the slab and is equivalent to a test of the validity of the energy deposition computation.

the mean angle of incidence from active diagnostics. Consequently, the energy deposition profiles, normalized to unit fluence, were obtained as follows. First, the deposition profile was measured in aluminum using a depth dosimeter (see Section 1.2 above). A series of Monte Carlo electron transport calculations were performed for aluminum with the PIE-1D code, using the electron energy spectrum based upon the accelerator voltage and several different values for the mean angle of incidence. The angle that produced best agreement between the computed and measured profiles was then assumed for subsequent calculations.

The optimum values obtained for the mean angles of incidence were 45 degrees for Model 738 Pulserad operating at 1.1 MeV and 37 degrees for the Model 312 Pulserad, operating at 0.6 MeV. Comparisons of the computed and measured deposition profiles are shown in Figures 2.1 and 2.2. These angles are consistent with postulated values of the beam conditions and the results of previous measurements (References 7, 29, and 33).

The time dependence of the deposition profile is known from the accelerator voltage monitor record.

In order to determine the fluence incident on the sample, total absorbing graphite calorimeters were placed surrounding the sample. In addition, thin bare thermocouples were placed around the perimeter of the samples. This setup is shown schematically in Figure 2.3. Preliminary experiments were performed to calibrate the output of the bare thermocouples in terms of the incident fluence. This was accomplished in a series of experiments in which the bare thermocouples were placed immediately in front of an array of graphite calorimeter blocks. A calibration curve from a number of shots is shown in Figure 2.4.

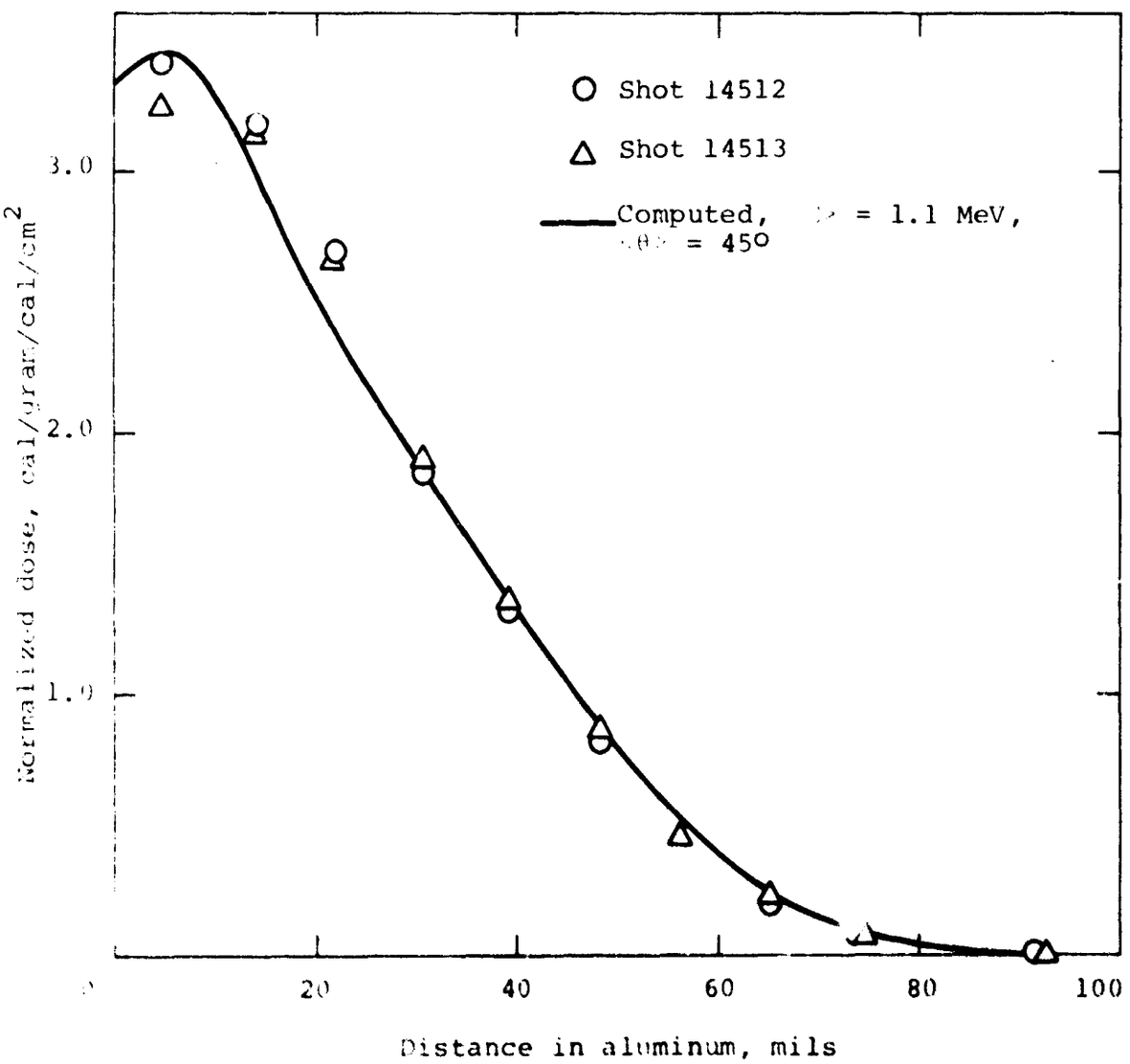

Figure 2.1 Comparison of calculated and measured energy deposition profiles--Model 738 Pulserad.

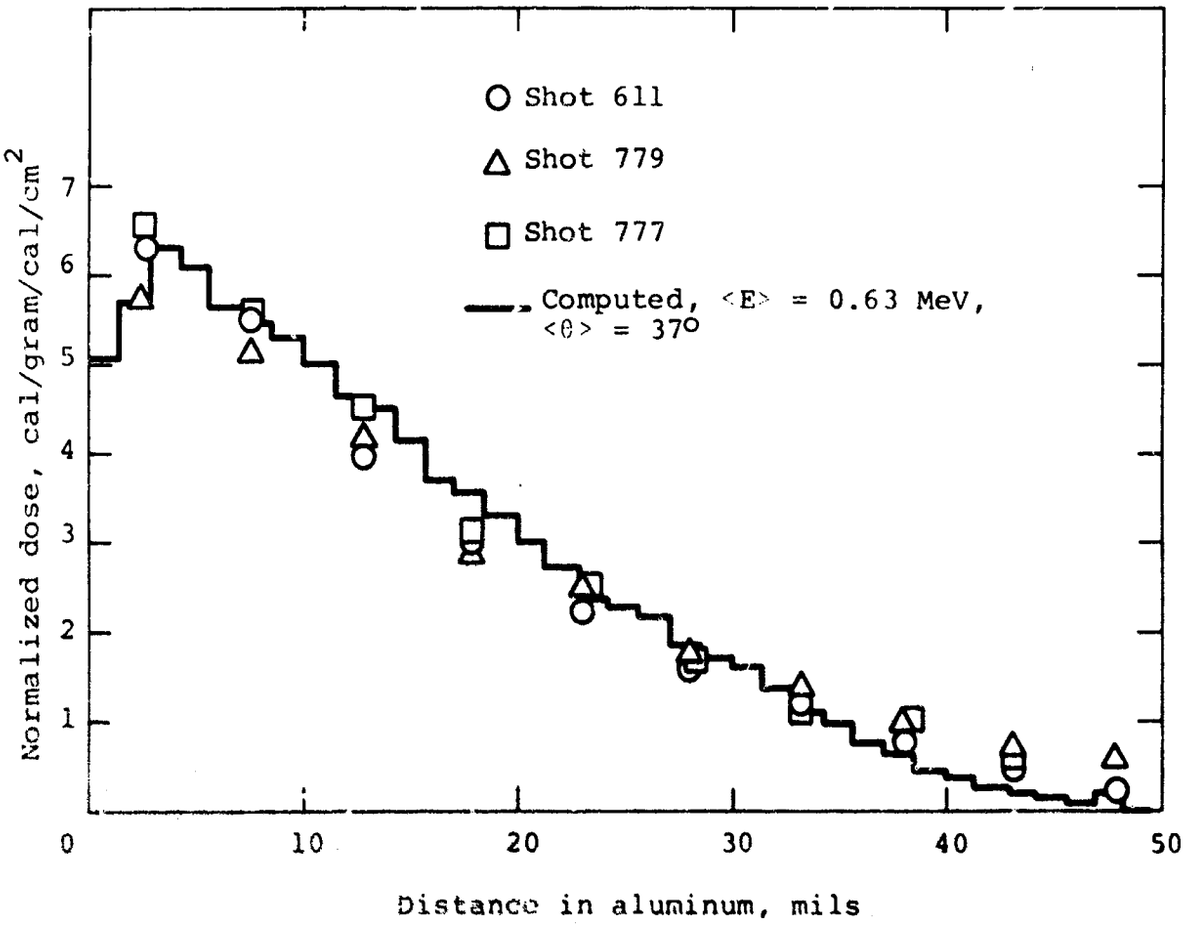

Figure 2.2 Comparison of calculated and measured energy deposition profiles--Model 312 Pulserad.

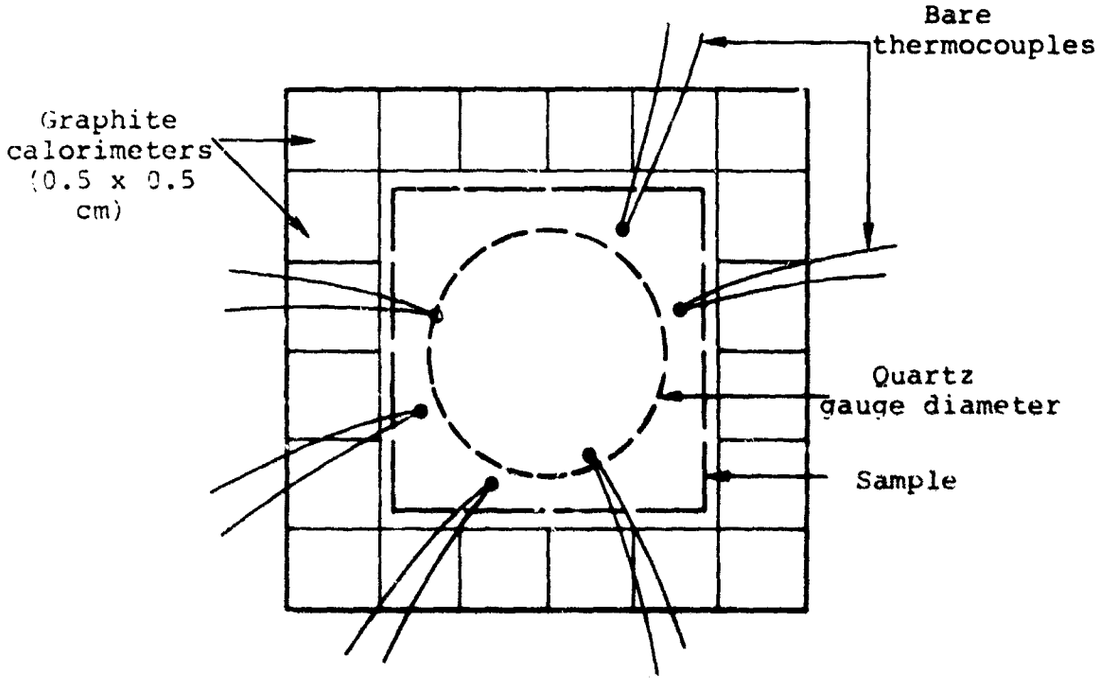

Figure 2.3 Sample configuration.

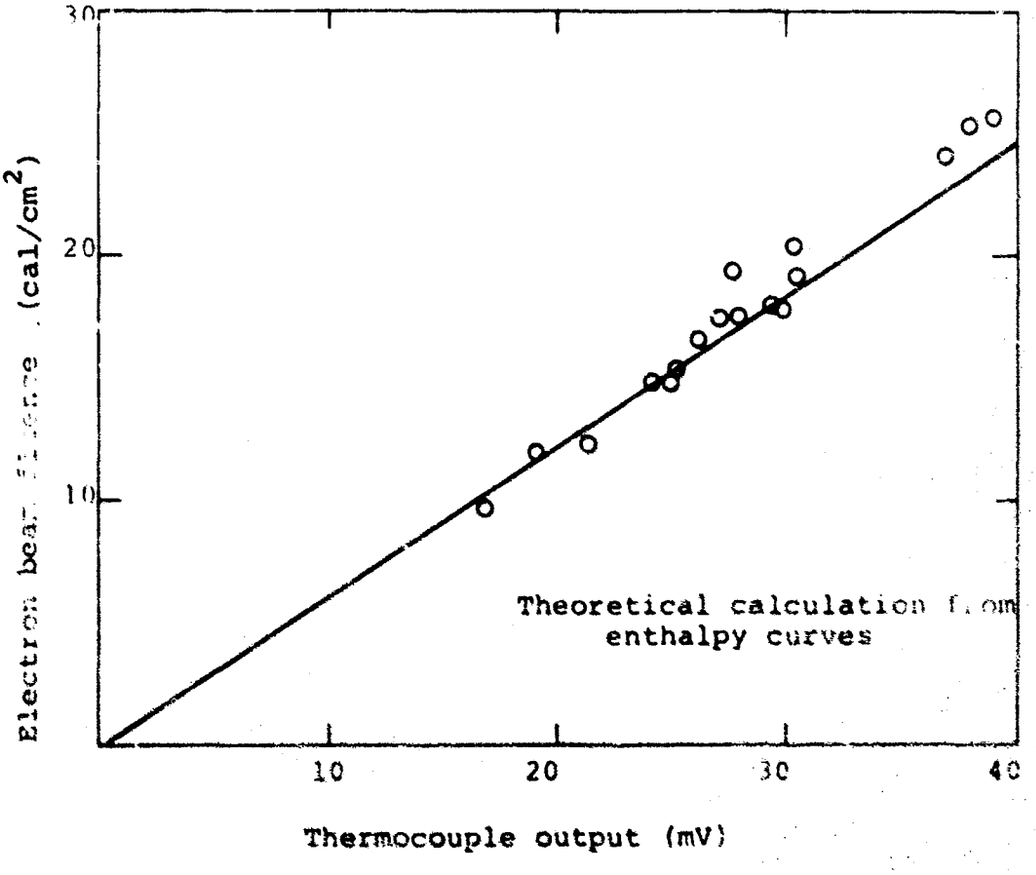

Figure 2.4 Bare thermocouple calibration curve for 1.1 MeV pulsed electron beam.

Some variation in the calibration curves will occur when the thermocouples are placed in front of target materials different from the graphite, due to differences in electron backscatter. Based upon Monte Carlo electron transport calculations, a three-percent correction was applied to the curves for the aluminum targets and a seven-percent correction was used when titanium targets were irradiated. It was possible to use the bare thermocouples up to doses of about 100 cal/gram, at which level they started to spall and/or melt.

On a given sample experiment the fluence over the sample area was obtained by interpolating the data from surrounding calorimeter blocks and the output readings of the bare thermocouples. Thus, it was possible to detect any significant variation in fluence over the sample region of interest. The fluences determined by the two methods were generally in good agreement.

The following procedure was used to deduce the Gruneisen coefficient. For each experiment the appropriate time dependent energy deposition, based on the measured fluence and the electron transport calculations, and sample geometry were input to Physics International's 1D Lagrangian material response code, "POD." The equations of state assumed are shown in Table 2.1. The computed stress history in the quartz at the specimen-quartz interface was compared to the measured quartz transducer record. Since the variation of the computed peak pressure is very nearly linear with the value assumed for the Gruneisen coefficient, the optimum value for the Gruneisen coefficient to fit a given experimental record could be obtained by simple scaling of the value assumed in the initial computation by the ratio of the peak measured to calculated stress.

TABLE 2.1 EQUATION-OF-STATE PARAMETERS USED IN THE MATERIAL RESPONSE CALCULATIONS (REFERENCE 18)

Material	Gruneisen Coefficient	Density (g/cm^3)	Shear Modulus (mbar)	Yield Stress (mbar)	$P = C_\mu + D_\mu^2 + S_\mu^3 + \Gamma(1+\mu)E$
2014-T6 aluminum	2.13	2.79	0.293	0.00414	C = 0.765 mbar D = 0.844 S = 1.34
Alpha titanium	1.18	4.5	0.474	0.0064	C = 1.05 D = S = 0
Quartz	1.17	2.65	0.376	0.02	C = 0.374 D = S = 0

2.3 RESULTS AND DISCUSSION

Representative quartz transducer records obtained for an aluminum sample and a titanium sample are shown in Figures 2.5 and 2.6. The first signal is a short pulse due to electron Bremsstrahlung radiation incident upon the cables for the transducer. This provides a precise fiducial point for the energy deposition. The compressive stress pulse arrives shortly thereafter and is completely recorded well within the 0.5 μsec reading time of the transducer. The time-dependent deposition profiles for these shots are shown in Figures 2.7 and 2.8, respectively.

Comparisons of the measured and computed stress profiles are shown in Figures 2.9 and 2.10. Reasonable agreement is obtained in the arrival and shape of the calculated and measured pulses.

The complete set of oscillogram records along with the associated energy deposition profiles and computer calculations are presented in Appendix A for the 2014-T6 aluminum and Appendix B for alpha titanium.

The results for 2014-T6 aluminum are summarized in Table 2.2 and Figure 2.11, while those for titanium are presented in Table 2.3 and Figure 2.12. The uncertainty associated with each datum point for the aluminum is estimated to be ± 15 percent, based upon the accuracy of the interpolation for the fluence incident upon the sample and to a lesser extent the observed shot-to-shot variations in the deposition profile.

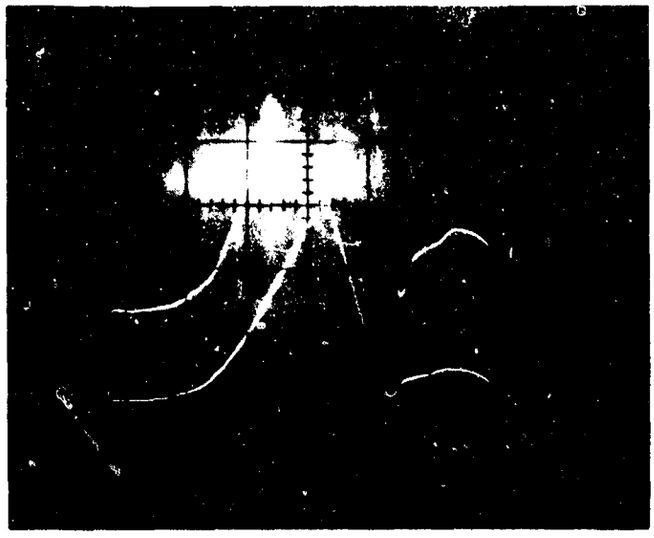

Shot 14523

Sensitivity sweep:

Upper trace: 2 V/cm
Lower trace: 5 V/cm

Time: 0.1 μsec/cm

Figure 2.5 Pressure response of a quartz gauge to deposition of electron energy in 2014-T6 aluminum--shot 14523.

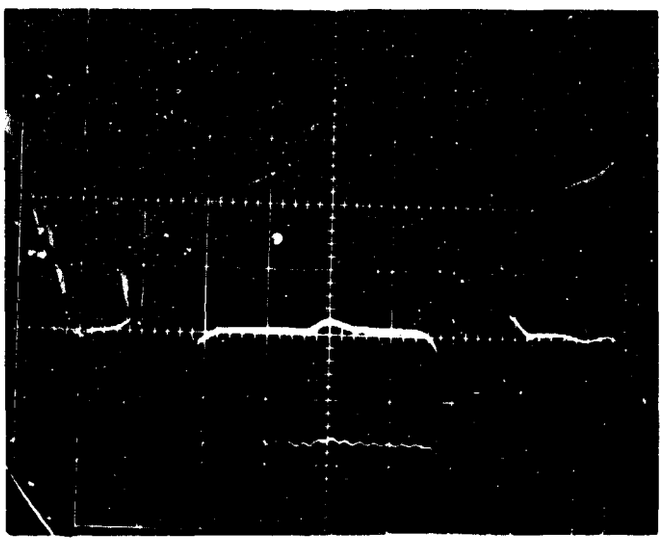

Shot 616

Sensitivity sweep:

Upper trace: 2 V/cm
Lower trace: 5 V/cm

Time: 0.1 μsec/cm

Figure 2.6 Pressure response of a quartz gauge to deposition of electron energy in α-titanium--shot 616.

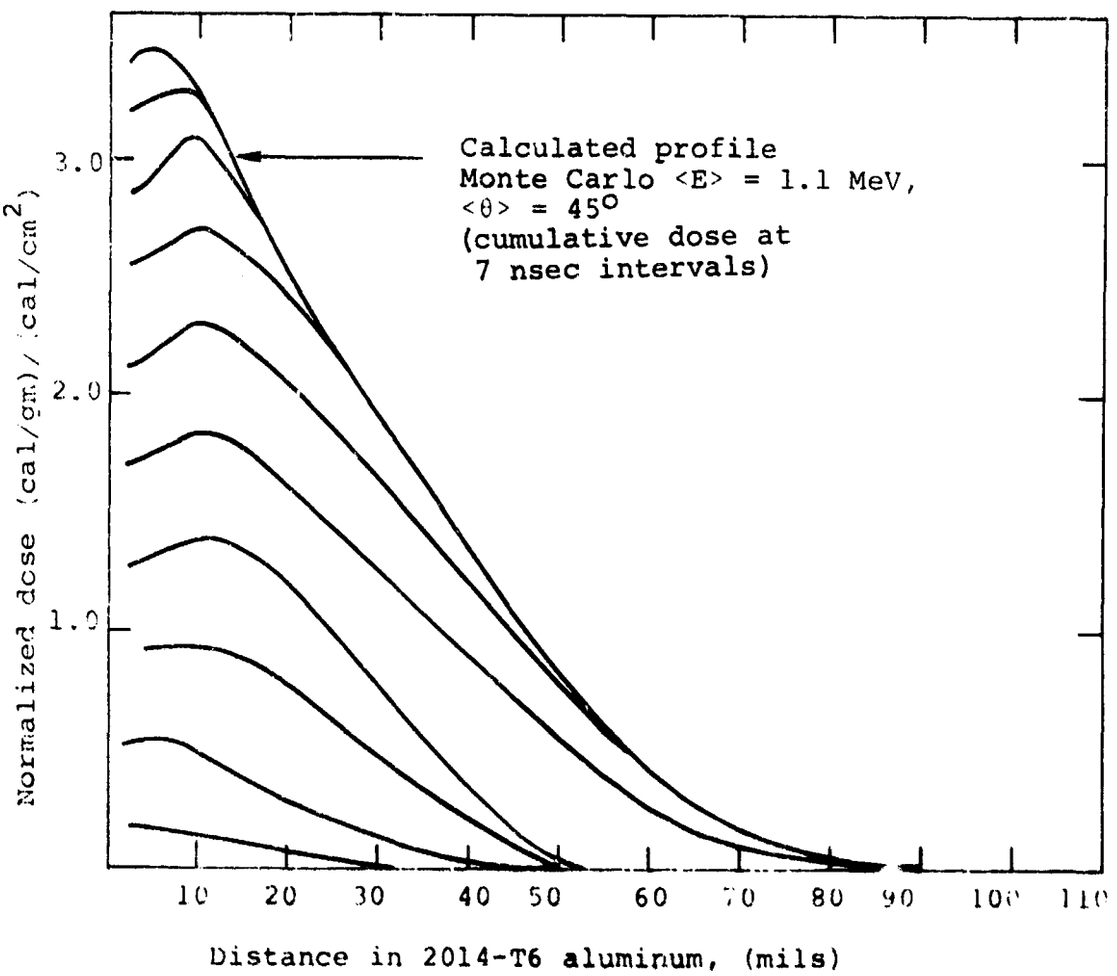

Figure 2.7 Calculated electron deposition profile for shots 14531, 14523 and 14529 in 2014-T6 aluminum.

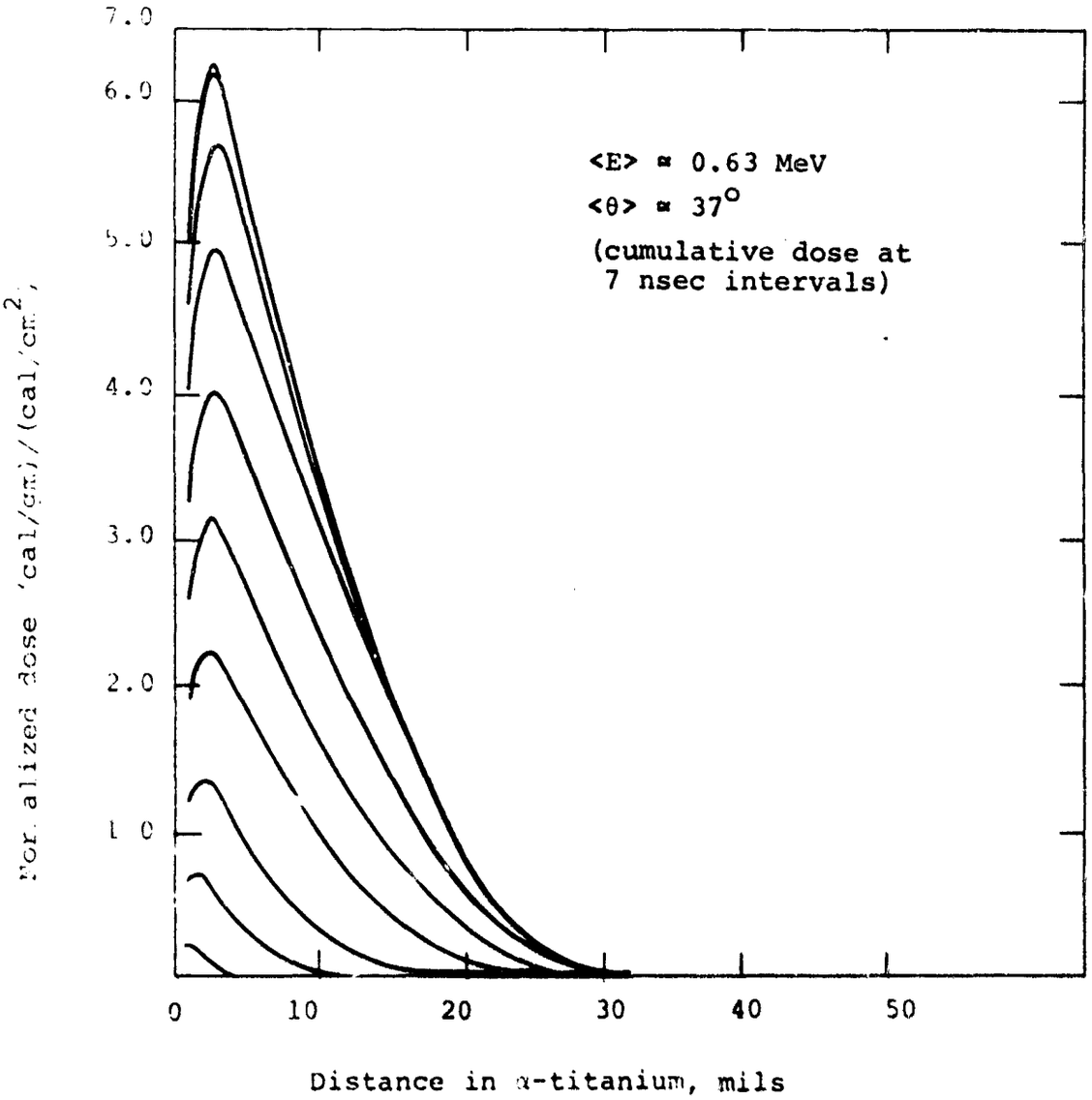

Figure 2.8 Calculated electron deposition profile for alpha titanium shots at 0.63 MeV mean electron energy.

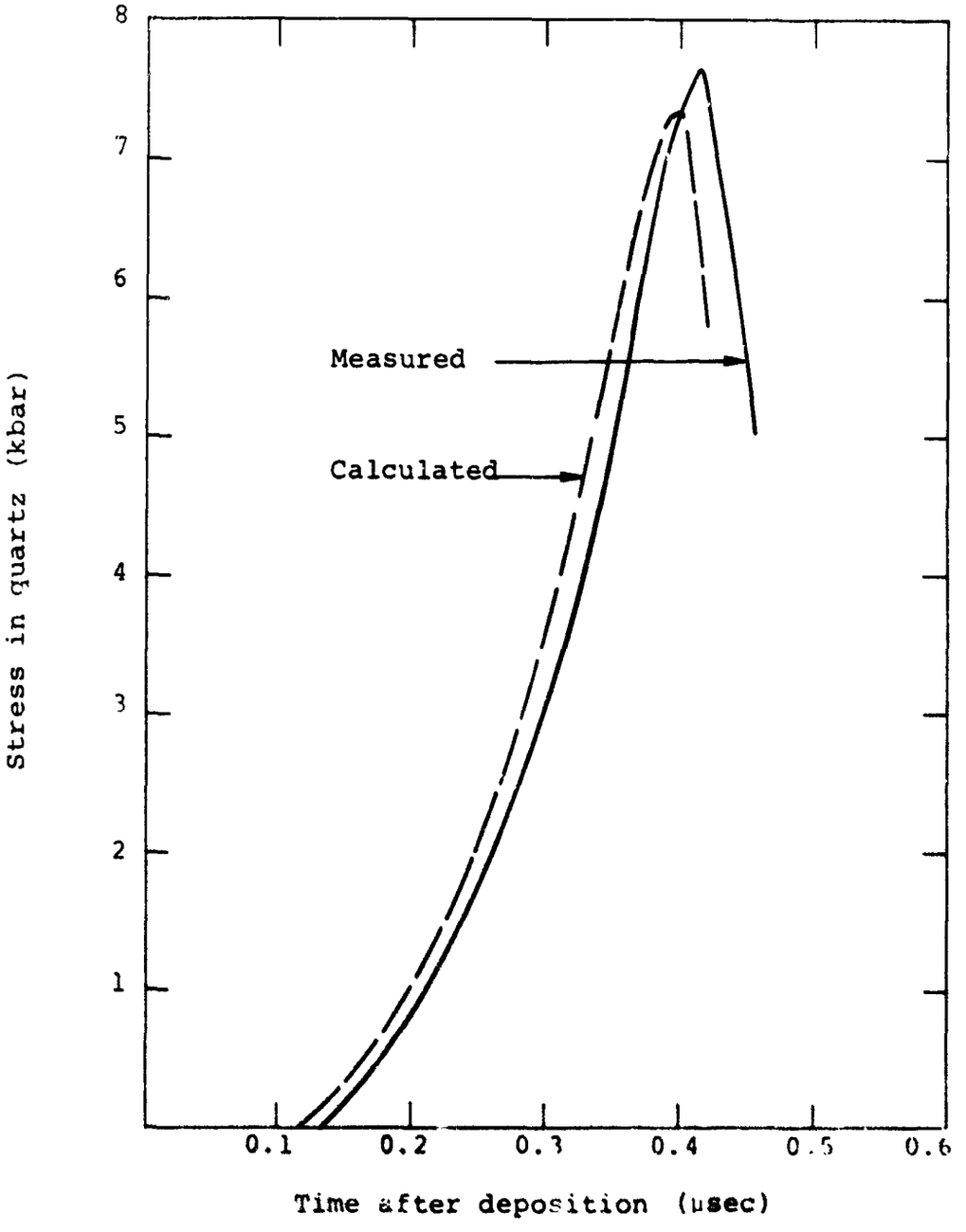

Figure 2.9 Comparison between measured and calculated stress profiles as shown by a quartz gauge, shot 14523, 2014-T6 aluminum.

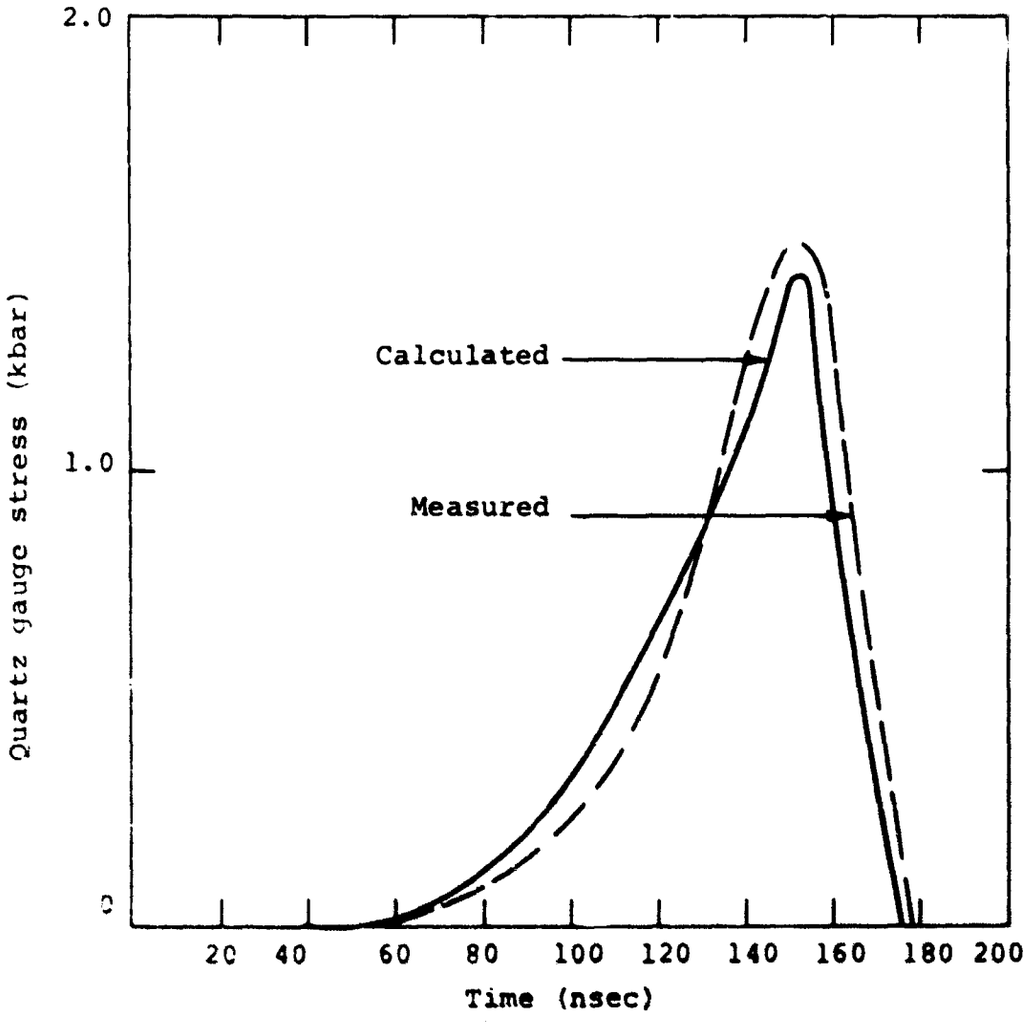

Figure 2.10 Comparison between measured and calculated stress profiles as shown by a quartz gauge, shot 616, α-titanium.

TABLE 2.2

2014-T6 ALUMINUM GRUNEISEN RESULTS

Shot No.	Mean Energy $\langle E \rangle$ (MeV)	Average Fluence (cal/cm^2)	Dose at Relief Depth (cal/gram)	Peak Stress in Quartz Measured (kbar)	Peak Stress in Quartz Calculated* (kbar)	Gruneisen Γ
14531	1.1	21.6	67	7.60	7.30	2.22
14523	1.1	21.6	67	7.60	7.30	2.22
14529	1.1	54.0	164	20.0	17.0	2.52
790	0.93	18.0	74	8.35	8.3	2.14
614	0.63	4.7	28	3.50	3.56	2.10
610	0.63	3.4	20	2.56	2.56	2.13
14522	0.91	18.4	64	6.7	7.0	2.04

$\Gamma = 2.20$

*Stress calculated assuming $\Gamma = 2.13$

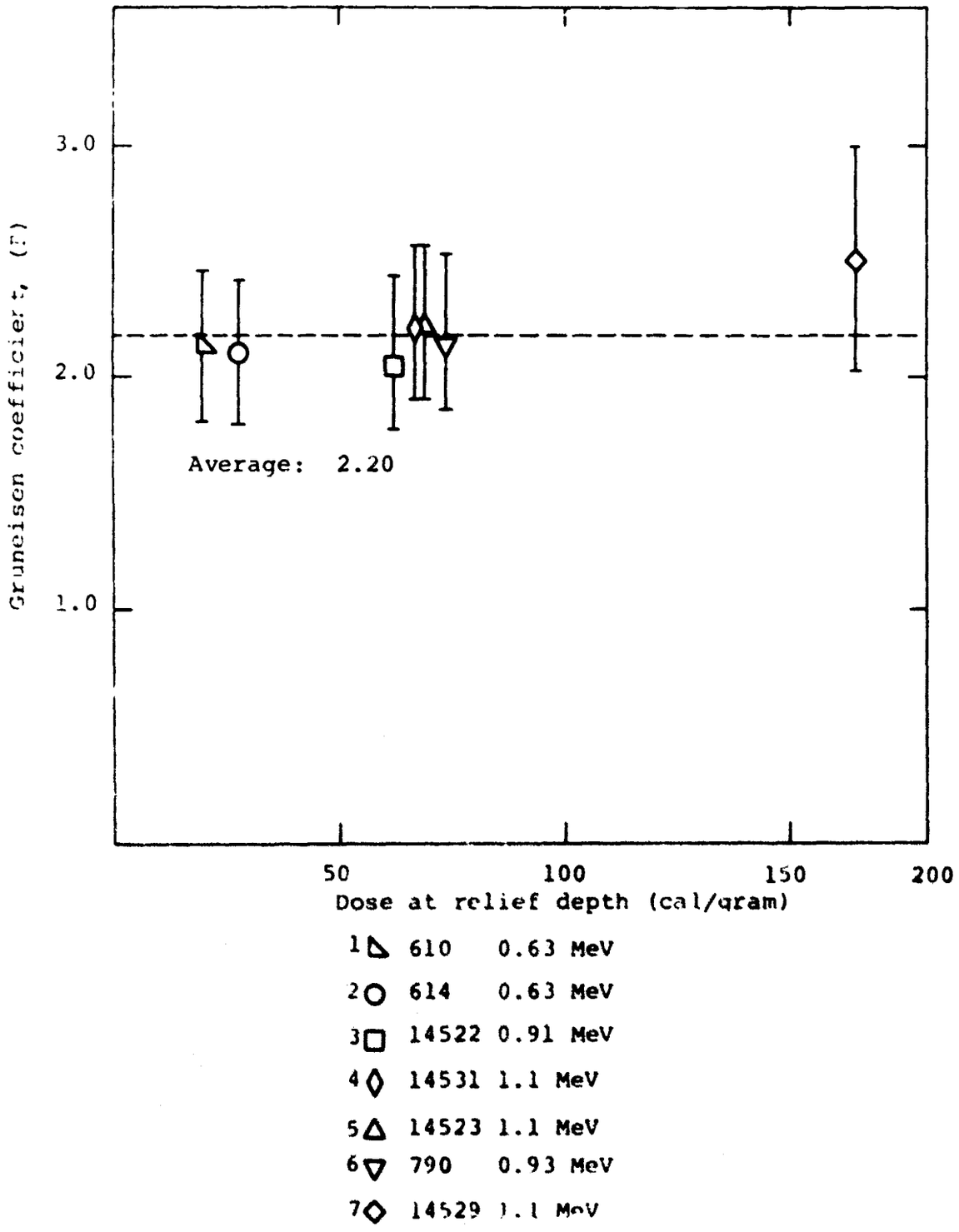

Figure 2.11 Energy dependency of the Grueneisen coefficient in 2014-T6 aluminum.

TABLE 2.3

GRUNEISEN RESULTS FOR ALPHA TITANIUM

Shot No.	Average Energy (⟨E⟩ MeV)	Average Fluence (cal/cm²)	Dose at Relief Depth	Peak Stress in Quartz Measured kbar	Peak Stress in Quartz Calculated* kbar	Γ
15018	0.9	14	36 cal/gram	3.86	3.52	1.28
15028	0.9	5.6	14	1.25	1.39	1.06
15030	1.1	15	38	3.59	3.20	1.32
15088	0.6	38	88	10.5	9.2	1.34
15089	0.6	38	88	9.5	9.2	1.22
618	0.6	4.8	21	1.90	2.03	1.11
616	0.6	3.3	14	1.49	1.43	1.23
787	0.6	19.5	81	8.0	8.1	1.17
788	0.7	9.3	36	3.42	3.66	1.10

*Stress calculated assuming Γ = 1.18

$\bar{\Gamma}$ = 1.20

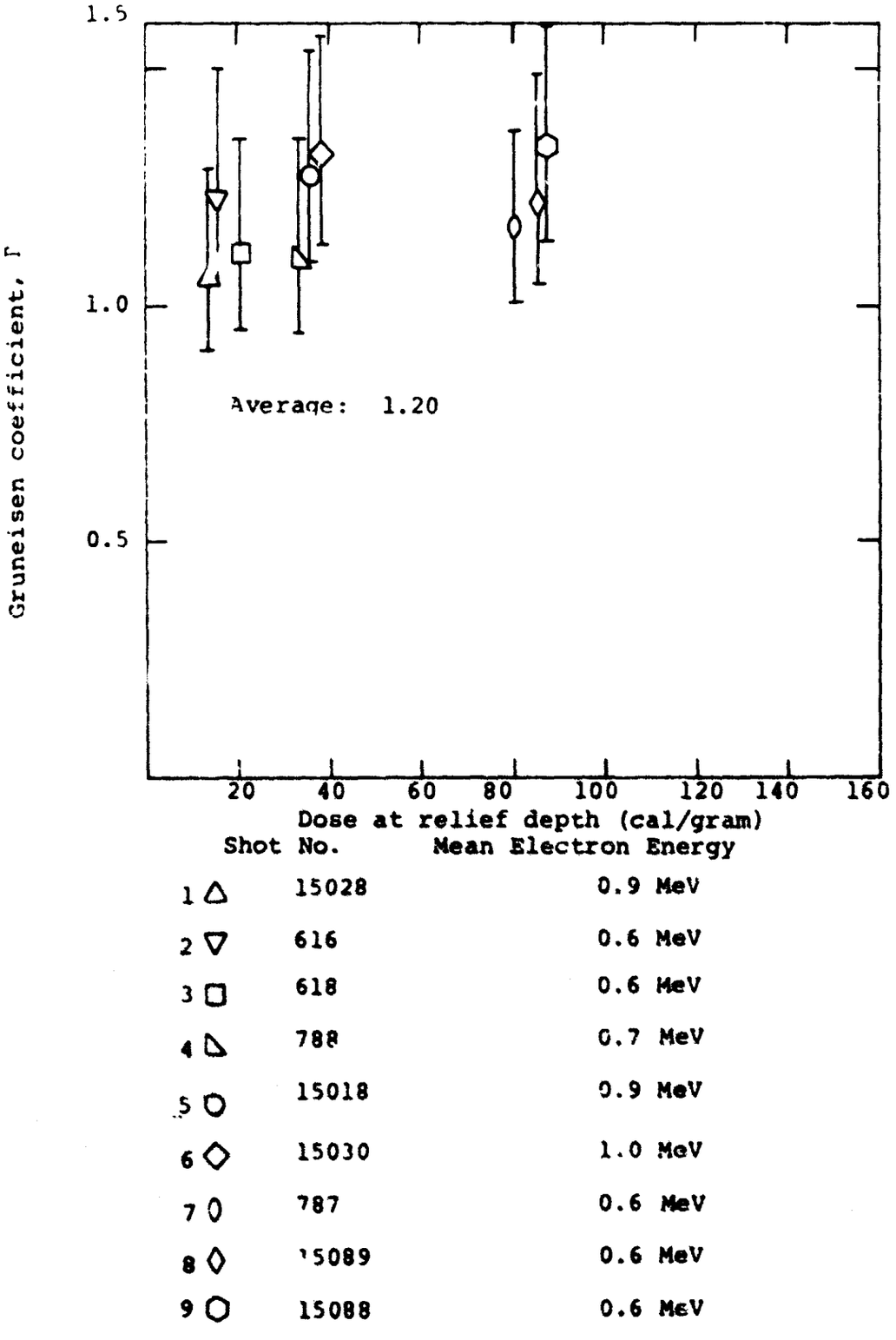

Figure 2.12 Energy dependence of the Gruneisen coefficient in alpha titanium.

The uncertainty in the fluence for the titanium shots is slightly greater, since the effect of electron backscatter was only estimated. Consequently, an additional two percent uncertainty is assumed for these data making a total uncertainty of ± 17 percent. On the highest fluence data shot for each material, the fluence was less uniform and an overall uncertainty of ± 20 percent is estimated for those shots.

The mean value for the Gruneisen coefficient that was obtained for the 2014-T6 aluminum was 2.20 with a standard deviation of 0.16, for specific energies of up to 160 cal/gram.

The standard deviation of the data, on the order of seven percent, falls well within the uncertainty associated with a given experimental point (~ ± 15 percent). This indicates that the data are consistent within themselves and even though the absolute uncertainty in the coefficient is ± 15 percent, any variation in the coefficient with specific energy must be less than 7 percent over the range in dose.

The value of 2.20 ± 0.32 for the Gruneisen coefficient of 2014-T6 aluminum compares favorably with the reported handbook value of 2.13 (Reference 18). The values obtained specifically for 2014-T6 aluminum computed from thermodynamic quantities are somewhat lower, 1.81 from Reference 11 and 1.88 from Reference 31. These latter values are 15 percent and 18 percent below the values obtained in this program and consequently lie just outside the estimated error band.

An average value for the Gruneisen coefficient for alpha titanium of $\Gamma = 1.20$ with a standard deviation of 0.10 is obtained from the experimental data up to specific energies of 95 cal/gram.

The total uncertainty associated with the Gruneisen coefficient is ± 0.18; the experimental results are therefore not significantly different than the handbook value of 1.18 (Reference 18) and the Reference 14 value of 1.11.

The standard deviation of the data is about ± 9 percent; this is less than the uncertainty associated with a given point (17 percent) and again indicates the self consistency of the data. Any variation in the Gruneisen coefficient with specific energy is therefore less than nine percent over the range in dose.

2.4 CONCLUSIONS

Measurement of the Gruneisen coefficient using pulsed electron beams and a transmitted stress technique has been demonstrated. Data were obtained on 2014-T6 aluminum and alpha titanium; the results up to the highest dose levels tested are in reasonable agreement with the Gruneisen coefficient obtained from thermodynamic data.

For simple materials and excluding changes in phase, greater precision in the Gruneisen coefficient is obtained from measurement of the specific heat, density, thermal expansion coefficient and adiabatic bulk modulus. However, determination of the constant volume energy-pressure coupling for materials with porosity, large heterogeneity, or changes in phase by the thermodynamic techniques becomes extremely difficult, and pulsed electron beam techniques are preferable.

In cases where the character of the material tested is such that dispersion alters the stress pulse between the heated

volume and the transducer, alternative techniques can be used (Reference 34). One such technique is to observe the velocity of an interface between the material being tested, which is uniformly heated by the beam, and a slab of fused silica. The velocity of the interface can be measured using a velocity interferometer, observing through fused silica. The pressure in the material can be calculated from the observed response since the Gruneisen coefficient and equation of state of the fused silica are known.

REFERENCES

1. ASM Metals Handbook, American Society for Metals, Metals Park, Ohio, 1964.

2. Aerospace Materials Handbook, 1968.

3. Minutes for the Sixth Technical Direction Meeting of the DASA PREDIX Program, November 5, 6, 1969.

4. Rads III Final Report, Material Data Handbook, Vol. X, Book 1, 1969.

5. Design Development of the AURORA Facilities, PISR-127-1, Oct. 15, 1968, Physics International Company, San Leandro, California.

6. T. Stefansky and J. Shea, Dynamic Fracture Experiments Using High Energy Pulsed Electron Beams, PIFR-108, Physics International Company, San Leandro, California (1971).

7. G. Yonas and P. Spence, Experimental Investigation of High ν/γ Beam Transport, Record of the Tenth Symposium on Electron, Ion and Laser Beam Technology, L. Marton, editor, San Francisco Press, Inc. (1970).

8. B. Alder, et al., Methods in Computational Physics, Vol. 1, Academic Press, New York, N. Y., 1963.

9. T. von Karman, On the Propagation of Plastic Deformation in Solids, NDRC A-71, OSRD 365 (1942).

10. T. Bechtel, Composite Heat Shield Structure, in Hardening of Materials for Reentry Vehicles, Vol. IV, National Materials Advisory Board, [illegible]ion NMAB-253-4, July 1969.

11. S. G. Babcock, et al., Characterization of Three Aluminum Alloys, AMMRC CR 71-3, January 1970.

12. L. E. Malvern, The Propagation of Longitudinal Waves of Plastic Deformation in a Bar of Material Exhibiting a Strain Rate Effect, J. Appl. Mech. 18 (1951) 203.

13. R. J. Rubin, J. Appl. Phys. 25 (1953) 528.

14. Measurements of Dynamic Properties of Materials, PREDIX Report, General Motors Corporation, June 1970.

15. Aerospace Structural Metals Handbook, Syracuse University Press, March 1967.

16. K. K. Kelly, High Temperature Heat Content, Heat Capacity and Entropy Data for the Elements and Inorganic Compounds, U. S. Bureau of Mines Bulletin, 584, Washington, D. C., 1960.

17. M. H. Rice, R. G. McQueen, and J. M. Walsh, Solid State Physics, 6 (1958).

18. L. H. Bakken and P. D. Anderson, An Equation of State Handbook, Report SCL-DR-68-123 (1969), Sandia Corporation, Livermore, California.

19. W. Herrmann, Constitutive Equation for the Dynamic Compaction of Ductile Porous Materials, J. Appl. Phys. 40, 2490 (1969).

20. W. Herrmann, On the Dynamic Compaction of Initially Heated Porous Materials, SC-DR-68-865 (1959); Sandia Corporation, Albuquerque, New Mexico.

21. L. Seaman and R. K. Linde, Distended Material Model Development, AFWL-TR-68-143, Vol. 1, Air Force Weapons Laboratory, Albuquerque, New Mexico (May 1969).

22. R. Fowles, Thermodynamic Compatibility of the Specific Heat and Gruneisen's Ratio, J. Appl. Phys. 39, 2963 (1968).

23. T. Stefansky and A. Mazzella, Dynamic Response of Porous Materials to Electron Energy Deposition, Bull. Am. Phys. Soc. 15, 1618 (1970).

24. B. Budiansky, Thermal and Thermoelastic Properties of Isotropic Composites, J. Composite Materials 4, 286 (1970).

25. J. Shea and A. Mazzella, Feasibility of Gruneisen Measurements Using Electron Beams, PIFR-077, Physics International Company, San Leandro, California (1968).

REFERENCES (cont.)

26. R. A. Graham and R. E. Hutchinson, Thermoelastic Stress Pulses Resulting from Pulsed Beams, Appl. Phys. Letters 11, 69 (1967).

27. R. B. Oswald, Jr., D. R. Schallhorn, H. A. Eisen, and F. B. McLean, Jr., Appl. Phys. Letters, 13, 279 (1968).

28. A. Goodman, The Direct Measurment of the Gruneisen Parameter, Rept. SC-TM-67-13, Sandia Corporation, Albuquerque, New Mexico.

29. P. W. Spence, G. Yonas, and D. K. Dean, Shock Generation in S-200 Beryllium Using a Pulsed Electron Beam, Bull. Am. Phys. Soc. 14, 1164 (1969).

30. J. Shea, A. Mazzella and L. Avrami, Equation of State Investigation of Granular Explosives Using a Pulsed Electron Beam, Proceedings of the Fifth Symposium on Detonation, August 1970.

31. L. Webster, The Equation of State of 2014-T6 Aluminum at Ambient and Elevated Temperatures, KN-70-526 (R), Kaman Nuclear, Colorado Springs, Colorado, August 1970.

32. R. A. Graham, F. W. Nielson, W. B. Benedick, Piezoelectric Current from Shock-Loaded Quartz--A Submicrosecond Stress Gauge, J. Appl. Phys. 36, 1775 (1965).

33. G. Yonas, et al., Dynamic Effects of High ν/γ Beam Plasma Interactions, DASA 2426, August 1969.

34. V. Bailey, Material Response Characterization of Several SPARTAN Materials to Pulsed Radiation Environments, PIFR-243, Physics International Company, San Leandro, California, in preparation.

APPENDIX A

ENERGY-PRESSURE COUPLING DATA AND CALCULATIONS FOR 2014-T6 ALUMINUM

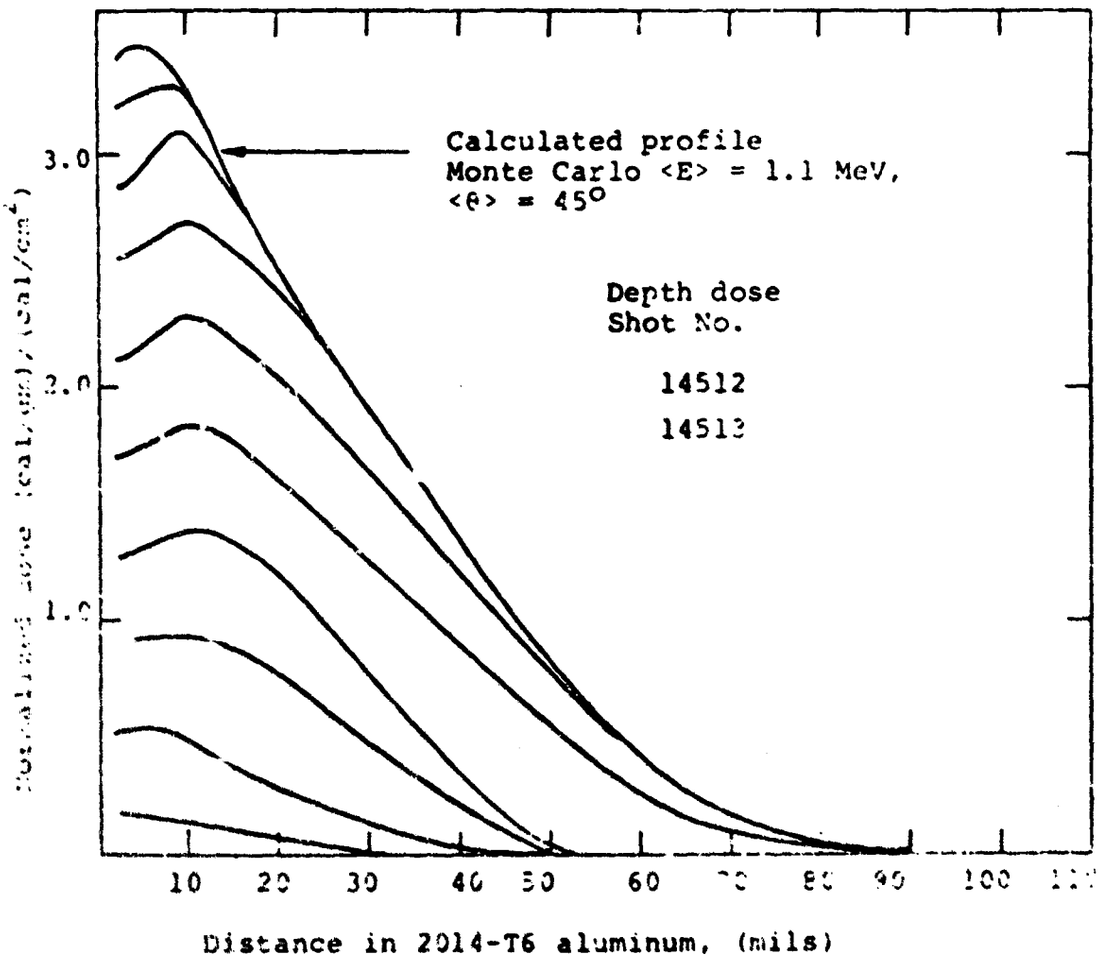

Figure A.1 Deposition profile for shots 14531, 14523 and 14529 in 2014-T6 aluminum.

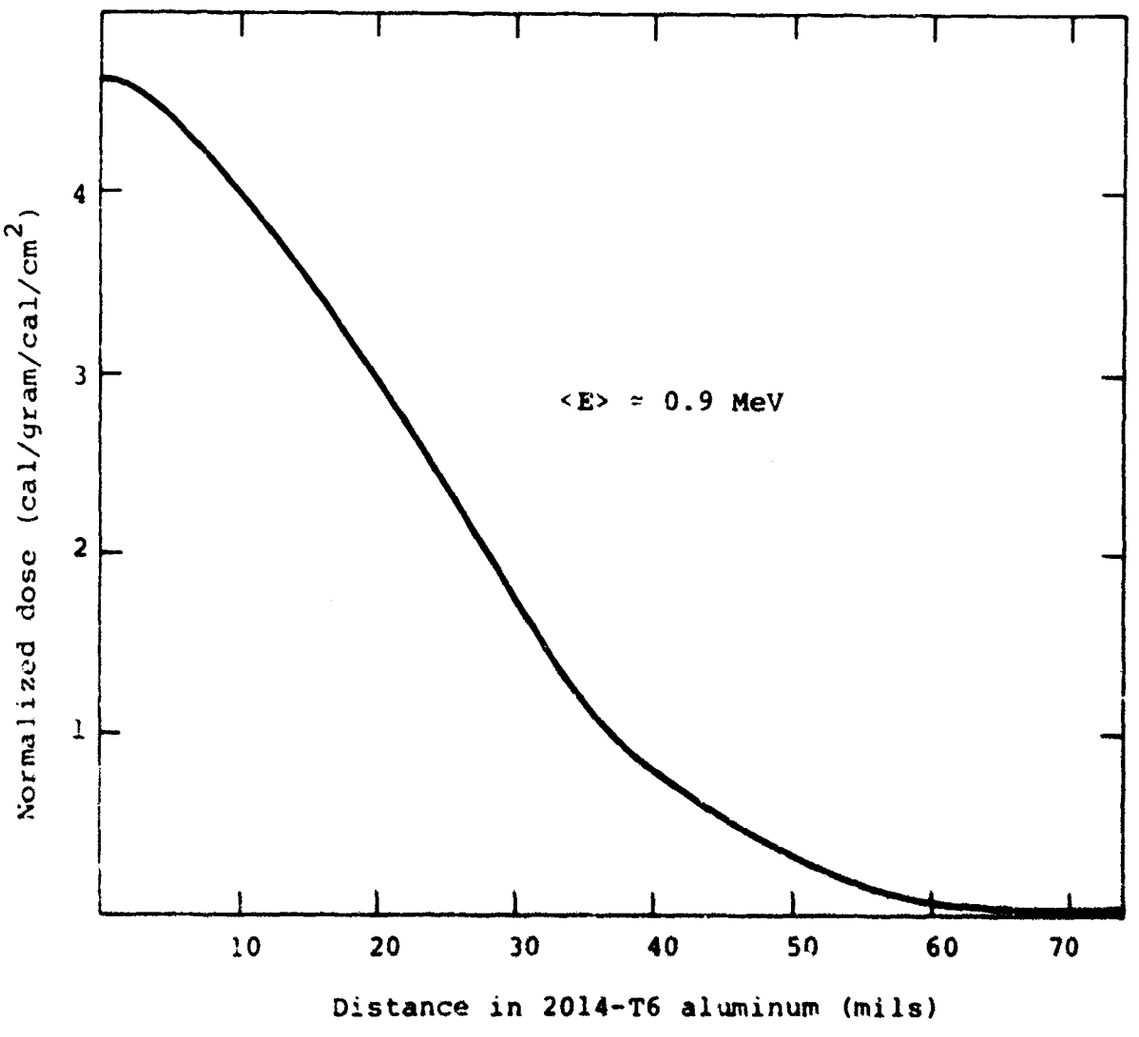

Figure A.2 Experimental deposition profile for data shots 790 and 14522 in 2014-T6 aluminum.

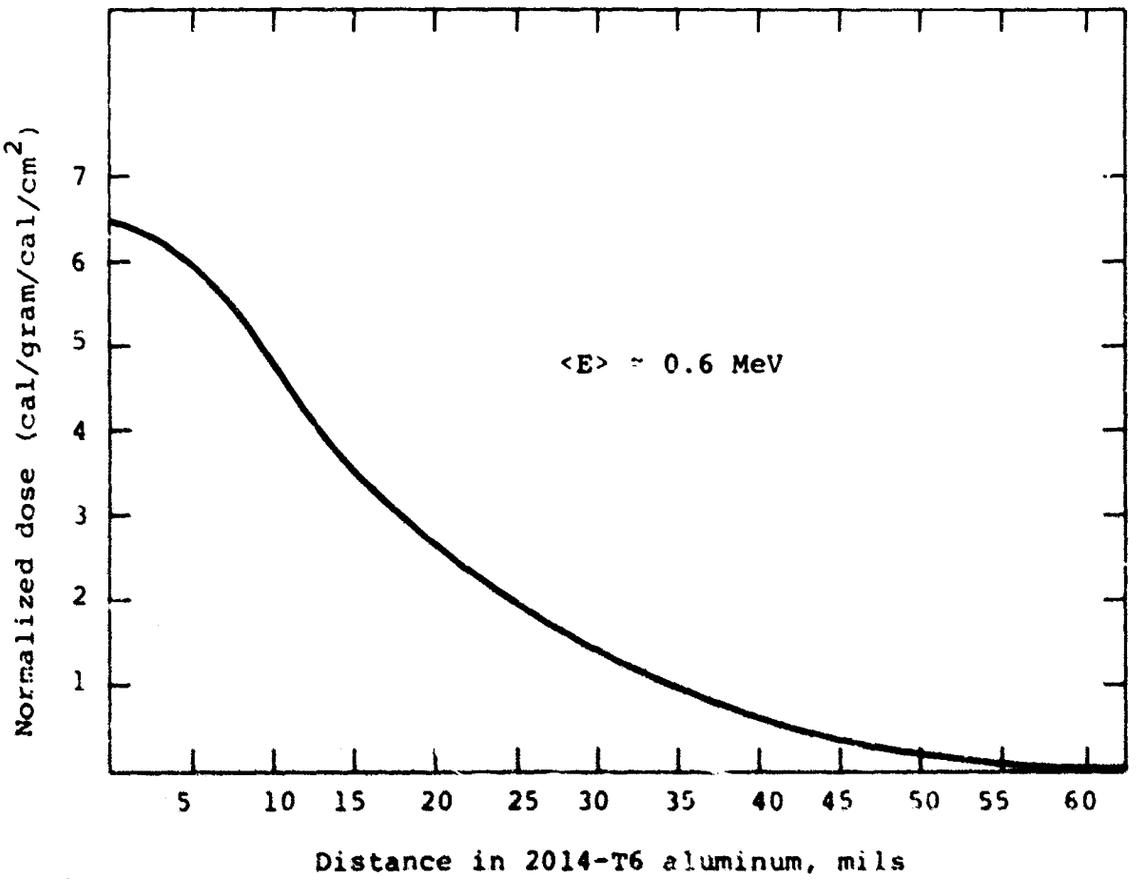

Figure A.3 Experimental deposition profile for data shots 610 and 614 in 2014-T6 aluminum.

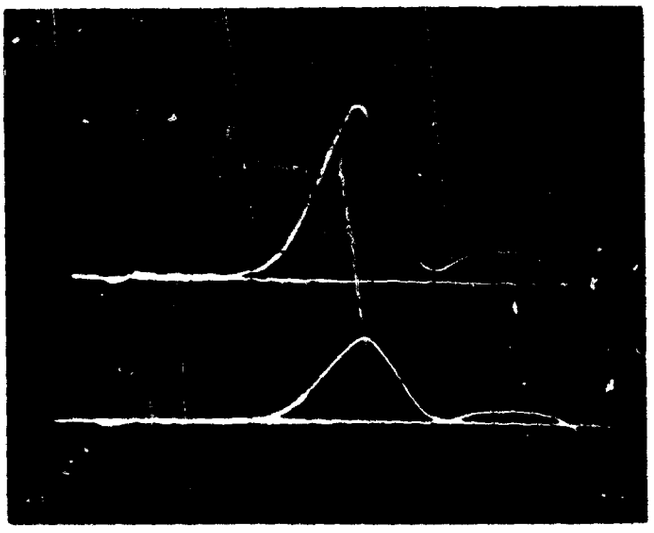

Shot 14522
Time: 0.10 μsec/cm
Pressure (Upper Trace): 5 V/cm
(Lower Trace): 10 V/cm

Figure A.4 Stress response of a quartz gauge to electron beam deposition in 2014-T6 aluminum.

NOT REPRODUCIBLE

Shot 14523
Time: 0.1 μsec/cm
Pressure (Upper Trace): 2 V/cm
(Lower Trace): 5 V/cm

Figure A.5 Stress response of a quartz gauge to electron beam deposition in 2014-T6 aluminum.

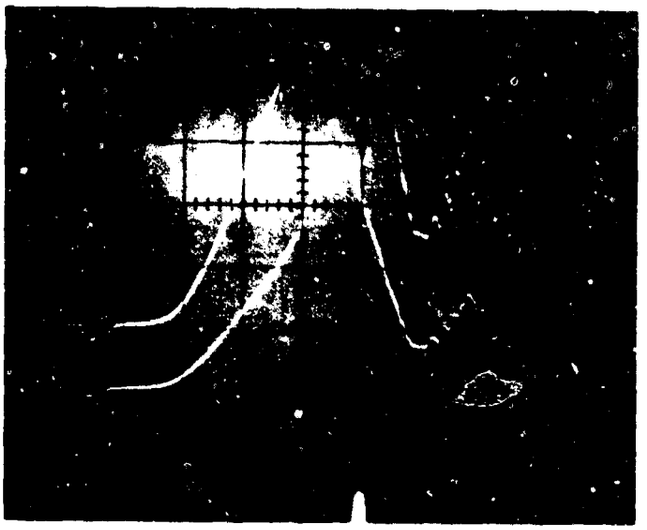

Shot 14529
Time: 0.1 μsec/cm
Pressure (Upper Trace): 5 V/cm
(Lower Trace): 10 V/cm

Figure A.6 Stress response of a quartz gauge to electron beam deposition in 2014-T6 aluminum.

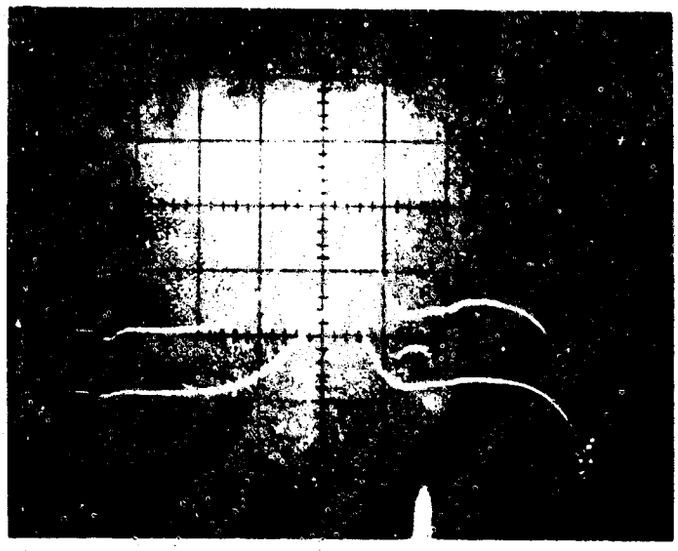

Shot 14531
Time: 0.1 μsec/cm
Pressure (Upper Trace): 5 V/cm
(Lower Trace): 10 V/cm

Figure A.7 Stress response of a quartz gauge to electron beam deposition in 2014-T6 aluminum.

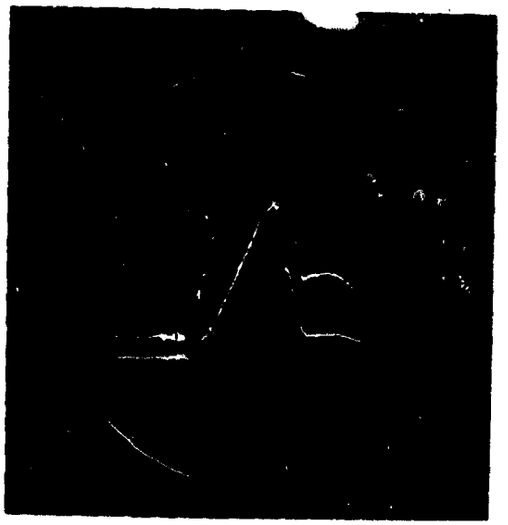

Shot 790

Time: 0.1 μsec/cm
Pressure:
Upper trace: 2 V/cm
Lower trace: 5 V/cm

Figure A.8 Stress response of a quartz gauge to electron beam deposition in 2014-T6 aluminum.

A698

NOT REPRODUCIBLE

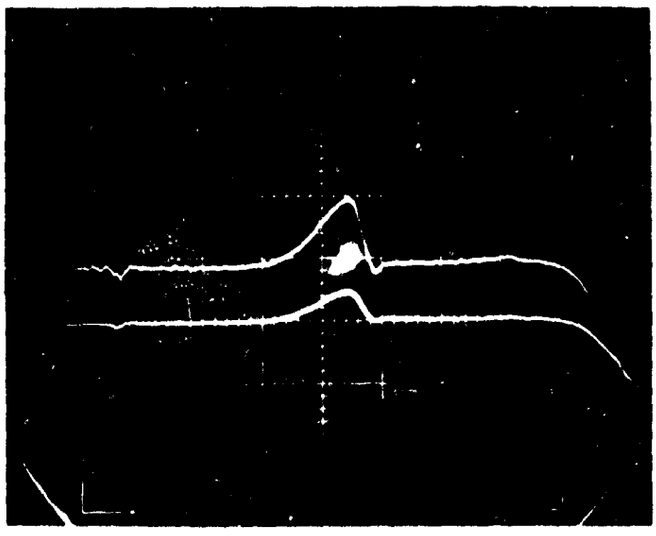

Shot 610

Time: 0.1 μsec/cm
Pressure:
Upper trace: 5 V/cm
Lower trace: 10 V/cm

Figure A.9 **Stress response of a quartz gauge to electron beam deposition in 2014-T6 aluminum.**

A699

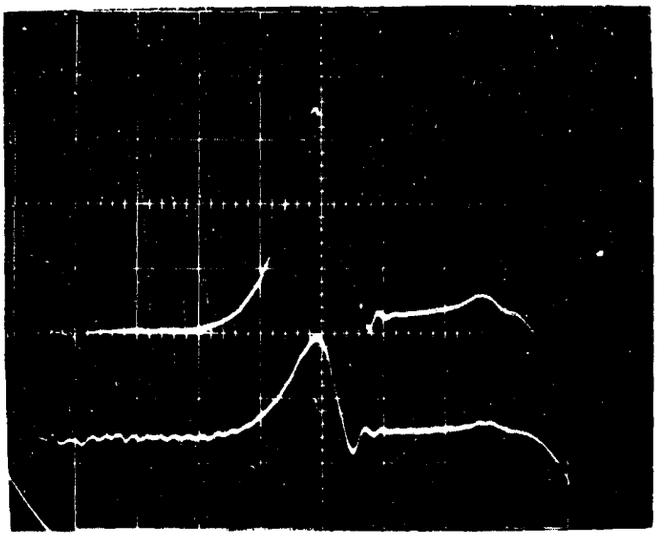

Shot 614

Time: 0.1 μsec/cm
Pressure:
Upper trace: 2 V/cm
Lower trace: 5 V/cm

Figure A.10 Stress response of a quartz gauge to electron beam deposition in 2014-T6 aluminum.

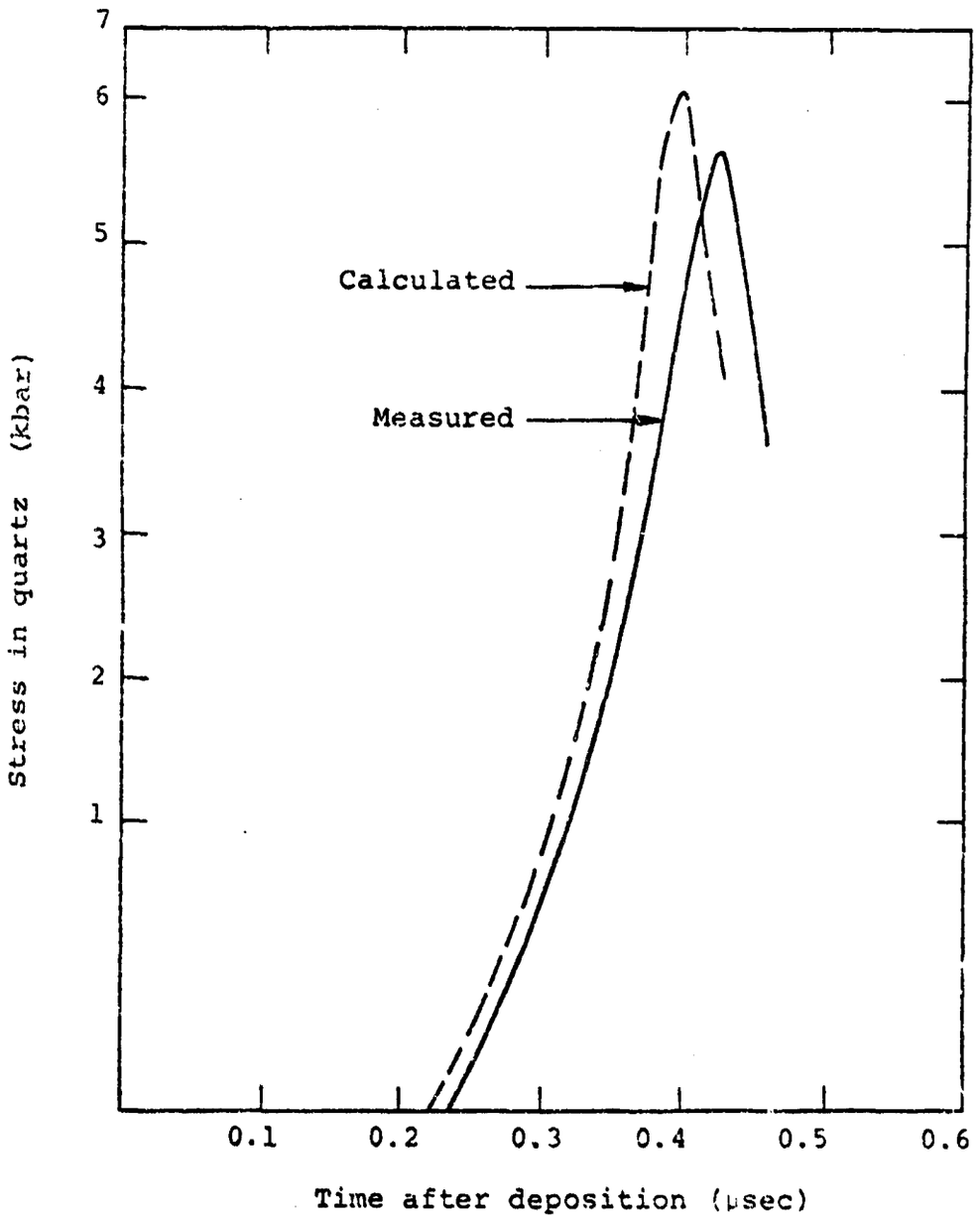

Figure A.11 Comparison between measured and calculated stress histories in quartz--shot 14522.

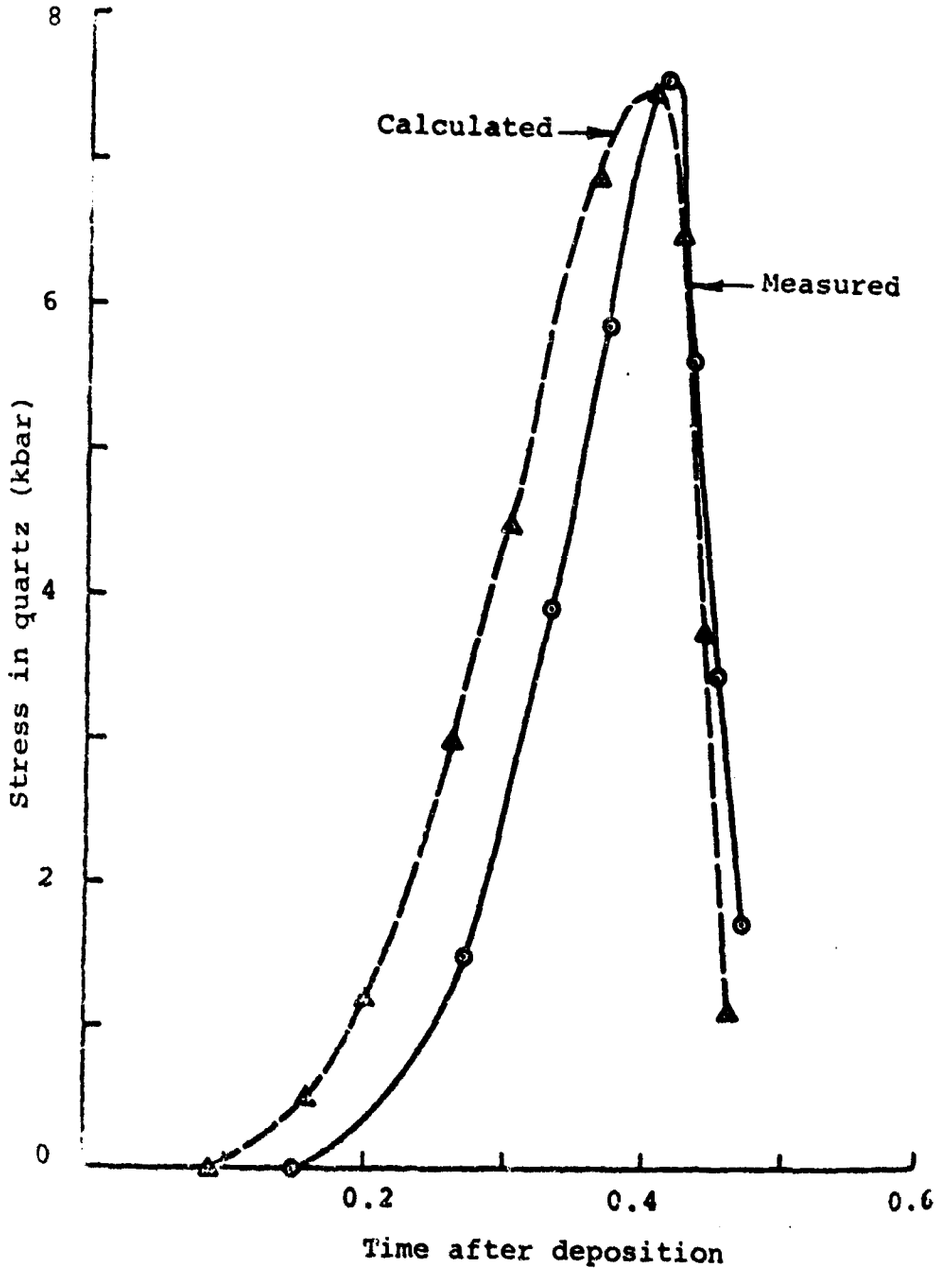

Figure A.12 Comparison between measured and calculated stress histories in quartz--shot 14523.

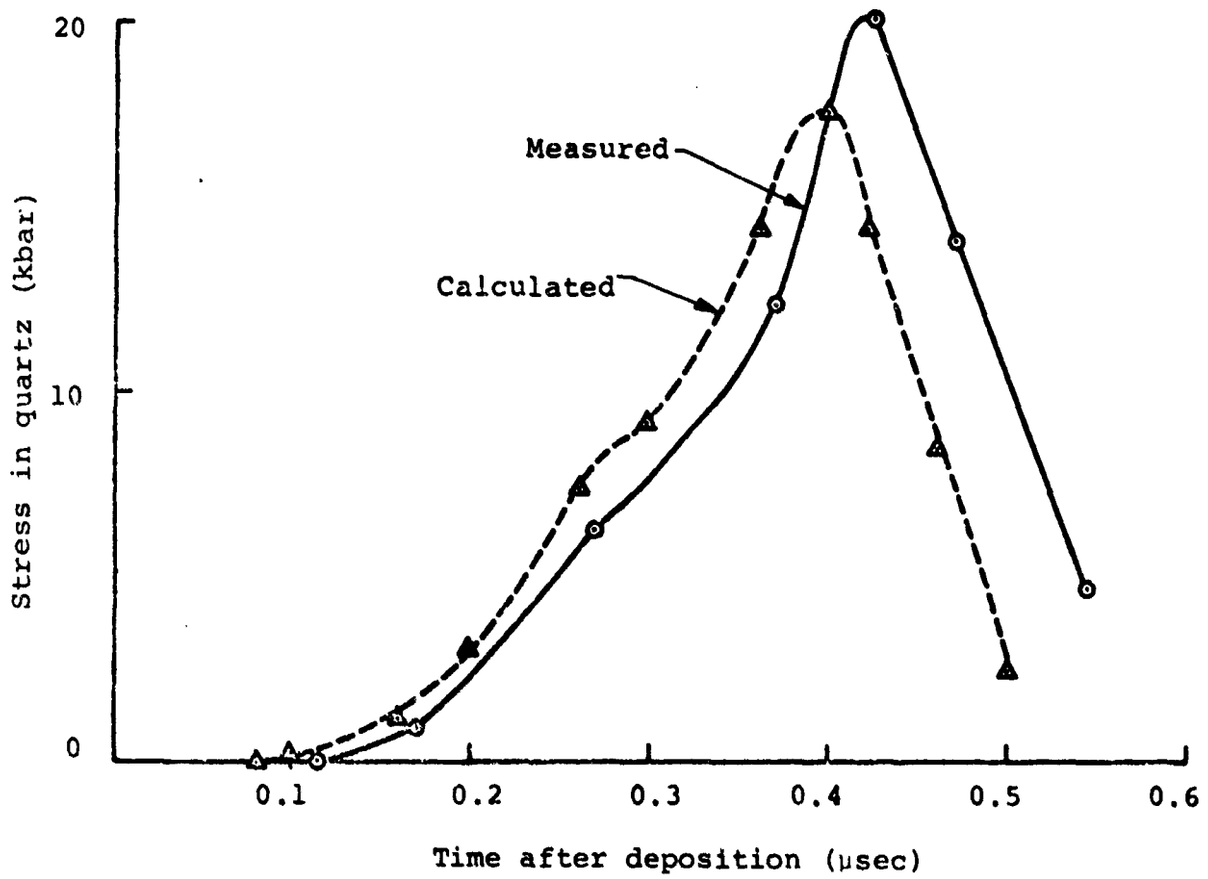

Figure A.13 Comparison between measured and calculated stress histories in quartz--shot 14329.

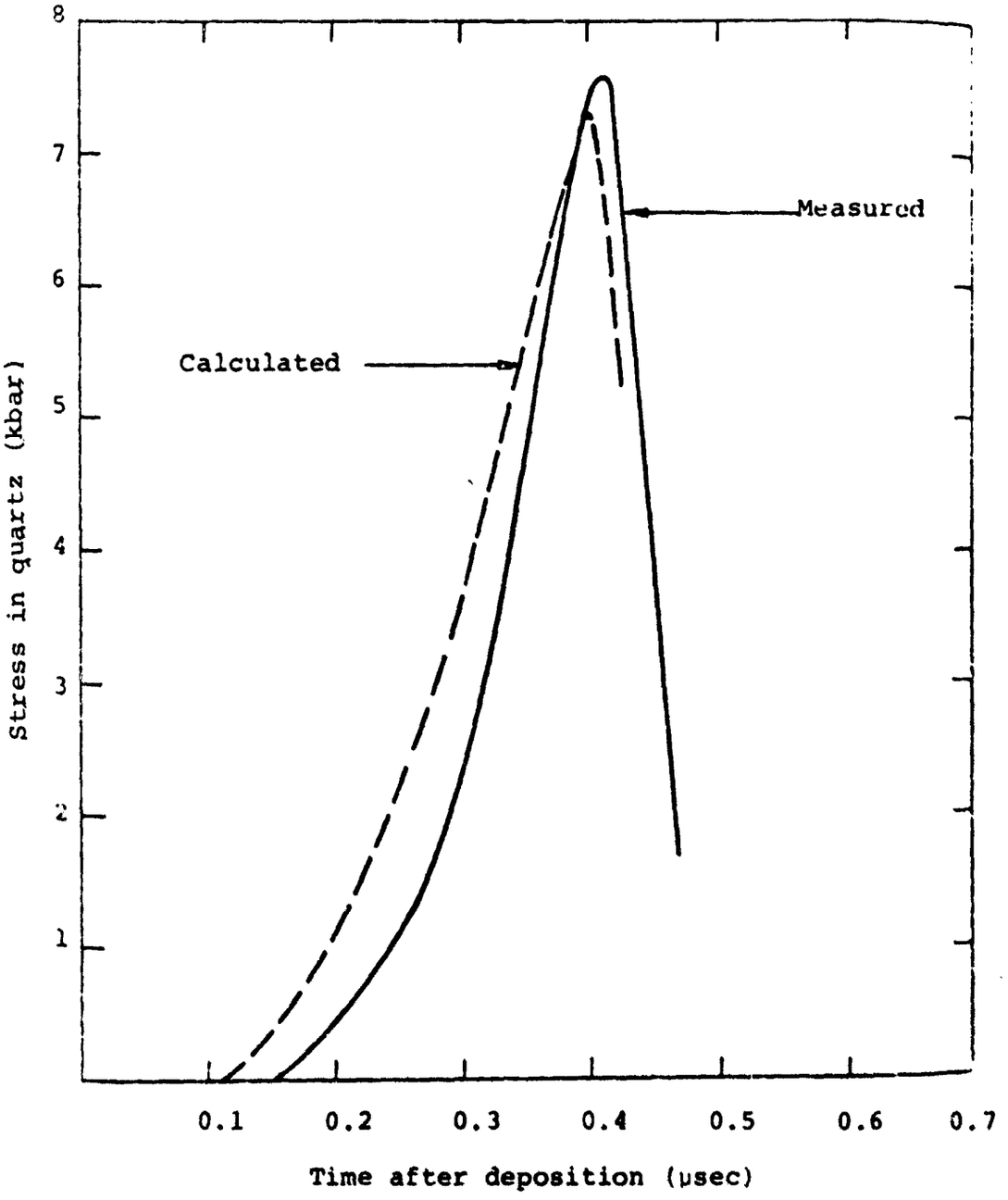

Figure A.14 Comparison between measured and calculated stress histories in quartz--shot 14531.

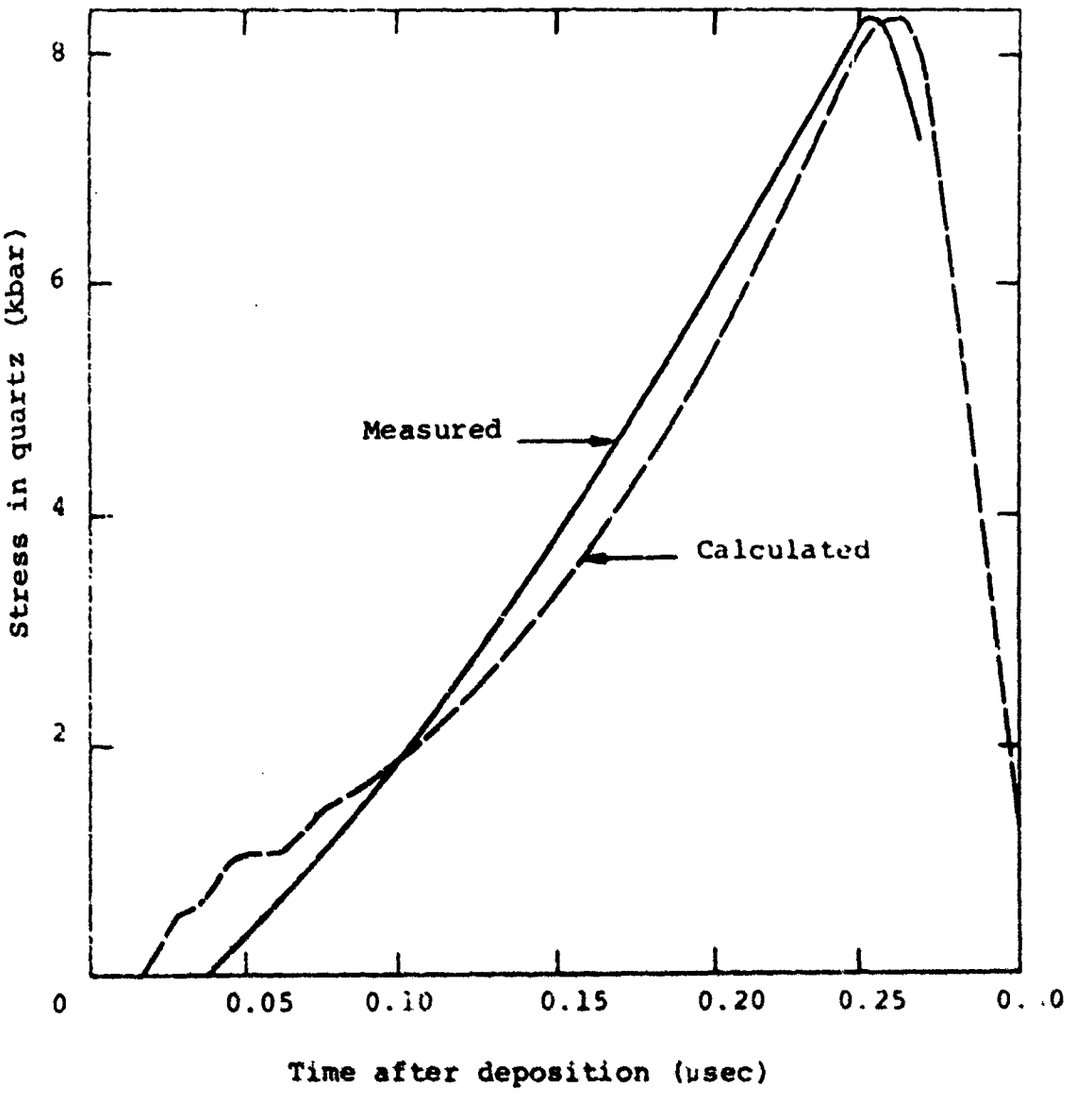

Figure A.15 Comparison between measured and calculated stress histories in quartz--shot 790.

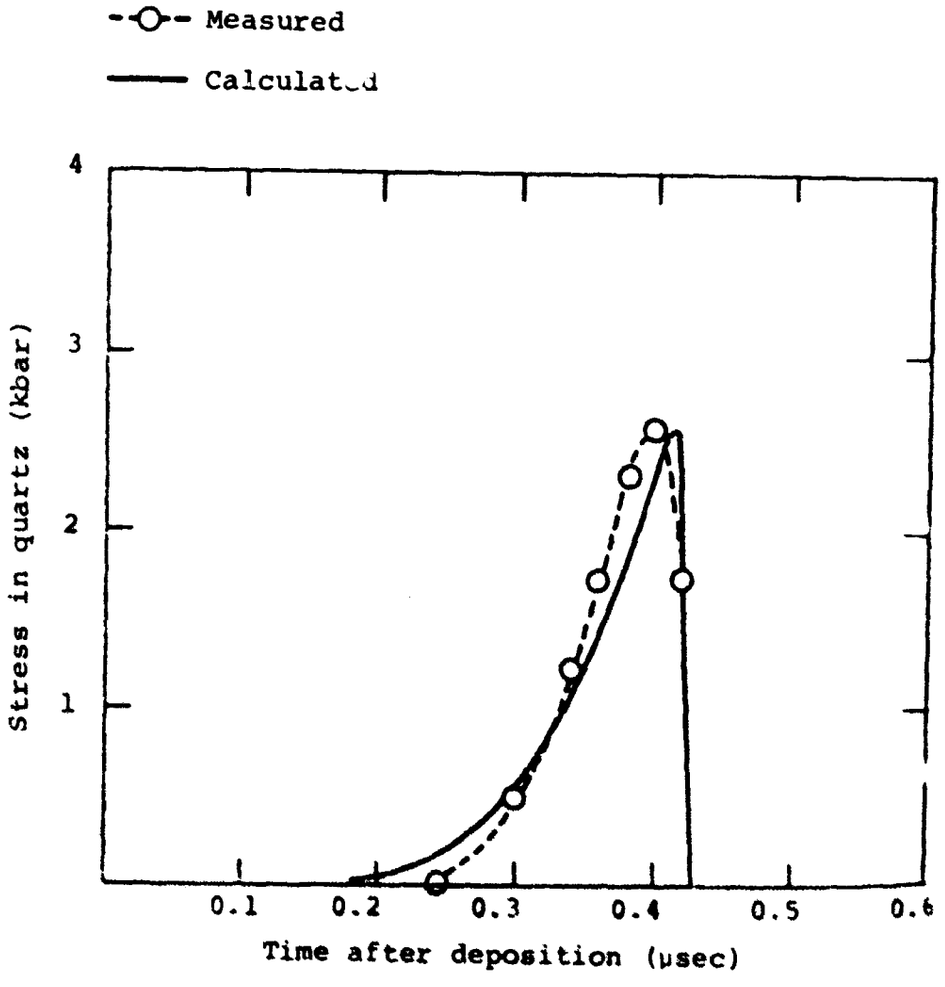

Figure A.16 Comparison between measured and calculated stress histories in quartz--shot 610.

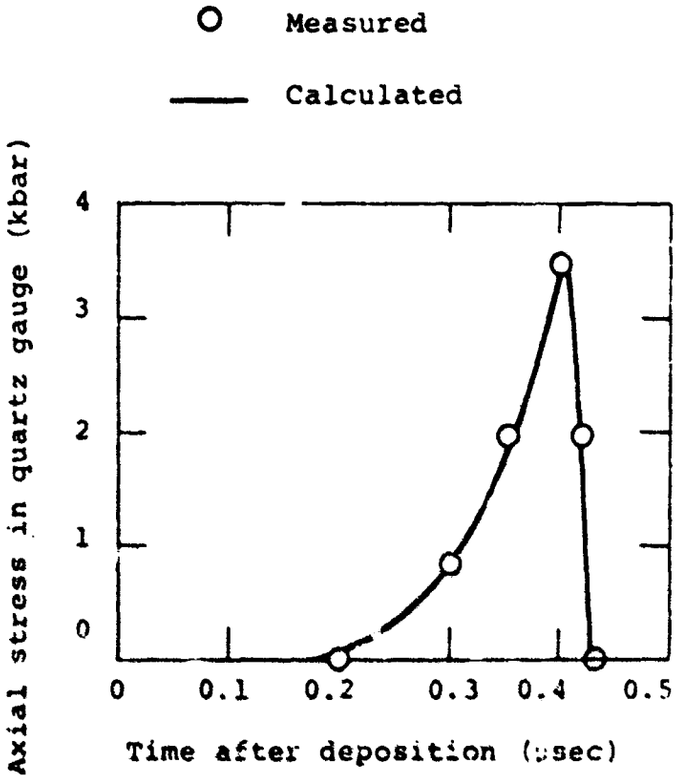

Figure A.17 Comparison between measured and calculated stress histories in quartz--shot 614.

APPENDIX B

ENERGY-PRESSURE COUPLING DATA AND CALCULATIONS FOR α-TITANIUM

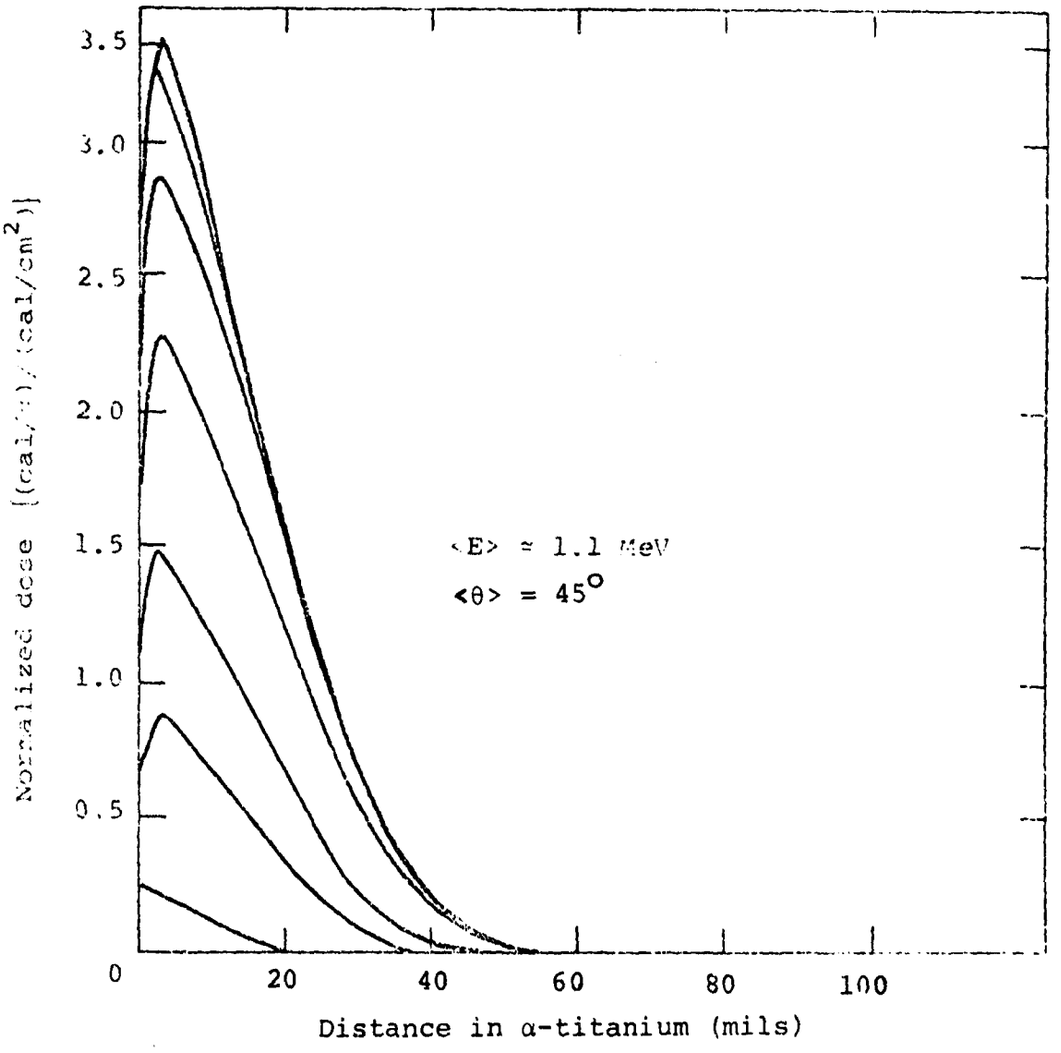

Figure B.1 Deposition profile for shot 15030 in α-titanium.

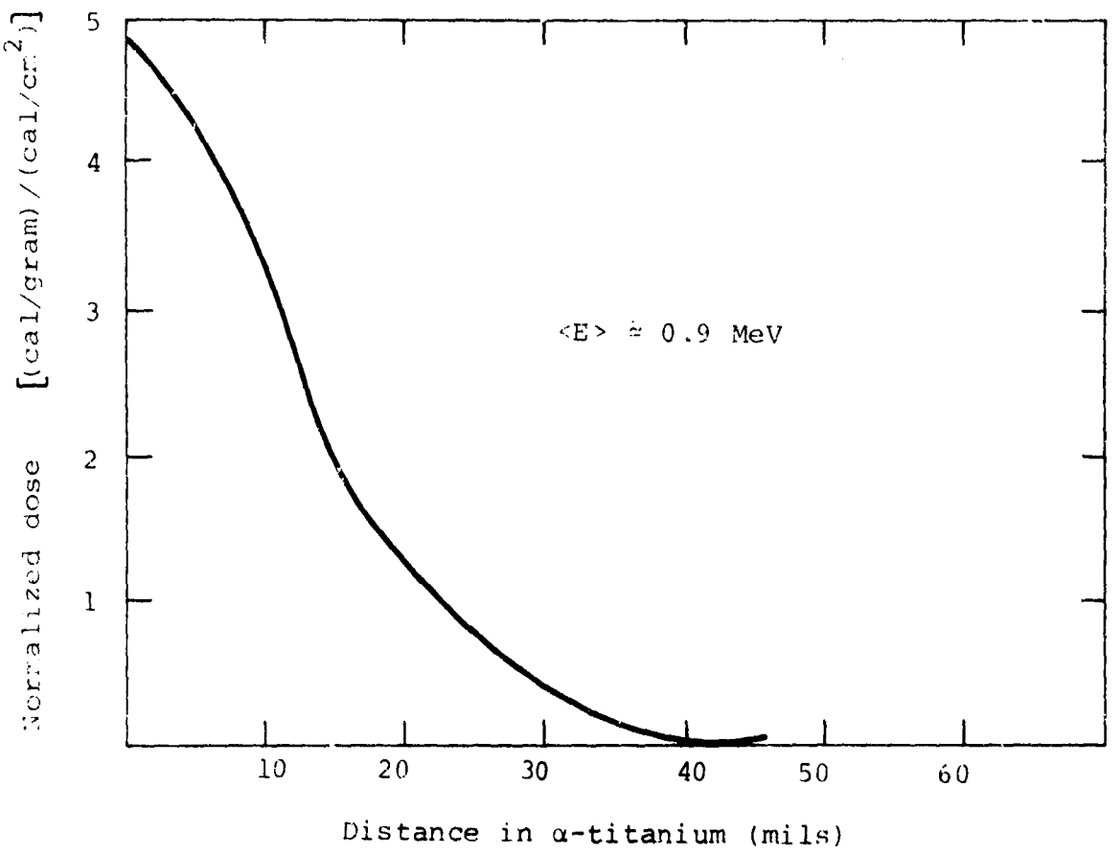

Figure B.2 Deposition profile for data shots 15018 and 15028 in α-titanium.

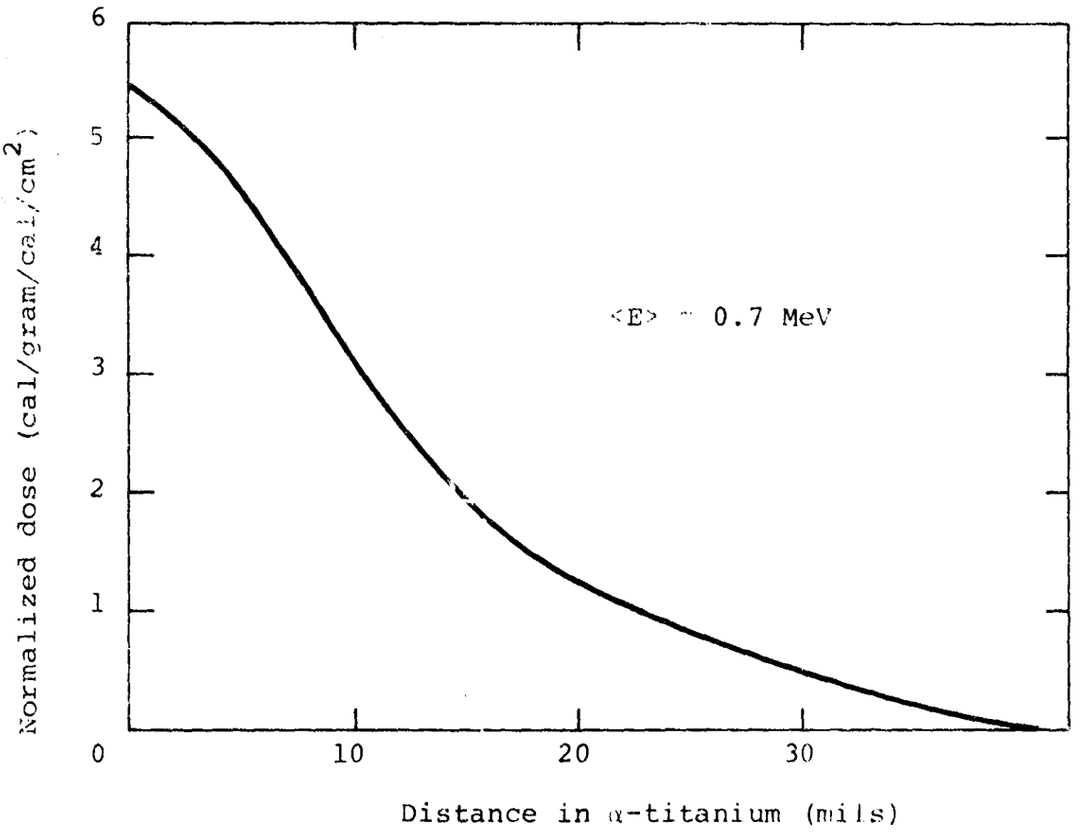

Figure B.3 Deposition profile for data shot 788 in α-titanium.

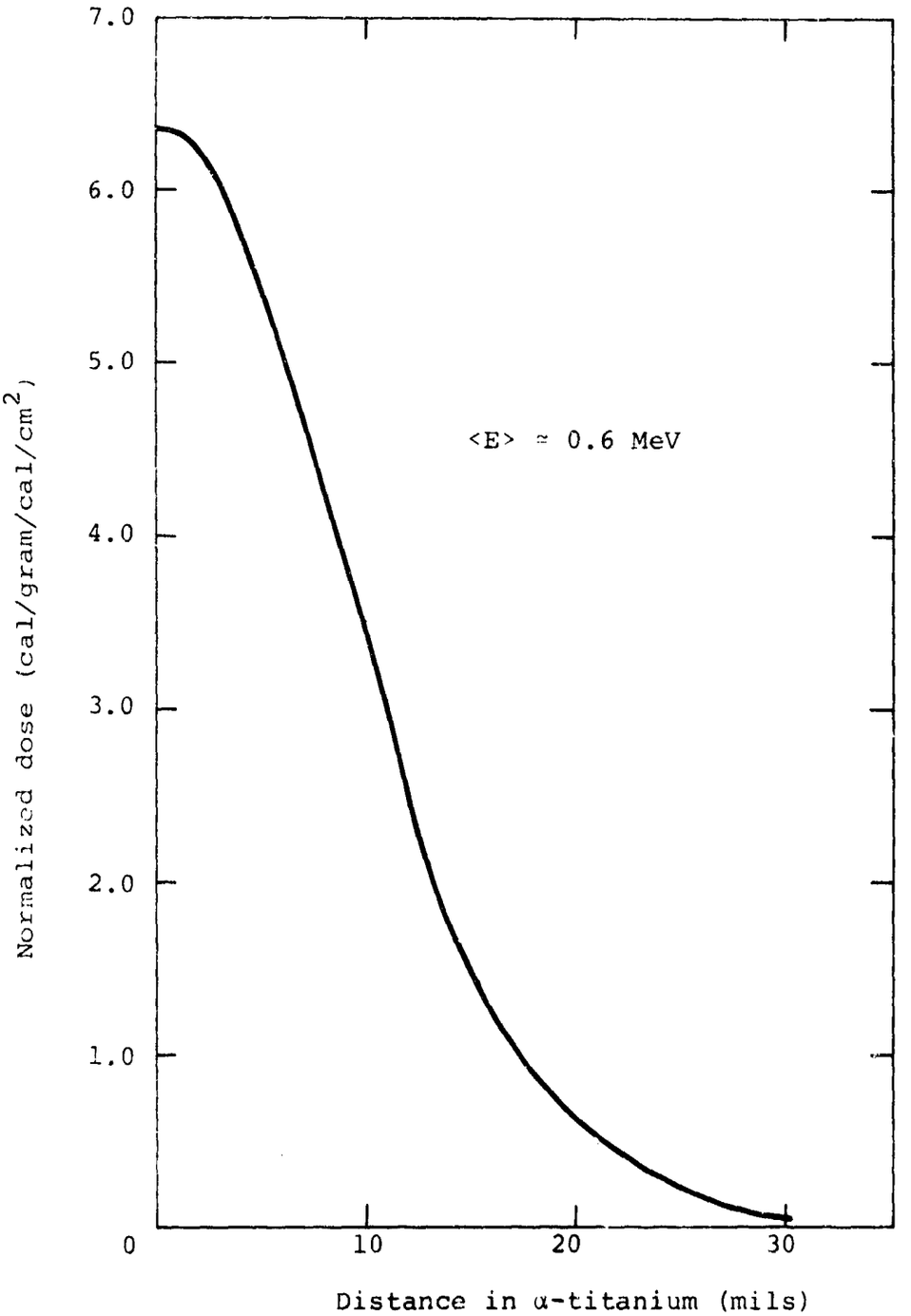

Figure 8.4 Deposition profile for data shots 15088 and 15089 α-titanium.

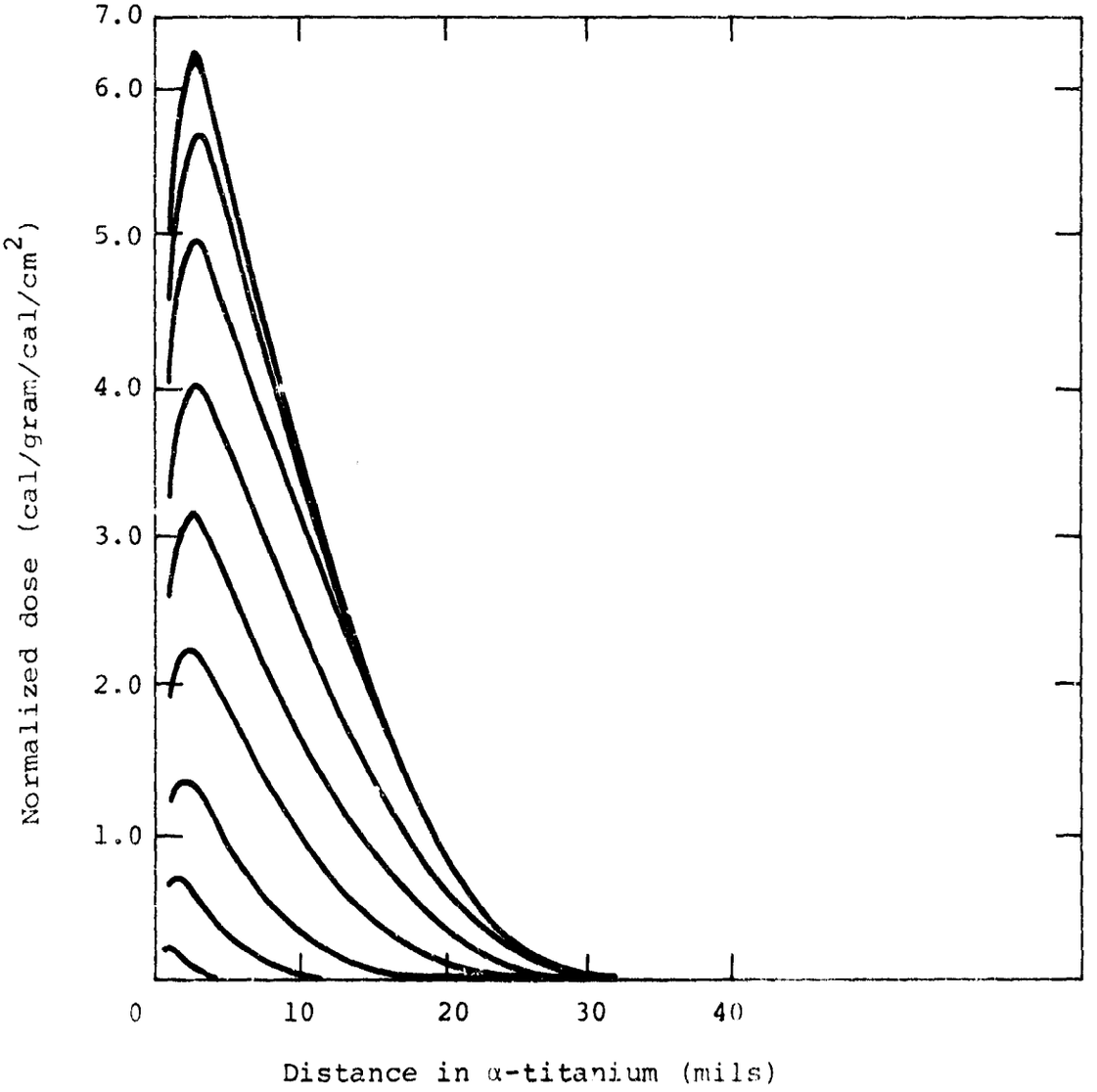

Figure B.5 Electron deposition profile for alpha titanium shots at 0.63 MeV mean electron energy.

Shot 15030

Time: 0.1 μsec/cm
Pressure:
Upper trace: 2 V/cm
Lower trace: 5 V/cm

Figure B.6 Stress response of a quartz gauge to electron beam deposition in α-titanium.

A701

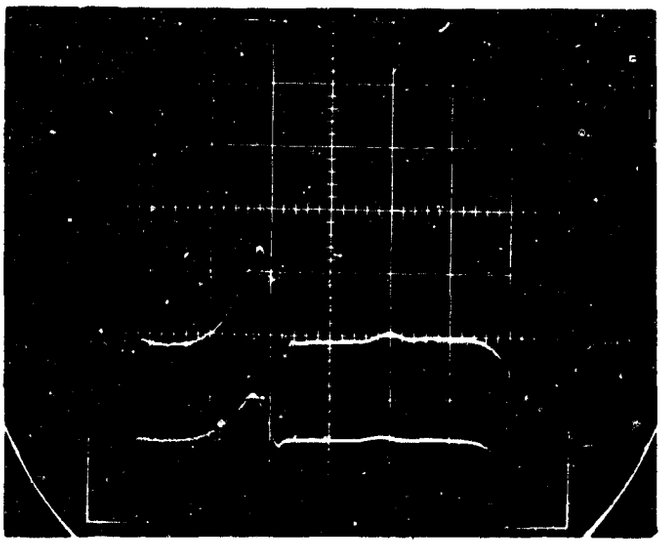

Shot 15018

Time: 0.1 μsec/cm
Pressure:
Upper trace: 5 V/cm
Lower trace: 10 V/cm

Figure B.7 Stress response of a quartz gauge to electron beam deposition in α-titanium.

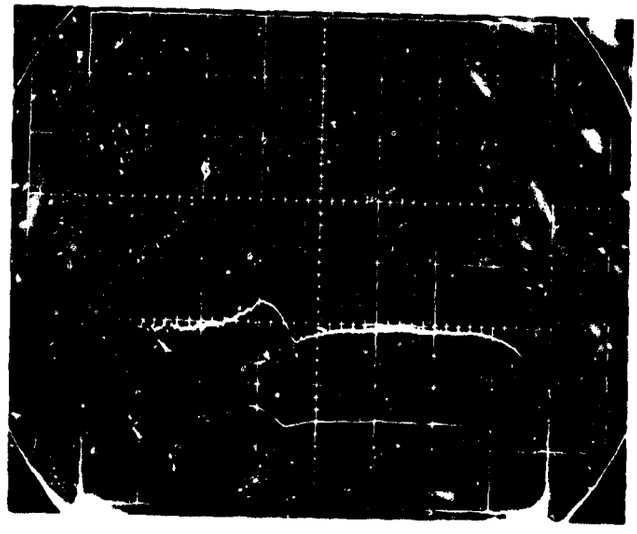

Shot 15028

Time: 0.1 μsec/cm
Pressure:
Upper trace: 5 V/cm
Lower trace: 10 V/cm

Figure B.8 Stress response of a quartz gauge to electron beam deposition in α-titanium.

Shot 788

Time: 0.1 μsec/cm
Pressure:
Upper trace: 2 V/cm
Lower trace: 5 V/cm

Figure B.9 Stress response of a quartz gauge to electron beam deposition in α-titanium.

NOT REPRODUCIBLE

Shot 15088

Time: 0.1 μsec/cm
Pressure:
Upper trace: 5 V/cm
Lower trace: 10 V/cm

Figure B.10 Stress response of a quartz gauge to electron beam deposition in α-titanium.

A705

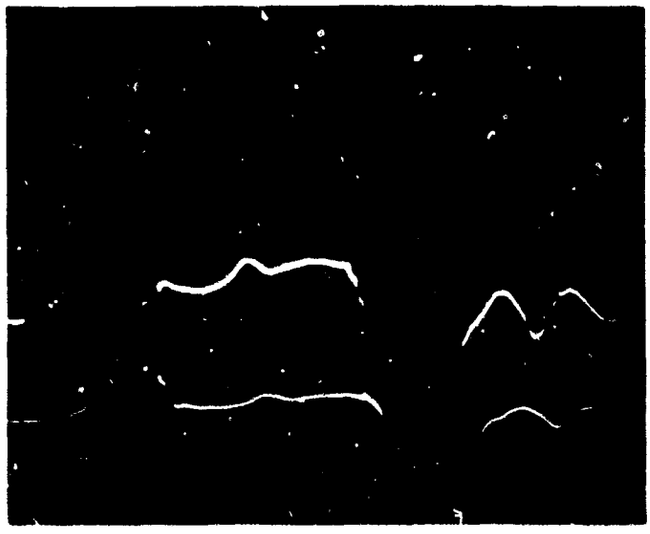

Shot 15089

Time: 0.1 μsec/cm
Pressure:
Upper trace: 2 V/cm
Lower trace: 5 V/cm

Figure B.11 **Stress response of a quartz gauge to electron beam deposition in β-titanium.**

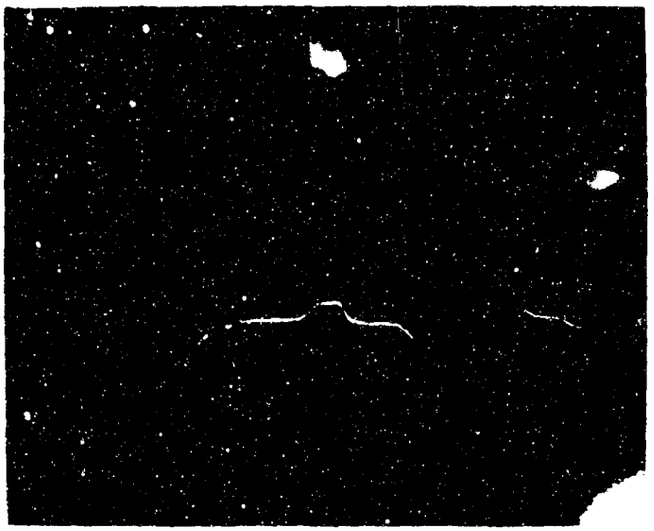

Scope 1

Time: 0.1 μsec/cm
Pressure:
Upper trace: 2 V/cm
Lower trace: 5 V/cm

NOT REPRODUCIBLE

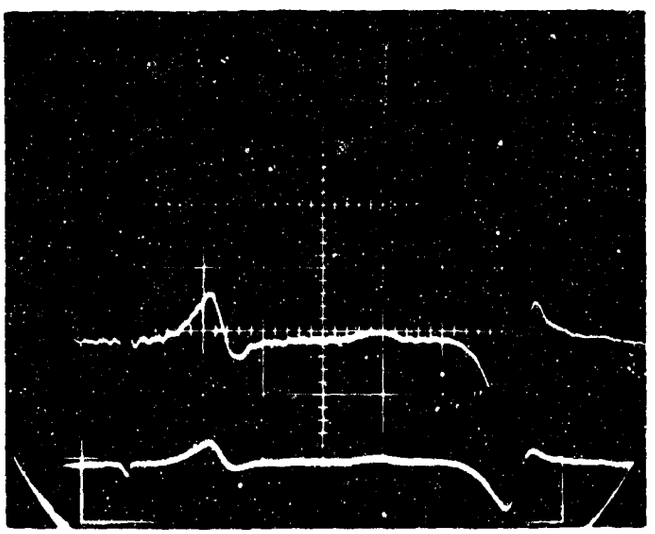

Scope 2

Time: 0.1 μsec/cm
Pressure:
Upper trace: 5 V/cm
Lower trace: 10 V/cm

Figure B.12 **Stress response of a quartz gauge to electron beam deposition in α-titanium, shot 618.**

A716

NOT REPRODUCIBLE

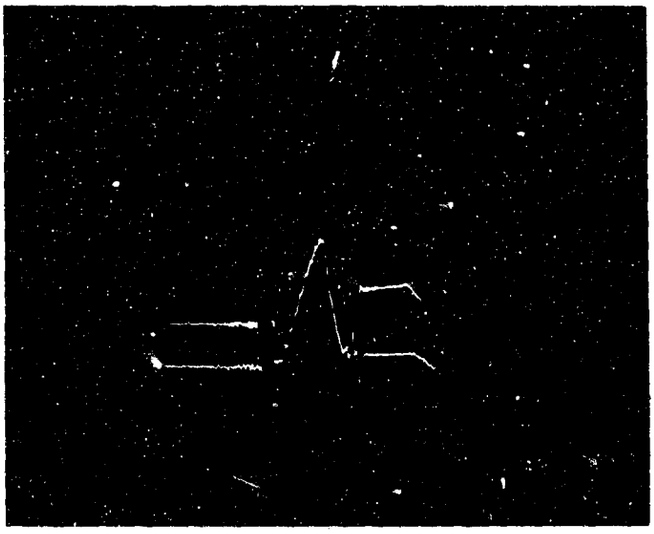

Shot 787

Time: 0.1 μsec/cm
Pressure:
Upper trace: 2 V/cm
Lower trace: 5 V/cm

Figure B.13 Stress response of a quartz gauge to electron beam deposition in α-titanium.

A718

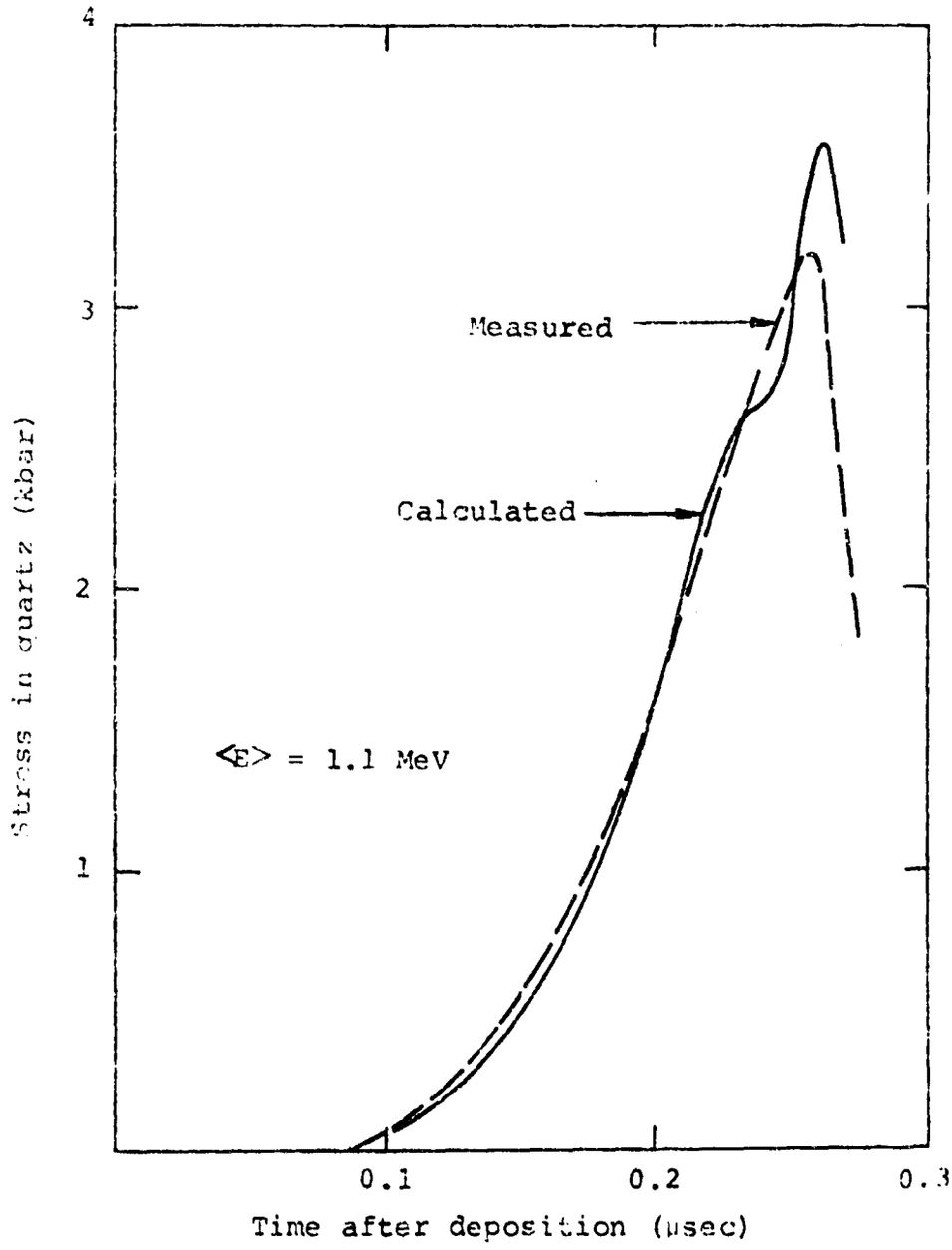

Figure B.14 Comparison between measured and calculated stress histories in α-titanium--shot 15030.

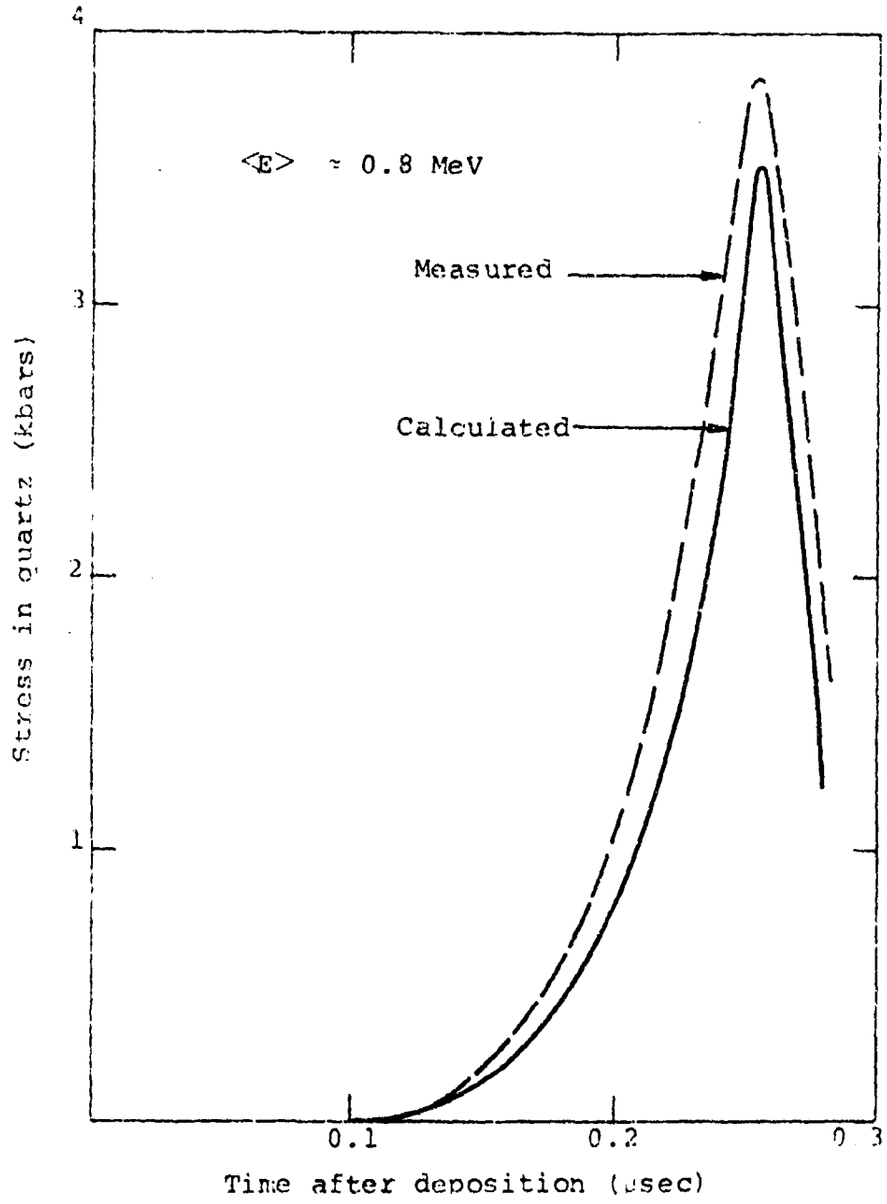

Figure B.15 Comparison between measured and calculated stress histories in α-titanium--shot 15018.

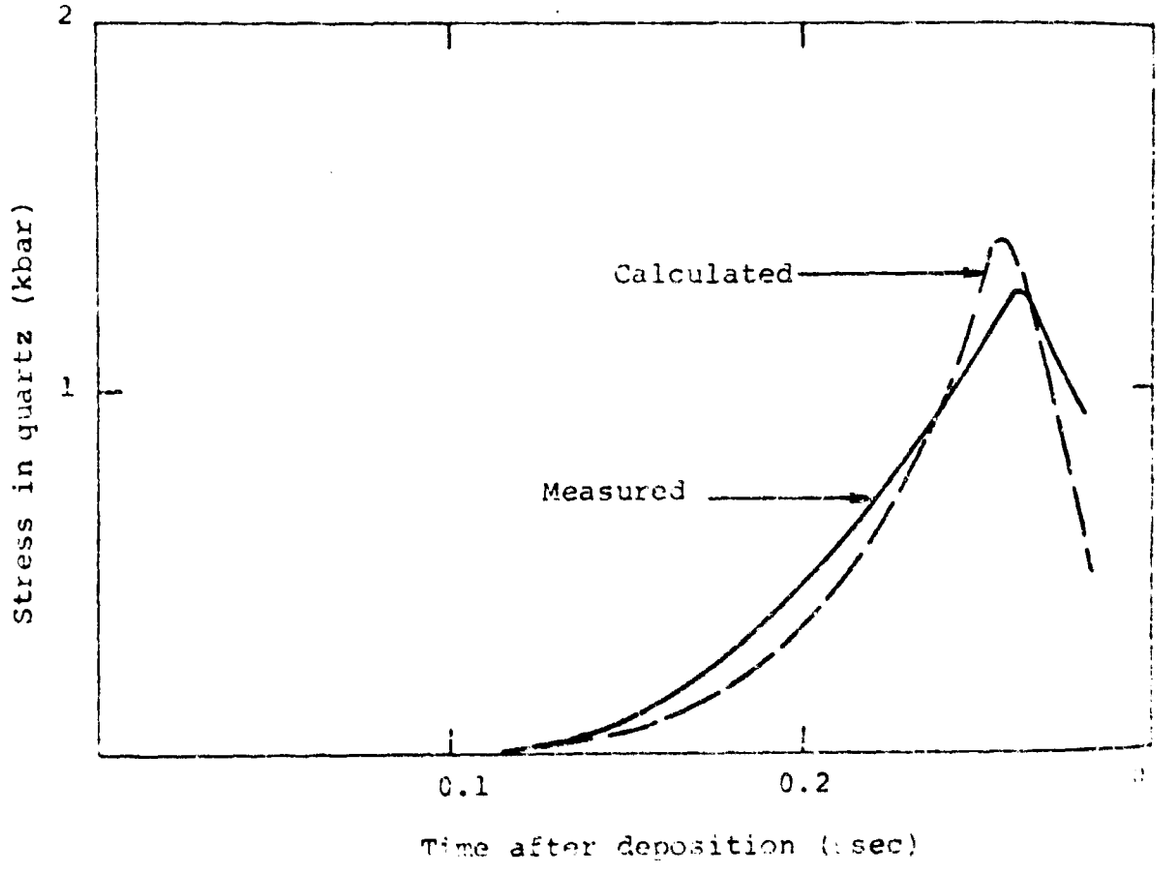

Figure B.16 Comparison between measured and calculated stress histories in α-titanium--shot 15028.

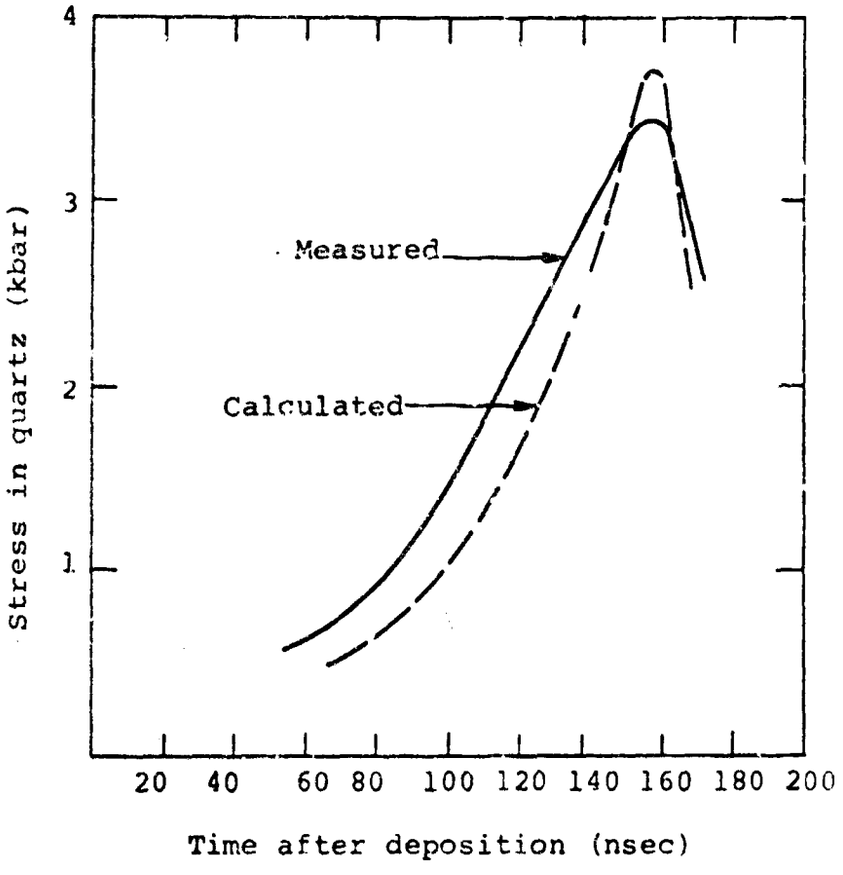

Figure B.17 Comparison between measured and calculated stress histories in α-titanium--shot 788.

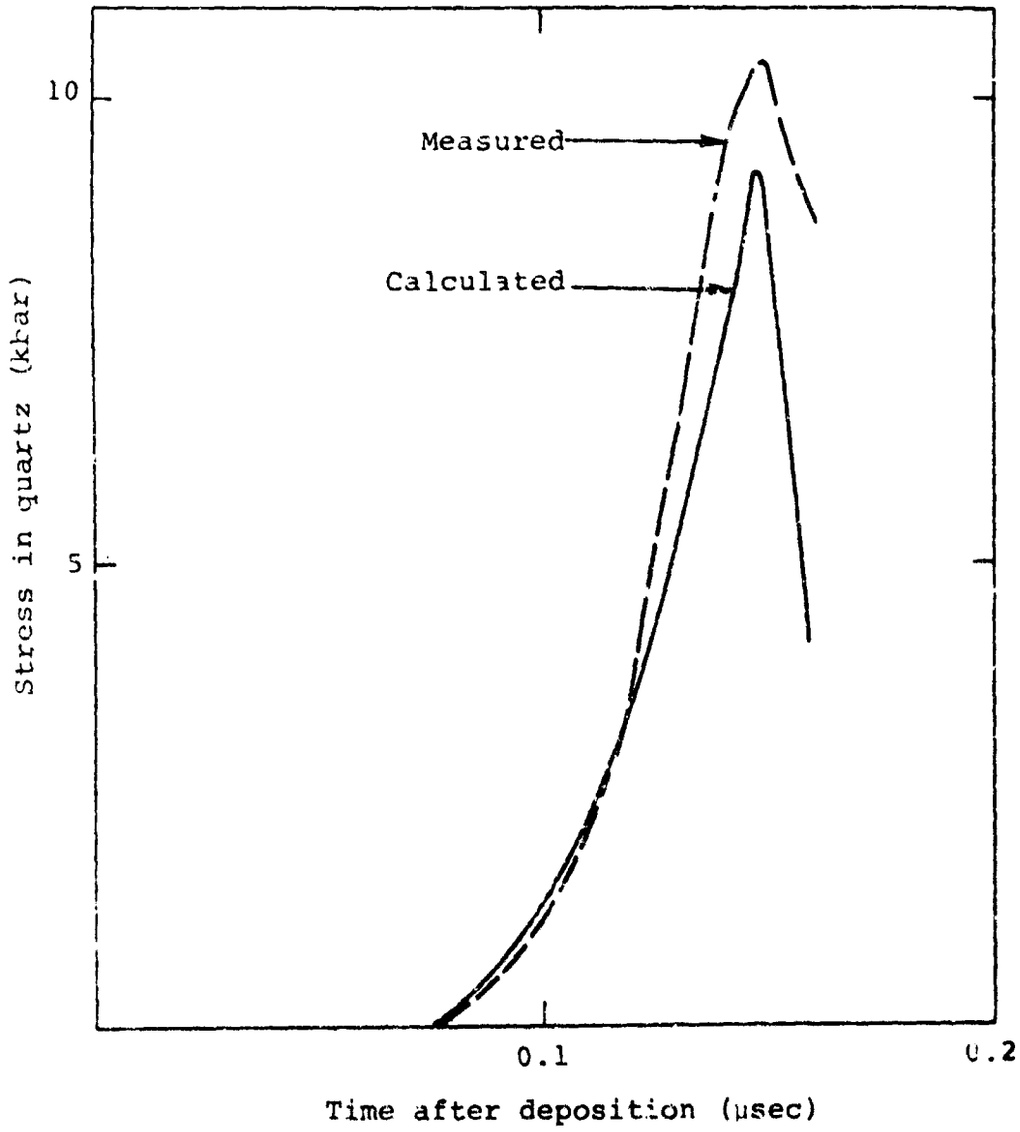

Figure B.18 Comparison between measured and calculated stress histories in α-titanium--shot 15088.

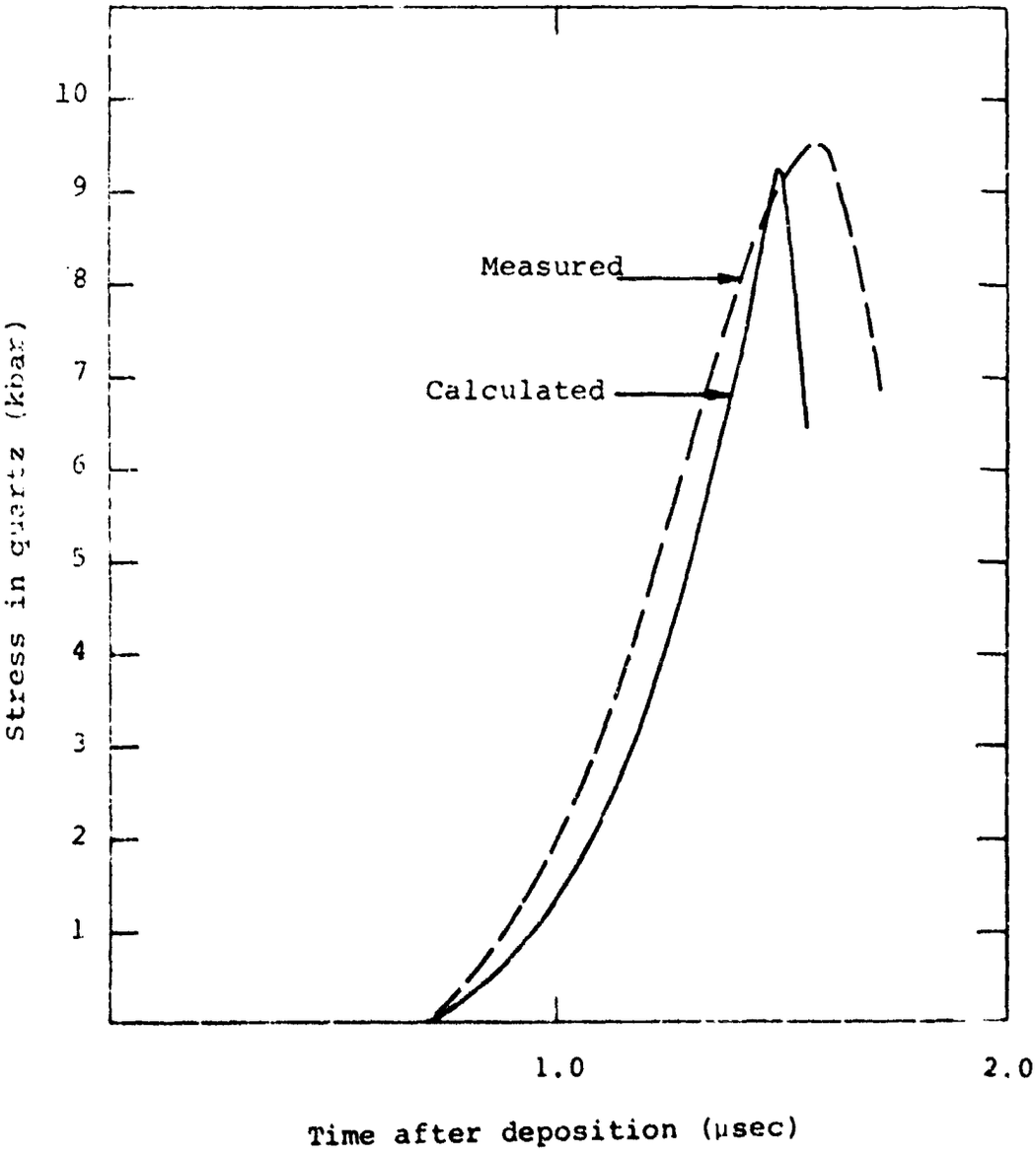

Figure B.19 Comparison between measured and calculated stress histories in α-titanium--shot 15089.

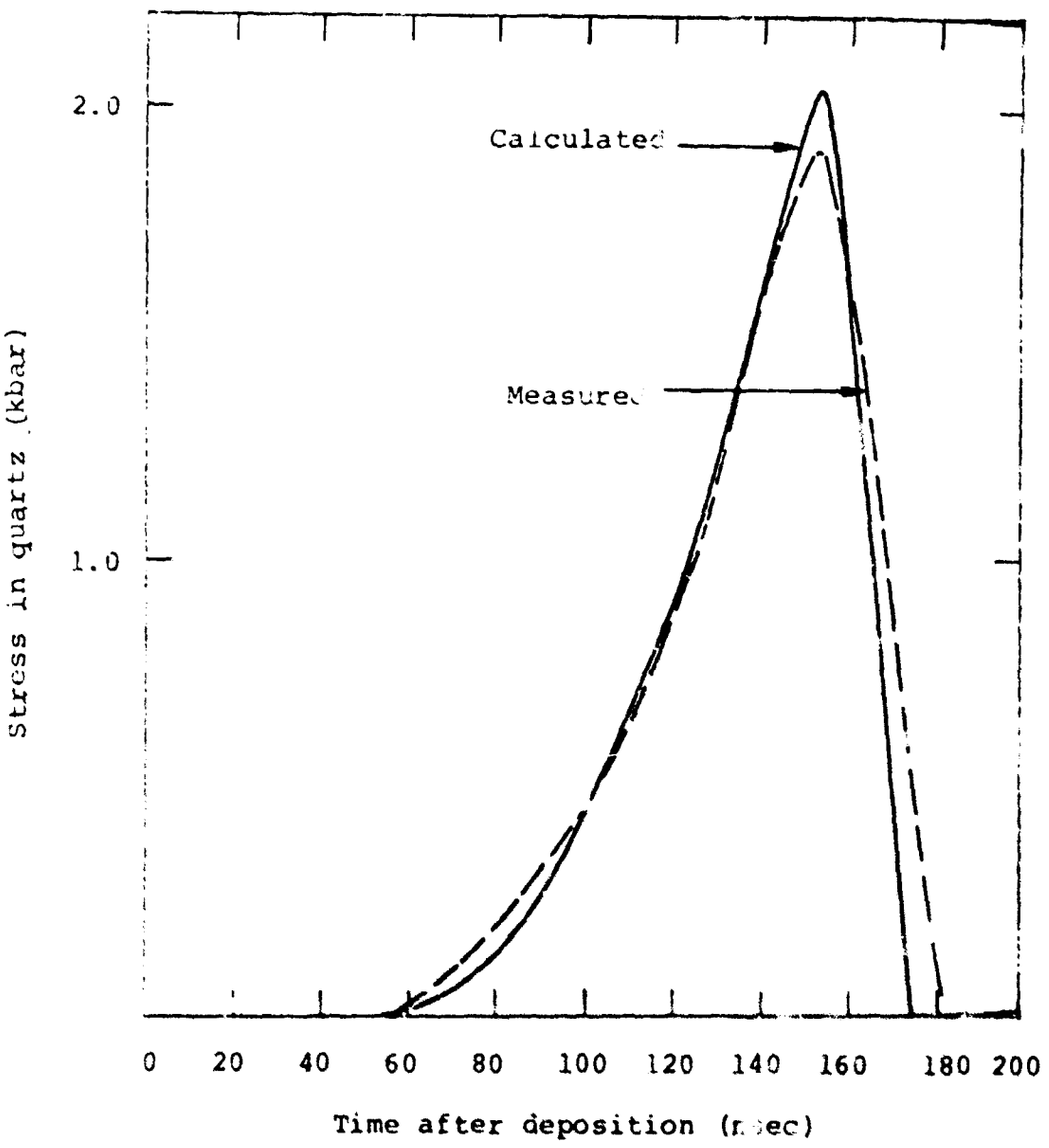

Figure 5.20 Comparison between measured and calculated stress histories in α-titanium--shot 618.

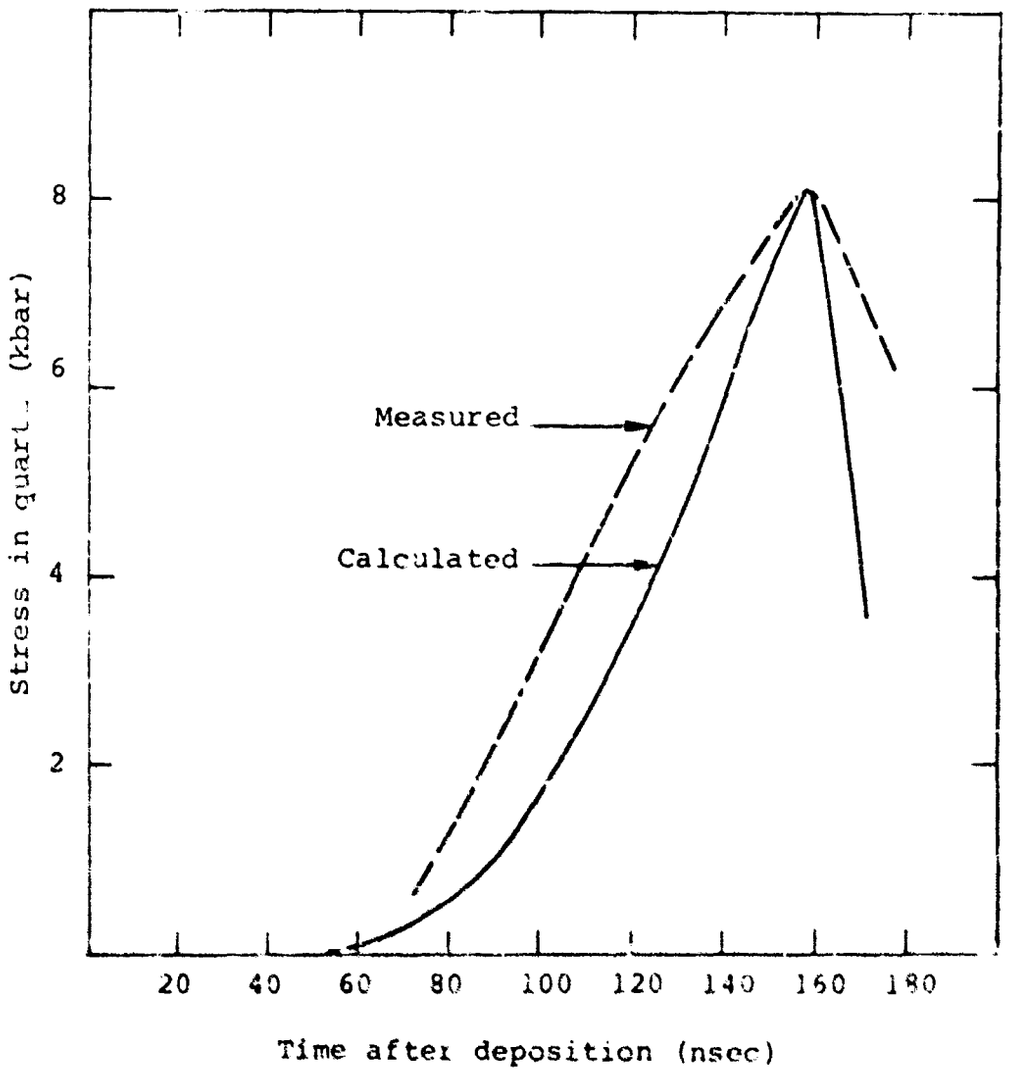

Figure B.21 Comparison between measured and calculated stress histories in α-titanium--shot 787.